Air quality modeling inter-comparison and multi-scale ensemble chain for Latin America

Jorge E. Pachón[1], Mariel A. Opazo[2], Pablo Lichtig[3], Nicolas Huneeus[2], Idir Bouarar[4], Guy Brasseur[4], Cathy W. Y. Li[4], Johannes Flemming[5], Laurent Menut[6], Camilo Menares[2], Laura Gallardo[2], Michael Gauss[7], Mikhael Sofiev[8], Rostilav Kouznetsov[8], Julia Palamarchuk[8], Andreas Uppstu[8], Laura Dawidowski[3], Nestor Y. Rojas[9], Maria de Fatima Andrade[10], Mario E. Gavidia-Calderón[10], Alejandro H. Delgado Peralta[10], and Daniel Schuch[10,11]

[1]Department of Environmental Engineering, Universidad de La Salle, Bogotá, 111711, Colombia
[2]Department of Geophysics and Center for Climate and Resilience Research (CR2), Universidad de Chile, Santiago, 8320000
[3]Consejo Nacional de Energía Atómica – CNEA, Buenos Aires, C1429BNP, Argentina
[4]Max Planck Institute for Meteorology, Hamburg, 20146, Germany
[5]European Centre for Medium-Range Weather Forecasts– ECMWF, Bonn, 53175, Germany
[6]Laboratoire de Météorologie Dynamique, Palaiseau, 91128, France
[7]Norwegian Meteorological Institute, Oslo, 0313, Norway
[8]Finnish Meteorological Institute, Helsinki, FI-00560, Finland
[9]Department of Chemical and Environmental Engineering, Universidad Nacional de Colombia, Bogotá, 111321, Colombia
[10]Instituto de Astronomia, Geofísica e Ciências Atmosféricas, Universidade de São Paulo, São Paulo, 05508-09B, Brazil
[11]Civil and Environmental Engineering, Northeastern University, Boston, 02115, USA

Correspondence: Guy Brasseur (guy.brasseur@mpimet.mpg.de)

Abstract. A multi-scale modeling ensemble chain has been assembled as a first step towards an Air Quality analysis and forecasting (AQF) system for Latin America. Two global and three regional models were tested and compared in retrospective mode over a shared domain (120W-28W, 60S-30N) for the months of January and July 2015. The objective of this experiment was to understand their performance and characterize their errors. Observations from local air quality monitoring networks in Colombia, Chile, Brazil, México, Ecuador and Perú were used for model evaluation. The models generally agreed with observations in large cities such as México City and São Paulo, whereas representing smaller urban areas, such as Bogotá and Santiago, was more challenging. For instance, in Santiago during wintertime, the simulations showed large discrepancies with observations. No single model demonstrated superior performance over others or among pollutants and sites available. In general, ozone and NO_2 exhibited the lowest bias and errors, especially in São Paulo and Mexico City. For SO_2, the bias and error were close to 200%, except for Bogotá. The ensemble, created from the median value of all models, was evaluated as well. In some cases, the ensemble outperformed the individual models and mitigated extreme over- or underestimation. However, more research is needed before concluding that the ensemble is the path for an AQF system in Latin America. This study identified certain limitations in the models and global emissions inventories, which should be addressed with the involvement and experience of local researchers.

1 Introduction

Latin America has some of the most populated urban areas in the world, notably, México City and São Paulo have populations exceeding 20 million, while Lima, Bogotá, Rio de Janeiro, and Buenos Aires have more than 10 million inhabitants each (Nations, 2018). These densely populated regions often experience air pollution events due to large emission sources and due to atmospheric conditions. Other major cities, such as Santiago and Medellin, with a population of ~7 and ~3.5 million, respectively, are also affected by poor air quality. This urban air pollution not only has long lasting effects on the health of the population but also has a significant negative impact on the environment, and possibly the regional climate (Busch et al., 2023; Gouveia et al., 2018; Molina et al., 2015; Rodríguez-Villamizar et al., 2018; Romieu et al., 2012). Latin America could greatly benefit from an air quality forecasting (AFC) system that informs the public about air pollution episodes and supports policy actions.

To better understand the causes of air pollution events in Latin America, it's important to consider the local emission sources. In addition to the usual urban pollution sources (e.g., industrial facilities, residential heating, energy production, and transportation sectors), plumes from biomass burning and long-range dust transport can occasionally reach major cities. In northern South America, increased pollution levels in the dry season have been associated with biomass burning (Ballesteros-González et al., 2020; Casallas et al., 2023; Mendez-Espinosa et al., 2019) and dust from the Sahara Desert (Mendez-Espinosa et al., 2020). The latter source also affects the Caribbean and central México in early spring (Kramer and Kirtman, 2021; Ramírez-Romero et al., 2021). Also, in the context of climate and land-use change, wildfires are a recurrent phenomenon in southern South America (Resquin et al., 2018; de la Barrera et al., 2018; Sarricolea et al., 2020). The Amazon is the largest forest in the world and a significant source of biogenic volatile organic compounds (BVOCs), precursors of CO, ozone and secondary aerosols (Nascimento et al., 2022; Zimmerman et al., 1988).

Air quality management in Latin America and the Caribbean (LAC) has been traditionally focused on surveillance and building emission inventories (Franco et al., 2019). Modeling activities for LAC are less frequent than North America, Europe, or Asia, mainly due to limited computing resources and scarce information of emission sources. Of more than 30 regional AQF systems identified worldwide only one exists in Latin America (Zhang et al., 2012). In addition to the restrictions already mentioned, LAC has other challenges: complex terrain where cities are situated in the valleys and canyons of the Andes, varying meteorological conditions due to their proximity to mountains and coastlines, deep convection in the tropics, extensive biomass burning in the Orinoco and Amazonian basins, and the presence of densely populated megacities and urban areas, among others. Despite limitations for applying air quality models in LAC, regional models have been successfully implemented since 2000.

The coupled Aerosol and Tracer Transport model to the Brazilian development of the Regional Atmospheric Modeling System (CCATT-BRAMS) was developed in the region (Longo et al., 2013) to investigate the impact of the Amazonian wildfires on air quality in major Brazilian cities (Pereira et al., 2011; Freitas et al., 2011). The North American Community Multiscale Air Quality Model (CMAQ), coupled with the Weather Research and Forecasting (WRF) meteorological model, has been used in Colombia and Brazil to predict pollutant concentrations and assess reduction strategies (Albuquerque et al., 2019; East et al., 2021; Pérez-Peña et al., 2017; Nedbor-Gross et al., 2018; Pachón et al., 2018). The WRF model coupled with

Chemistry (WRF-Chem) online has been actively used to study the impact of regional sources on air quality in urban centers across Colombia (Ballesteros-González et al., 2020, 2022; Casallas et al., 2024; González et al., 2018; Mendez-Espinosa et al., 2019), Chile (Saide et al., 2016) and São Paulo (Gavidia-Calderón et al., 2024). CHIMERE (Menut et al., 2013) and MATCH (Andersson et al., 2015) models have been applied in Chile to assess pollutant chemical transformation and dispersion as well as emission reduction strategies (Gallardo et al., 2002; Lapere, 2018; Lapere et al., 2021; Mailler et al., 2017). Additionally, CAMS reanalysis data has been compared against air quality observations, observing well-captured temporal trends for PM_{10}, $PM_{2.5}$ and SO_2 but not for NO_X (Casallas et al., 2024).

This work conducts the first model inter-comparison effort and ensemble construction for Latin America, which was assembled under the Prediction of Air Pollutants in Latin America (PAPILA) project (https://papila-h2020.eu/papila). The aim of PAPILA was to develop an AQF system for the region with increasing capabilities in major cities. This objective is in line with the WMO GAFIS initiative that supports the implementation of AQF systems, especially in countries and regions where they do not exist, such as Africa and South America (WMO, 2022). This manuscript presents a retrospective (hindcast) analysis and it's organized as follows: Sect. 2 presents model descriptions, emission inventories utilized in the models, and observations employed for model evaluation. In Sect. 3 we analyze the model performance and conduct inter-comparisons for each pollutant (NO_2, O_3, CO, SO_2, $PM_{2.5}$). We also discuss the season variability of predictions and the analysis of large vs small urban areas. Finally, Sect. 4 summarizes our findings and outlines directions for future development.

2 Methodology

The model inter-comparison and construction of the ensemble required relevant activities, such as: the execution of global and regional models in a common domain, harmonization of the model output, ensemble construction, collection of air quality observations, analysis of temporal and spatial variability, and model evaluation.

2.1 Description of the models and modeling set-up

For the model inter-comparison, two global models (CAMS and SILAM) and three regional models (CHIMERE, WRF-Chem, EMEP MSC-W) were selected based on the expertise of the research groups working on the PAPILA project (Table 1). WRF-Chem was implemented by two different groups, the Max Planck Institute for Meteorology (MPIM) in Germany and the University of São Paulo (USP) in Brazil, with different set-ups. It's worth to note that the early simulations analyzed hereby do not represent the best performance of each model in the LAC region or over individual urban areas. The different models are briefly described in the following paragraphs.

The Copernicus Atmosphere Monitoring Service (CAMS) provides state-of-the-art global atmospheric composition data based on the IFS (Integrated Forecasting System) model of the European Centre for Medium-Range Weather Forecasts (ECMWF) (Inness et al., 2019). The chemical mechanism of IFS is an extended version of the Carbon Bond 2005 (CB05) and complements the MACC aerosol module (Flemming et al., 2017; Morcrette et al., 2009). The CAMS reanalysis data used for this project is a combination of satellite observations of atmospheric composition and the IFS modeling setup. Anthro-

pogenic emissions from the MACC/CityZen (MACCity) inventory (Granier et al., 2011) and biomass burning emissions from the Global Fire Assimilation System GFASv1.2 (Kaiser et al., 2012) were used in the simulations (Table 1). The biogenic emissions were simulated off-line by the Model of Emissions of Gases and Aerosols from Nature (MEGAN) version 2.1 model (Guenther et al., 2006) using an offline emission inventory (ECCAD, 2021). CAMS has been extensively evaluated against

85 ozone sondings, aircraft profiles, surface observations, and global satellite retrievals (Flemming et al., 2015).

Table 1. Description of the models included in the ensemble.

Institution and model	Model type	Vertical resolution	Grid cells	Projection	Initial and Boundary conditions	Chemical mech. - Aerosol model	Meteo - rology	Emissions
FMI - SILAM	Global and regional offline v5.7	25 layers of varying depth up to 5.25 Pa. Lowest level ∼20m	590 x 526	lat-lon	IC and BC from a global SILAM simulation with a coarser resolution.	Chemistry: Gas-phase CBM-IV	C-IFS ECMWF	CAMS-GLOB-ANT-v2.1 IS4FIRES v1.0. Biogenic MEGAN 2.1
ECMWF - CAMS	Global	60 levels up to 0.1 hPa (65km). Lowest level ∼20m	450 x 460	lat-lon	IC for meteorology from the ECMWF´s operational analysis and for chemistry from the previous forecast.	Chemistry: CB05 - Aerosol: AER bulk	C-IFS	CAMS-REG-AP_v3.1/2016 provided by CAMS_81. MACCITY GFAS v1.2 Biogenic MEGAN 2.1
LMD & UCL - CHIMERE	Regional offline V2017r4.2	Variable, 8 levels from the surface up to 500 hPa. 7 levels below 2 km	450 x 455	Lambert-conformal	BC CAMS-Global IFS IC previous day forecast.	Chemistry: SAPRC 07 A - Aerosol: 10 bins and 15 species LMDz-INCA (gas, aerosols) and GOCART (mineral dust)	C-IFS	Anthropogenic EDGAR-HTAP Biogenic online MEGAN v2.1
UCL - EMEP	Global and regional offline	20 layers up to 100 hPa with approximately 10 in the Planetary Boundary layer	450 x 460	lat-lon	BC CAMS-Global IFS IC previous day forecast.	Chemistry: CBMZ - Aerosol: EMEP scheme MARS	C-IFS	Anthropogenic EDGAR-HTAP FINN v1.0 Biogenic Included with internal calculation of emissions
MPIM - WRFChem	Regional online v3.6.1	36 vertical levels up to 50 hPa Lowest level ∼50m	455 x 450	Mercator	BC and IC for meteorology from GFS, for Chemistry from CAM-Chem.	Chemistry: MOZART 4 - Aerosol: GOCART	WRF	CAMS-GLOB-ANT v4.2 FINN v1.5 Biogenic MEGAN v2.1
USP - WRFChem	Regional online WRF-Chem v3.9.1	35 vertical levels up to 50 hPa Lowest level ∼50m	455 x 450	Mercator	BC and IC for meteorology from GFS, for Chemistry from CAM-Chem.	Chemistry: MOZART - Aerosol: GOCART	WRF	CAMS-GLOB-ANT v5.3 FINN v1.5 Biogenic MEGAN v2.1

Abbreviations: FMI – Finnish Meteorological Institute, ECMWF – European Center for Weather and Modeling Forecast, LMD – Laboratoire de Météorologie Dynamique, MPIM – Max Planck Institute for Meteorology, UCL – University of Chile, USP – University of São Paulo

The system for Integrated modelling of Atmospheric composition (SILAM, http://silam.fmi.fi) is a chemical transport model for global-to-local simulations of atmospheric composition and air quality developed at Finish Meteorological Institute (FMI) (Sofiev, 2002; Kouznetsov and Sofiev, 2012; Sofiev et al., 2010, 2006, 2015). Briefly, SILAM employs the CBM-IV mechanism

for gas-phase chemistry (Gery et al., 1989). For further details on the model characteristics, refer to (METEO-FRANCE, 2020).

For this work, the SILAM simulations were driven by the meteorological IFS model of ECMWF. Anthropogenic emissions were adopted from the CAMS global emission inventory v2.1, whereas the biomass burning emissions were generated by the Integrated Monitoring and Modeling System for Wildland fires (IS4FIRES) (http://is4fires.fmi.fi, last access: 03 July 2024), (Sofiev et al., 2009; Soares and Sofiev, 2014). The biogenic emissions were simulated off-line by the MEGAN v2.1 model (Guenther et al., 2006), particularly, isoprene and monoterpene emissions computed for the year 2010, as found on the MEGAN website (Table 1). The model has been extensively evaluated in numerous international retrospective studies (Marécal et al., 2015; Kukkonen et al., 2012; Blechschmidt et al., 2020; Petersen et al., 2019) and real-time operational applications. SILAM is included in the regional European forecasting system provided by CAMS together with CHIMERE, EMEP MSC-W and eight other models (Colette et al., 2020).

CHIMERE is a Eulerian chemistry-transport model (CTM). It's able to perform simulations from urban to hemispheric scale (Lapere, 2018; Lapere et al., 2021; Mailler et al., 2017; Menut et al., 2021). The model can be used online (with WRF only) or offline (with several meteorological models). The model characteristics are published elsewhere (METEO-FRANCE, 2020). For this study, the meteorological forcing is the IFS global simulation provided by ECMWF. The biogenic emissions are online calculated using the MEGAN v2.1 model (Guenther et al., 2006) using the 30s horizontal resolution database. Fire emissions are those of CAMS (Kaiser et al., 2012) and reformatted for CHIMERE using the dedicated preprocessor (Menut et al., 2021). The mineral dust is calculated online using the (Alfaro and Gomes, 2001) scheme and the sea-salt emissions are also calculated online using the (Monahan, 1986) scheme. NOx by lightning are calculated using the scheme described in (Menut et al., 2020). CHIMERE is used for analysis and forecast in tens of countries around the world and at various spatial scales, including the CAMS forecast. More specifically for Latin-America, it was used for several studies about anthropogenic emissions, deposition of black carbon on snow, indirect effects and impact of megafires fires on clouds formation (Lapere et al., 2021; Mailler et al., 2017; Lapere, 2018). For this exercise, CHIMERE were run for the 31 days of January and July of 2015, however due to problems in the output files 15 days were missing (5 days from January 14th to 18th and 10 days from July 11th to 19th and July 9th).

The EMEP MSC-W model ('EMEP model' hereafter) is an offline chemical transport model developed at the Norwegian Meteorological Institute (MET Norway). It's used to simulate photo-oxidants as well as organic and inorganic aerosols in scales ranging from local to global scales (Simpson et al., 2012). Details regarding the model characteristics can be found in (METEO-FRANCE, 2020). For this study the model was driven by meteorological data from the IFS model of ECMWF. Gas phase chemistry from the "EMEP scheme", comprising 70 species and 140 reactions (Andersson-Sköld and Simpson, 1999; Simpson et al., 2012), inorganics from the MARS equilibrium module (Binkowski and Shankar, 1995) and organics from the CBM-Z mechanism (Zaveri and Peters, 1999). Emissions from forest and vegetation fires are taken from the Fire INventory from NCAR (FINN v1.0) (Wiedinmyer et al., 2011). Biogenic emissions of isoprene and (if required) monoterpenes are calculated in the model for every grid-cell (Simpson et al., 2012). The EMEP model has for several decades been the main tool for underpinning air quality policies under the UNECE convention on long-range transboundary air pollution. However, it should be noted that the runs for this study were the very first EMEP model simulations ever conducted on a regional scale

for LAC and should thus be considered only as a first demonstration of model capabilities. For PAPILA, the EMEP model was run by the modeling team at the University of Chile in Santiago with some support by MET Norway.

The WRF-Chem is the Weather Research and Forecasting (WRF) model coupled with Chemistry, developed at the National Center for Atmospheric Research (NCAR) with the purpose of simulating urban- to regional-scale fields of trace gases and particulates. The air quality and meteorological components share the same transport and physics scheme, as well as horizontal and vertical grid (Fast et al., 2006; Grell et al., 2005). The MPIM WRF-Chem uses version 3.6.1 to simulate meteorology and chemistry simultaneously online in South America at ~20 km horizontal resolution and 36 vertical levels extending from the surface to 21 km altitude. The gas-phase chemistry is represented by the Model for Ozone and Related Chemical Tracers (MOZART-4) chemical scheme (Emmons et al., 2010). The Goddard Chemistry Aerosol Radiation and Transport (GOCART) bulk aerosol module coupled with MOZART is used in this study to consider the aerosol processes (Chin et al., 2002; Ginoux et al., 2001). Boundary and initial conditions for the meteorology were set up from GFS, and for the chemical species concentrations from CAM-Chem. The anthropogenic emissions were from CAMS-GLOB-ANT v4.2, which consists of $0.1°x 0.1°$grid maps of several species including CO, SO_2, NO, NMVOC, NH_3, BC and OC. Daily varying emissions of trace species from biomass burning were taken from the (FINN v1.5) dataset (Wiedinmyer et al., 2011). Biogenic emissions of trace species from terrestrial ecosystems are calculated online using the MEGAN model v2.04 (Guenther et al., 2006). Further details on the MPIM WRF-chem model settings can be found in (Bouarar et al., 2019).

The WRF-Chem run by USP (version 3.9.1) uses similar characteristics as previously described with a horizontal resolution ~22 km and 35 vertical layers. Some differences from the MPIM configuration are the version of global emissions CAMS-GLOB-ANT v5.3 (ECCAD, 2020), the speciation of the chemical boundary condition from the CAM-Chem model (Buchholz et al., 2019; Emmons et al., 2010) and the speciation of FINN v1.5 emissions which are suitable for simulation over São Paulo. For this exercise, WRF-Chem did not include Mexico City in the modeling domain.

CHIMERE, IFS, EMEP, WRF-Chem, LOTOS-EUROS and SILAM models are used in an ensemble mode to configure the MarcoPolo-Panda prediction system in Asia (Brasseur et al., 2019; Petersen et al., 2019). It has been observed that, under specific circumstances, a model ensemble can outperform individual models, demonstrating the potential benefits of this approach. With the desire to replicate the experience in Latin America, the selected models were applied in a common domain, defined by the south-eastern corner at 119°54'W 59°54'S, and the north-eastern corner at 28°6'W 29°54'N. The models were run at a spatial resolution of ~0.2°x 0.2°(~20x20km). Input meteorology and emissions were up to the modeling group (Table 1). The simulation period covers January (southern hemisphere summer) and July (southern hemisphere winter) of 2015.

2.2 Model Evaluation

The performance of the models was assessed by comparing the simulated concentrations with the average of the observations for each available city, pollutant, and considered period. The observation's average was constructed by computing the arithmetic mean of all air quality stations available in the network within the city's polygon. On the other hand, the simulated concentrations for the models were estimated as the average of the models' closest grid point to the location of each station that is within the city's polygon for every city and pollutant considered in this study. This results in a weighted average of the

model where the weight is given by the number of stations that measure the pollutant closest to each grid point, resulting in the same geographical sampling for the observations and the models, thus reducing any potential station's sampling bias to the best of our abilities. This approach was chosen with the objective of assessing the model performance in cities, rather than for each air quality station separately. It's outside the scope of this work to conduct an intra-urban variability study of the model performance given the chosen resolution of 0.2 degrees. The model evaluation was focused on nitrogen dioxide (NO_2), ozone (O_3), carbon monoxide (CO), sulphur dioxide (SO_2), and particulate matter less than 2.5 micrometers ($PM_{2.5}$) and less than 10 micrometers (PM_{10}).

For each period, pollutant and city, the model evaluation included the following metrics: Model/Observations ratio, mean bias (BIAS), modified normalized bias (MNBIAS), root mean square error (RMSE), fractional gross error (FGE) and correlation coefficient (R). The formulas were replicated from the MarcoPolo-Panda project (Petersen et al., 2019) and are presented in Table A1. These evaluation metrics were computed for all models and the ensemble.

2.3 Air quality monitoring networks in Latin America

Several air quality monitoring networks (AQMN) are available throughout Latin America, especially in major cities. However, worldwide access to the datasets can be difficult due to language barriers and the lack of a centralized platform. A comprehensive list of AQMN in Latin America was assembled for the PAPILA project (https://papila-h2020.eu/observations). For the year 2015, we collected air quality data for 12 cities in México, Colombia, Ecuador, Perú, Chile, Brazil, and Uruguay. Only stations with a minimum of 75% data completeness were considered when calculating the city average of the observations, resulting in eight cities with enough data to use for this study. This data completeness requirement considers a minimum of 75% of days available for each period, as well as a minimum of 75% of hourly data to construct their daily average. We focus in this study on the four major cities (from North to South): México City, Bogotá, São Paulo and Santiago (Figure 1). However, data of all available cities were used in the model evaluation (Tables B1 through B8).

3 Results

Simulated concentrations of all pollutants from all models were compared against observations from every city and for both periods (January and July) in 2015. In this section, we present results from the model evaluation, the spatial and temporal variability of simulate fields and the impact of large versus small urban areas in the model inter-comparison.

3.1 Model evaluation

The following results are presented for every pollutant: analysis of observations from AQMN, simulated concentrations by the models, comparison of evaluation metrics, discussion of model performance including the ensemble and analysis of model variation.
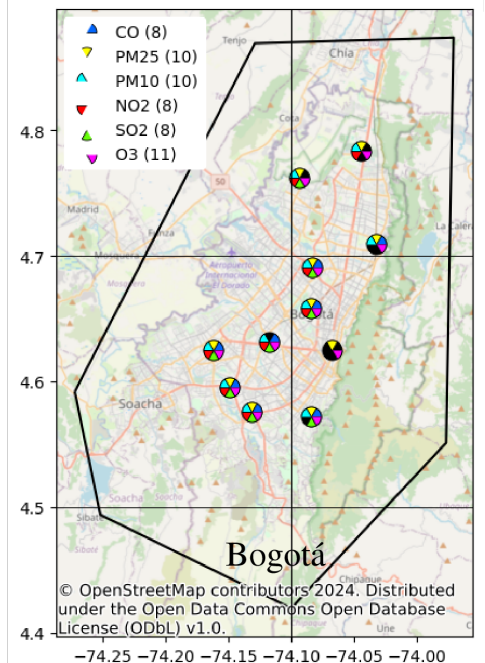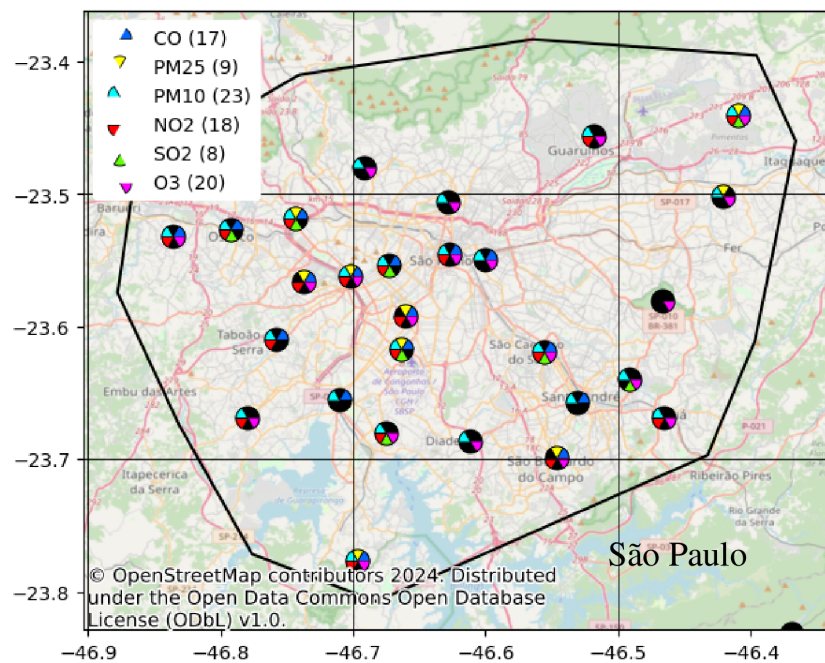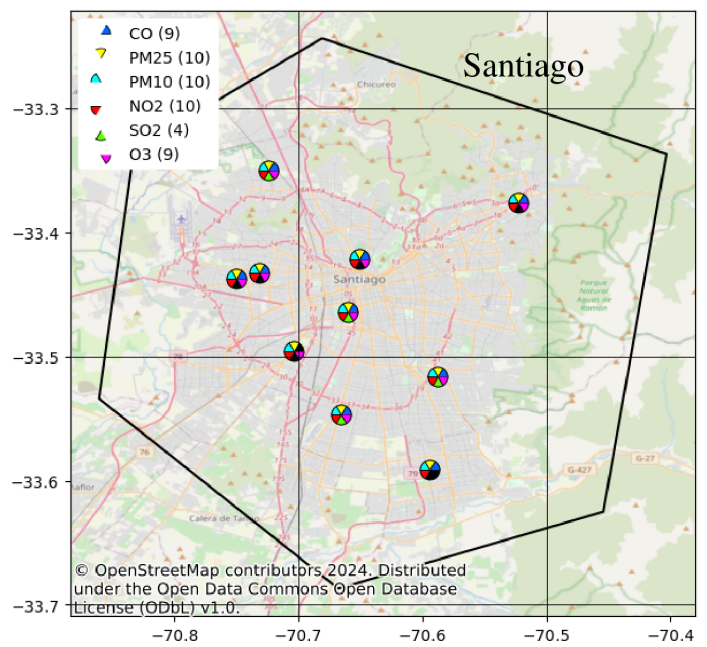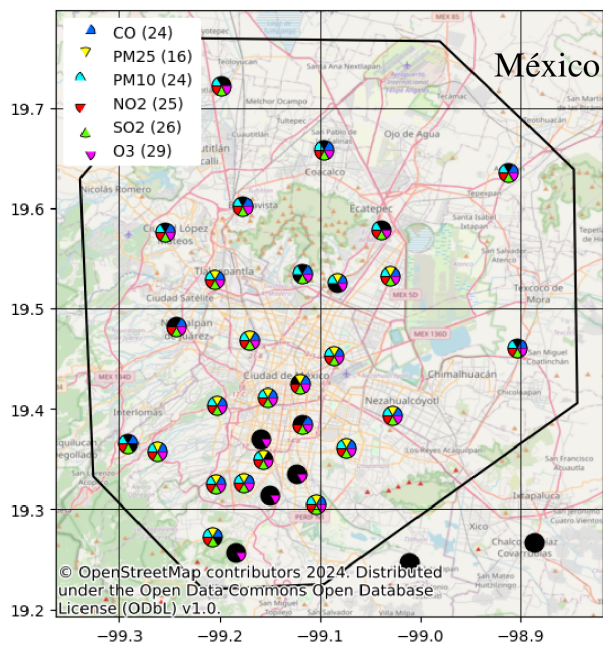
Figure 1. Location of air quality stations in major Latin American cities (Santiago, Bogotá, México City, São Paulo) alongside the city's definition for computing the modeled city average. © OpenStreetMap contributors 2024. Distributed under the Open Data Commons Open Database License (ODbL) v1.0.

3.1.1 Nitrogen dioxide - NO$_2$

Observations

The number of stations per city recording NO$_2$ during January and July of 2015 varies between 7 in Bogotá and 24 in Mexico City (Appendix B). The highest daily average concentration of NO$_2$ is observed in Santiago during winter at around 30 ppb (Figure 2). This can be attributed to adverse meteorological conditions and emissions from transportation and residential combustion in the surrounding municipalities (Mazzeo et al., 2018; Saide et al., 2016) whereas in the summer NO$_2$ levels fall to 11 ppb. The second largest values are shown in México City and São Paulo with a daily average NO$_2$ levels of 27 and 20 ppb respectively, due to the heavy use of fossil fuels in transportation and power generation. The lowest levels of NO$_2$ are measured in Bogotá with 16.4 ppb on average.

Model performance

In Bogotá and Santiago, NO$_2$ is underestimated by the ensemble members (Figure 2). In Santiago, the mean of the models is 10.3 ppb in summer and 22.1 ppb in winter, lower than the mean of the observations. Similarly, in Bogotá the mean of the modeled values is 6.6 ppb, much lower than observations. In contrast, in São Paulo and México City, the models both over and under predict the ambient concentrations and the average of the modeled fields (23.6 ppb and 30.3 ppb respectively) are in the same order of magnitude of observations.

São Paulo and México City exhibit the lowest MNBIAS and FGE for NO$_2$ (Table A2).The correlation between the models and observations hovers around 0.7, which is larger than the goal benchmark proposed for this pollutant (r $\geq$ 0.6) (Zhai et al., 2024).

In Santiago, the MNBIAS is mostly negative during both seasons except the SILAM and EMEP models that resulted in a positive bias. The degree of which the models are underestimating the observations is notably higher in the winter than in summer and with a larger FGE (Table A2). The correlation between models and observations in Santiago is larger in summer than in winter, with some models achieving the criteria benchmark (r > 0.5, (Zhai et al., 2024). In Bogotá, the MNBIAS are large and consistently negative and the FGE varies between 50% and 156% (Table A2). Despite these lower scores, the correlation between observations and models are moderate around 0.6 in January meeting criteria benchmarks and demonstrate that certain models can successfully replicate the temporal variations but not the magnitude of the pollutant.

The adequate performance in São Paulo and México City may be attributed to an accurate portrayal of the temporal and spatial variability that is achieved in large urban areas like these (>3500 km^2) which encompass at least nine model cells (20 km x 20 km). The lower simulated NO$_2$ levels in Bogotá likely stems from an underestimation of emissions. A study by (Rojas et al., 2023) utilized local data to estimate on-road emissions in Colombia and revealed substantial underestimation of NO$_X$ emissions by global inventories such as EDGAR 6.1, CAMS, and the Community Emissions Data System (CEDS). Their findings recommend adjustments to the emission factors used for NO$_X$, particularly for heavy-duty and passenger vehicles, followed by a recalculation of the resulting emissions. The underestimation of NO$_2$ can also be noted in other cities such as Medellin, Guadalajara, Lima, and Quito (Figure 8). These cities, along with Bogotá, possess urban areas ranging from 235 to 890 km^2 and are confined within one or two cells of the models (20km x 20km). It's possible that the average of observations
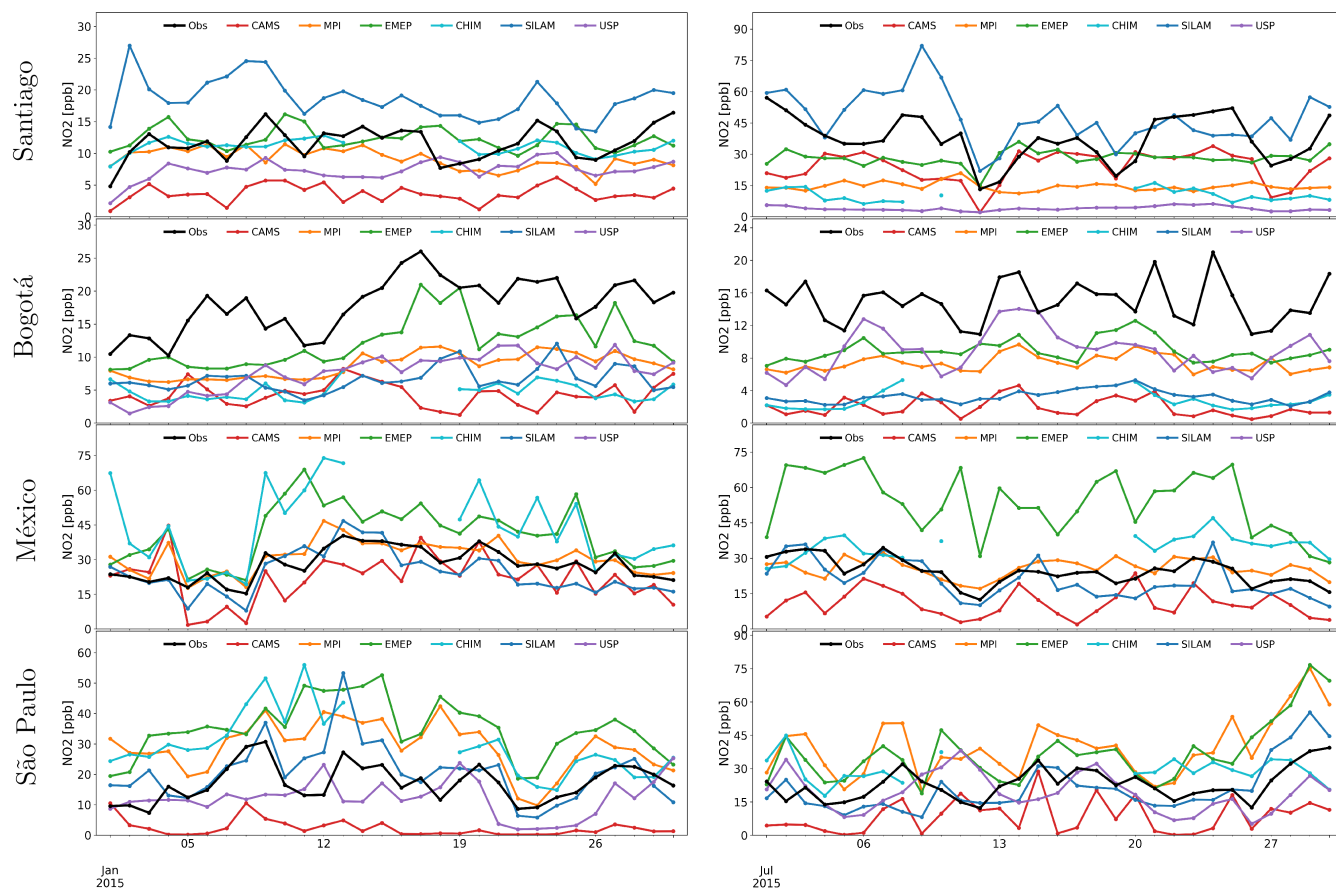
Figure 2. Observed (black) and simulated NO$_2$ daily mean concentrations in Santiago, (top) Bogotá, México City, São Paulo (bottom) for January (left) and July (right) 2015.

is heavily influenced by local sources, in which case a finer modeling resolution is required to accurately capture the spatial variability of air pollution.

Model intercomparison

For NO$_2$, CAMS underestimates the observations in the four cities whereas SILAM underestimates this pollutant in Bogotá,
225 Mexico City and São Paulo (only in July) and overestimates the observations in Santiago and in São Paulo (in January). CAMS displayed larger MNBIAS and FGE than SILAM. In general, SILAM reproduces at least 80% of the NO$_2$ levels, with the exception in Bogotá where only 30% is simulated. The correlation coefficient is better for SILAM (R $\sim$0.6) than for CAMS (R $\sim$0.3).

The results from regional models are very diverse. In general, WRF-MPI, CHIMERE and EMEP have lower values of
230 MNBIAS and FGE for NO$_2$ in São Paulo and México City (Table A2). In São Paulo, except for WRF-USP, regional models tend to overestimate NO$_2$ with MNBIAS between 20% and 70%. WRF-USP reproduces about 76% of NO$_2$ concentrations. In

México City, the tendency of regional models is to overestimate the NO_2 levels (MNBIAS: 10 to 75%). In Santiago, CHIMERE achieves the lowest MNBIAS (-2%) in January but not in July (-119%). In Bogotá, the MNBIAS in regional models remains consistently negative.

From Figure 2 is visible the model variation. In Santiago in winter the range of NO_2 values is 48 ppb, which corresponds to a coefficient of variation (C.V.) of 71% (Table A8), this contrasts with the range in summer of 15 ppb (C.V.=49%). Other large variations are observed in México City in July (range 54 ppb, C.V. 57%) and São Paulo (range 32 ppb, C.V. 46 to 58%). It's interesting to note the case of Bogotá where all models consistently underestimate NO_2, but the model variation is the lowest (8ppm with C.V. 39 and 56%).

Ensemble performance

The median ensemble underestimates NO_2 concentrations in Bogotá and in a lesser extent in Santiago. This is consistent with the underestimation trend by most of the models. The ensemble in these two cities has some of the lowest MNBIAS, FGE and R, but not always better than individual models (Table A2). On the contrary, in Mexico City and São Paulo, the ensemble median outperforms the models for NO_2. In summer and winter, the ensemble presents the lowest FGE in both cities. The correlation coefficient range between 0.5 and 0.8 within the criteria benchmark R>0.5 (Zhai et al., 2024). The MNBIAS are also the lowest (-2.9 to 17.7%).

3.1.2 Ozone - O_3

Observations

The number of stations per city recording O_3 during January and July of 2015 varies between 9 in Santiago and 29 in Mexico City (Appendix B). The highest observed ozone concentration was in México City in July with an average of 31 ppb. However, this value is significantly lower than the surface ozone concentrations reported in the MAM (March-April-May) season with values larger than 70 ppb (Barrett and Raga, 2016; Silva-Quiroz et al., 2019). The second largest ozone value occurs in São Paulo during January with daily averages of 24 ppb. This is probably due to an abundance of ozone precursors, in particular, volatile organic compounds (VOC) from the use of biofuels in the transportation sector (de Fatima Andrade et al., 2017; Gavidia-Calderón et al., 2024) and biogenic VOCS (Martins et al., 2006). Santiago experiences a marked seasonal cycle of ozone concentrations with summer values of approximately 22 ppb and winter concentrations around 3.6 ppb. This seasonal difference has been observed in other studies (Seguel et al., 2024). In Bogotá, ozone concentrations are the lowest and below 13 ppb.

Model performance

In the four cities, simulations of O_3 are mainly overestimated (Figure 3). In the summer in São Paulo and México City, simulations can reach up to 100 ppb, which is significantly above the observations. In Santiago in the winter, the mean of models ($\sim$ 20 ppb) is significantly larger than observations, indicating that the models have difficulty reproducing low values of this secondary pollutant. In the summer, ozone estimates are much closer to observations. Similarly, in Bogotá, models estimate an average of 17 ppb which is in the same order of magnitude as the observations.
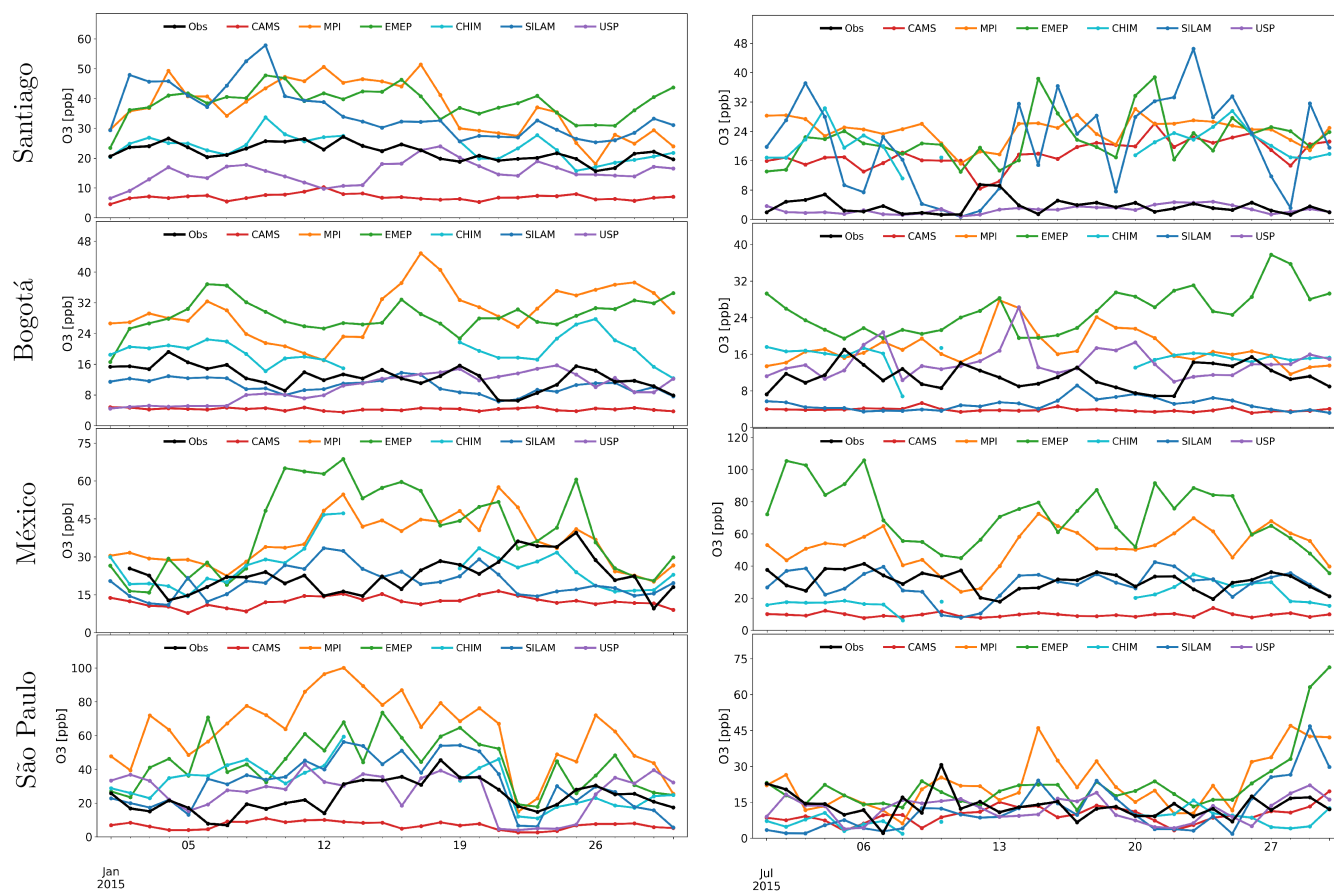
Figure 3. Observed (black) and simulated O_3 daily mean concentrations in Santiago, (top) Bogotá, México City, São Paulo (bottom) for January (left) and July (right) 2015.

265   The overestimation of O_3 in Santiago might be related to the underestimation of NO_2 previously described and the inadequate titration of ozone. Ozone formation in Santiago has been found VOC-limited (Seguel et al., 2020). This situation is also observed in Bogotá where most models overestimate O_3 with MNBIAS between 25% and 80% (Table A3). In contrast, in Mexico and São Paulo, the models that overestimate NO_2 are also overestimating O_3. This complex situation is explained by the non-linearities in the formation of ozone (Grewe, 2004). In general, correlation coefficients for O_3 are very low (R < 0.3),

270 especially in São Paulo and México City, indicating the challenge to adequately reproduce the spatial and time variability of this pollutant. Only in Santiago in January, the criteria benchmark for O_3 (R > 0.5) is achieved by some models (Emery et al., 2017).

Model intercomparison

In the case of global models, CAMS underestimates O_3 in the four cities except in Santiago during winter. Additionally,

275 CAMS tends to have low correlation levels along with large bias and errors (Table A3). SILAM displays lower bias and errors

compared to CAMS. However, just like with CAMS, SILAM significantly overestimates O_3 levels in Santiago during the winter. In Bogotá, SILAM underestimates O_3 to a lesser extent than CAMS, with a larger FGE in July (74%) than in January (22%).

In São Paulo, daytime concentrations of ozone are generally overestimated by most models (except for CAMS). The largest overprediction of O_3 (MNBIAS from 30 to 90%) is associated with overestimation of NO_2, especially for MPI, EMEP and CHIMERE models. For the models with NO_2 levels in reasonable agreement with observations (SILAM, USP) the ozone overprediction is lower (MNBIAS <25%). Among the regional models, EMEP and WRF-MPI consistently overestimate O_3 levels in all cities, with relatively high MNBIAS and FGE. In contrast, WRF-USP proves particularly suitable for São Paulo, achieving some of the lowest FGE. CHIMERE also performs well in Santiago in the summer, likely owing to local adjustments and parameterizations tailored to these specific cities.

Figure 3 shows a relatively large model variation for ozone. The largest ozone variability is shown in México City in summertime with a range of 62 ppb and a C.V. of 72% (Table A8). This wide variability is caused by the simulation of the EMEP model (71 ppb) and CAMS (9.6 ppb), that represent the extreme cases of over and underestimation. In a similar manner, in Bogotá, São Paulo and Santiago, the C.V. are 61%, 49% and 47% respectively, explained by the strong underestimation of CAMS and severe overestimation by EMEP and WRF-MPI.

Ensemble performance

In Santiago in January, the median ensemble showed one of the lowest MNBIAS and FGE, surpassed only by CHIMERE (Table A3), and achieved the goal benchmark for this pollutant (R>0.75) (Emery et al., 2017). In July, the overestimation of ozone by most models impacts the performance of the ensemble, which also overestimates O_3 concentrations. In Bogotá, the ensemble has some of the best scores for NMBIAS and FGE and represents an intermediate value between all models. In São Paulo, in wintertime, the ensemble has superior metrics (MNBIAS -2%) compared to any individual model, while in the summer the ensemble overestimates the observations as most models do. In México City, the ensemble median performs better than all individual models with MNBIAS between 4% (summer) and 13% (winter) and FGE less than 32%. Similar to the individual models, for most of the cases, the correlation coefficient for the ensemble does not meet any of the benchmarks (Emery et al., 2017).

3.1.3 Carbon monoxide - CO

Observations

The number of stations per city recording CO during January and July of 2015 varies between 7 in Bogotá and 24 in Mexico City (Appendix B). CO levels are generally below 1.0 ppm for all cities (Figure 4). However, in Santiago during winter some values surpass 1.5 ppm due to a combination of adverse meteorological conditions and emissions from the transportation sector and residential combustion, commonly employed for heating in neighboring municipalities (Saide et al., 2016; Gallardo et al., 2012).

There is a slight increase of CO in São Paulo in July with respect to January, due to the atmospheric conditions where lower winds and lower boundary layer increased primary pollutant concentration during winter. Additionally, biomass burning from
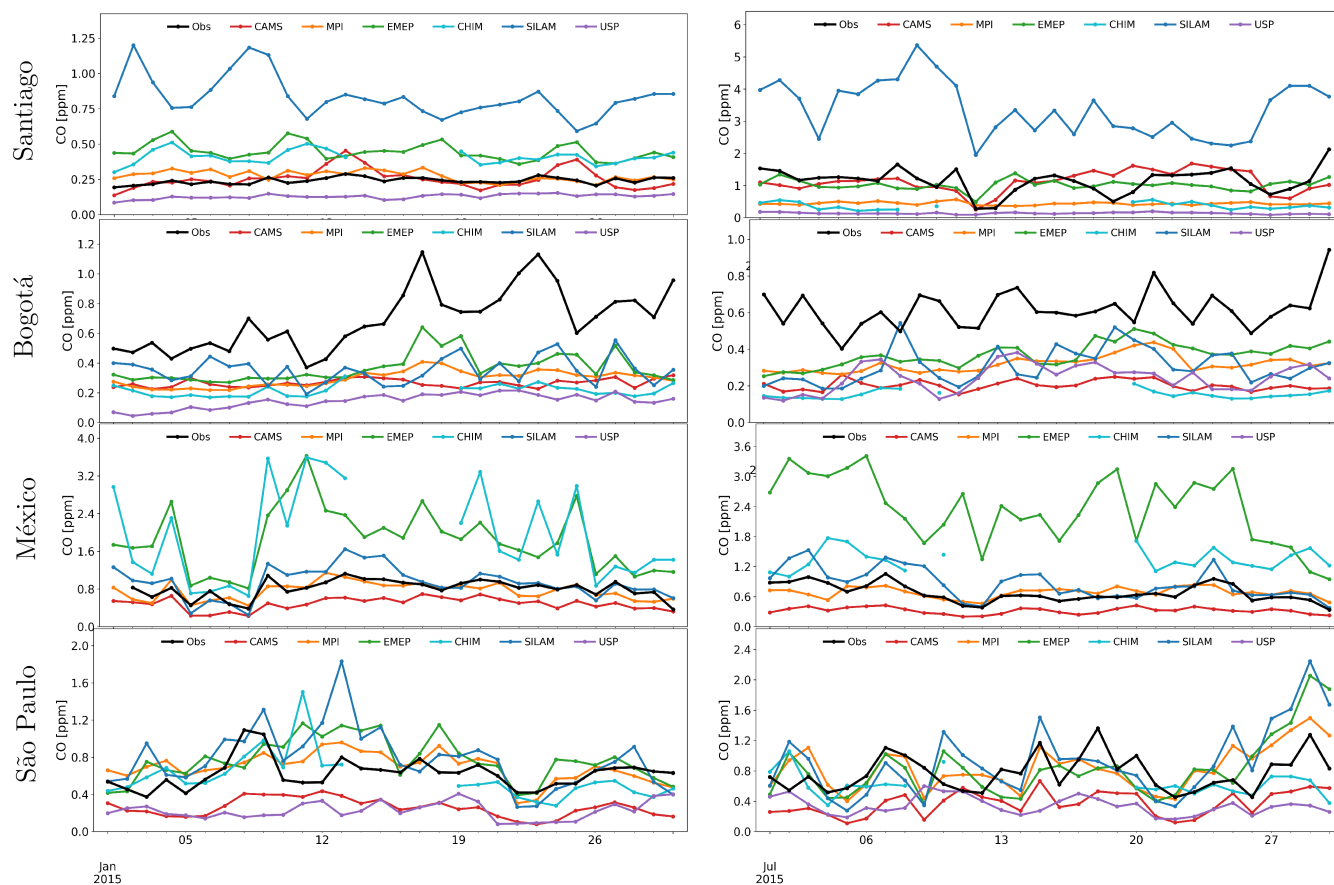
Figure 4. Observed (black) and simulated CO daily mean concentrations in Santiago, (top) Bogotá, México City, São Paulo (bottom) for January (left) and July (right) 2015.

310 wildfires which begin in July and peak in August and September for the southern part of the Amazon rainforest can bring more CO (Marlier et al., 2020). Likewise, larger CO concentrations in Bogotá in January are part of the wildfire season in northern South America lasting from the end of December until April (Mendez-Espinosa et al., 2019).

Model performance

315 Santiago records the largest simulated value of CO in winter with peak of 5.0 ppm (Figure 4). The second largest values are observed in Mexico City with values around 3.0 ppm. In both cases, model estimates severely overestimate the observations with some NMBIAS larger than 100% (Table A4). São Paulo displays intermediate values with an average CO of 0.5ppm, and Bogotá has the lowest modeled values with an average of 0.27 ppm.

CO simulations in Santiago, São Paulo, and México City, are both over and underpredicting observations (Figure 4). How-
320 ever, in Santiago in winter only the SILAM model overpredicts CO values (MNBIAS 98%), the other models underpredict

(MNBIAS between -152 and -1%). This situation could be explained by emissions, synoptic or the models' simulation of the boundary layer (Mazzeo et al., 2018). In Bogotá, all models consistently underestimate the CO with MNBIAS between -50 and -131% (Table A4). In January correlation coefficients for CO hover around 0.6 achieving benchmarks (R > 0.4) (Zhai et al., 2024). This result demonstrates the model's capability to reproduce the time variability of this pollutant in Bogotá, even if the levels are under or overestimated. The same situation is observed in Mexico City and São Paulo, where goal (R>0.6) and criteria (R>0.4) benchmarks are often achieved (Zhai et al., 2024).

The underestimation in Bogotá is similar to that observed for NO_2, which we attributed to a shortfall in emissions. According to the local inventory, CO emissions are predominantly attributed to mobile sources (99%), with motorcycles contributing to 45% of these emissions, automobiles accounting for 36%, and the remainder originating from other vehicles (SDA -Secretaria Distrital de Ambiente, 2018). Notably, it has been identified that motorcycle emissions are underestimated in Colombia (Rojas et al., 2023). The significant rise in the number of motorcycles in the country and their declining condition is not accurately reflected in global emission inventories, such as EDGAR 6.1.

Observed CO mixing ratios are also underestimated in cities such as Medellin, Guadalajara, Quito, and Lima (Figure 8), which might be explained by the coarse resolution of the model not capturing the local characteristics. It's possible that issues with CO emissions in global inventories or excess of OH radicals in photochemistry also contribute to this trend. In addition, a major source of atmospheric CO is the oxidation of BVOCs (Worden et al., 2019), which are significantly underestimated in the Southern Hemisphere (Zeng et al., 2015).

In São Paulo, five out of six models slightly underestimate CO with a relatively high correlation coefficient. The simulated concentrations for daily values range from 0.1 to 2.0 ppm, similar to that found in other studies (Deroubaix et al., 2024). Nevertheless, concentrations exceeding 1.2 ppm are simulated only for certain days (Jan. 13 and July. 30) and are probably due to wood burning (Figure C1).

Model intercomparison

Global models, particularly CAMS, tend to underestimate CO levels in Bogotá, São Paulo, and México City with MNBIAS < -50%. In Santiago, CAMS adequately simulates CO levels with MNBIAS (< ± 2.5%) and FGE (<25%). The correlation coefficient achieves the criteria benchmark (R > 0.4) proposed by (Zhai et al., 2024). SILAM underestimates CO in Bogotá (Model/Observations ~0.6) and overestimates it in Santiago, while it performs relatively well in São Paulo and México City (MNBIAS < 22%) and correlation coefficients meeting the criteria and goal benchmarks (R > 0.4 and R>0.6) proposed by (Zhai et al., 2024).

When it comes to regional models, WRF-USP consistently underestimates CO levels with large bias (MNBIAS < -60%) and errors (FGE > 60%). WRF-MPI has better performance especially in São Paulo and Mexico City (MNBIAS < ± 15%) and correlation coefficients within the goal benchmark (Zhai et al., 2024). EMEP and CHIMERE largely overestimate observations in México City while in São Paulo they closely match observations. In Santiago, these models tend to overpredict CO in the summer and underpredict it during the winter.

The largest model variation is observed in Santiago during wintertime with a range of 3.2 ppm and C.V. of 106% (Table A8). México City also shows large variation in summer (C.V. 72%) and winter (C.V. 56%). Bogotá and São Paulo present less

variation between model results.

Ensemble performance

In winter in Santiago and Bogotá in both periods the ensemble follows the underestimation pattern of all models (Table A4). In São Paulo there are models with better performance than the ensemble, but the ensemble results are reasonable with MNBIAS close to -15% and R approximately 0.7. In México City, the overestimation of CO by the EMEP and CHIMERE models (MNBIAS > 60%) is reduced in the ensemble (MNBIAS ~15%).

3.1.4 Sulfur dioxide - SO_2

Observations

The number of stations per city recording SO_2 during January and July of 2015 varies between 4 in Santiago and 26 in Mexico City (Appendix B). The largest concentration of SO_2 is observed in México City with values between 3.0 ppb (January) and 4.4 ppb (July) due to volcanic emissions (de Foy et al., 2009) and the heavy consumption of coal in power generation and cement production, especially in the proximity of the "Tula-Vito-Apasco" industrial area (SEMARNAT and INECC, 2020). On the other hand, SO_2 in Bogotá, Santiago and São Paulo are lower with concentrations ranging from 1.0 to 1.8 ppb (Figure 5).

Model performance

The largest simulation is shown in México City with an average of 45 ppb SO_2, followed by São Paulo, with a mean concentration of 8.5 ppb. In Santiago, the average SO2 value is 8.5ppb. The lowest modeled values are found in Bogotá with an average of 0.97ppb (Table A5).

The models' simulated SO_2 exhibits significant discrepancies when compared to the observations, with severe overestimation in Santiago, México City, and São Paulo (Figure 5), with MNBIAS reaching up to 190% and FGE up to 200% (Table A5). On the contrary, for Bogotá the predicted SO_2 values are in reasonable alignment with the observations, except for the WRF-Chem USP simulation, which drastically underestimates SO_2 (MNBIAS -200%) (Table A5).

The overestimation of SO_2 levels could stem from issues within global emission inventories. In fact, an overestimation of SO_2 emissions in CAMS was observed for Buenos Aires and Santiago when compared to the PAPILA inventory (Castesana et al., 2022). These emissions primarily originate from the energy and industrial sectors, where the sulfur content in coal appears to be significantly contributing to this overestimation.

The good performance in Bogotá might be related to less SO_2 emissions apportioned in the city. In fact, the vast majority of SO_2 emissions (~90%) in Colombia originate from the industrial and energy production sectors (IDEAM, 2020). However, these facilities are typically located outside major urban areas. Bogotá contributes only 1.5% of the total national SO_2 emissions (de Ambiente, 2018).

Model intercomparison

CAMS and SILAM severely overestimate SO_2 in México City, São Paulo and Santiago with MNBIAS and FGE larger than 100%. In Bogotá, both global models underestimate SO_2 concentrations (MNBIAS from -56 to -80%) but with lower FGE (< 80%) than CAMS. In January, correlation coefficients met the criteria benchmark (R > 0.35) suggested by (Zhai et al., 2024).
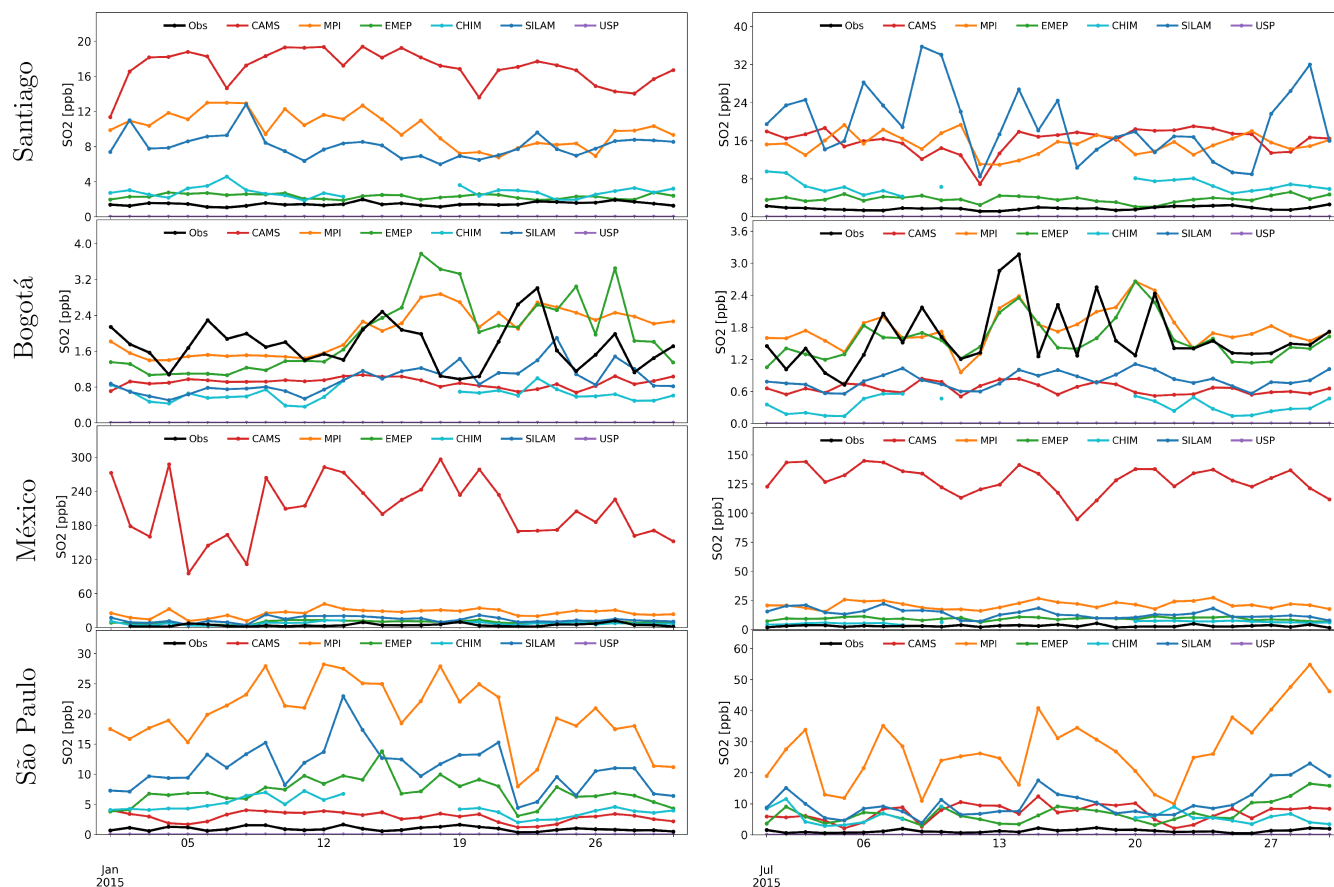
Figure 5. Observed (black) and simulated SO$_2$ daily mean concentrations in Santiago, (top) Bogotá, México City, São Paulo (bottom) for January (left) and July (right) 2015

The performance of regional models for SO$_2$ is quite diverse. WRF-USP severely underestimates SO$_2$ in all cities (MNBIAS close to -200%). In Santiago, México City and São Paulo the models overestimate SO$_2$ in a similar fashion than global models. In Bogotá, EMEP and WRF-MPI show the lowest MNBIAS (< 16%).

The largest model variation for SO$_2$ is found in México City where the range of models is 200 ppb, and the C.V. is larger than 150% (Table A8). In Santiago and São Paulo, the model variation is close to C.V. 95%. In Bogotá, the variation is the lowest (C.V. ∼75%).

Ensemble performance

In México City, Santiago and São Paulo, SO$_2$ is overestimated by all models, except USP. Therefore, the median ensemble also overestimates SO$_2$ concentration and does not represent any improvement in the evaluation metrics (Table A5). In Bogotá, the ensemble tends to underestimate the concentrations (MNBIAS ∼ -55%) to a lesser extent than individual models.

3.1.5 Fine particulate matter - PM$_{2.5}$

Observations

The number of stations per city recording PM$_{2.5}$ during January and July of 2015 varies between 9 in Bogotá and 16 in Mexico City (Appendix B). The largest PM$_{2.5}$ concentrations are found in Santiago during the southern hemispheric winter with daily values around 56 μgm^{-3}. This can be attributed to adverse meteorological conditions and emissions from transportation and residential combustion in the surrounding municipalities (Mazzeo et al., 2018; Saide et al., 2016). The second largest values are shown in México City with an average of 23 μgm^{-3} due to local emission sources. In São Paulo, PM$_{2.5}$ levels are larger in July (19 μgm^{-3}) than January (16 μgm^{-3}), due to the impact of wildfires from the Amazon basis and sugarcane burning (de Fatima Andrade et al., 2017). In Bogotá, PM$_{2.5}$ concentrations are the lowest in July (13 μgm^{-3}) due to the influence of the trade winds (Pachón et al., 2018) but with larger values in January (19 μgm^{-3}) due to biomass burning events and frequent thermal inversions (Ramírez et al., 2018).

Model performance

In Santiago in wintertime, the mean of the models is larger than observation whereas in summer the simulations are mostly below observations. In Mexico City, simulated values are approximately double the observations. In São Paulo, PM$_{2.5}$ is under and overpredicted by the models. In Bogotá, most of the simulations are below the observations (Figure 6).

In Santiago, Bogotá, and México City, models over and underpredict PM$_{2.5}$ (Table A6). In São Paulo, overestimation is observed in all models with exception WRF-USP and may be linked to an excess of fire emissions, as suggested by other studies (Deroubaix et al., 2024). The MNBIAS vary from 39% to 120% except for WRF-USP whose MNBIAS is negative (Table A6). The correlation coefficients for PM$_{2.5}$ are in some cases larger than the goal (R > 0.7) or criteria (R > 0.4) benchmarks proposed by (Emery et al., 2017). It's worth noting the case of México City in January and São Paulo in July, where most models achieve the goal metric. In smaller urban areas like Medellin, Lima, and Quito (Figure 8), most models tend to underestimate observations, potentially due to the coarse resolution of the models.

Hourly simulations of PM$_{2.5}$ are useful to understand the discrepancies between model and observations. In Figure C2, we show the hourly data and model outputs. In São Paulo, the highest PM$_{2.5}$ concentrations are simulated by SILAM in January 13 (> 320 μgm^{-3}) and July 30 (> 400 μgm^{-3}), which corresponds to days with high simulated CO values as well (Figure C1) and may indicate an overestimation of biomass burning by the IS4FIRES module in SILAM. From Jan 15 to 30 there is also an excess of PM$_{2.5}$ from SILAM.

In México City, the highest PM$_{2.5}$ concentrations are simulated by the CAMS model with about 250 μgm^{-3} in January and 160 μgm^{-3} in July (Figure C3) which are severely overestimated. The large PM$_{2.5}$ values are distributed in the whole period rather than specific days and do not correspond with high CO concentrations to suspect the influence of fires. This situation might indicate a local and continuous source of PM$_{2.5}$.

Model intercomparison

Both global models consistently overestimate PM$_{2.5}$ in Santiago, São Paulo and México City, but they behave differently in Bogotá. In Mexico City, CAMS has a greater overestimation than SILAM but in São Paulo and Santiago SILAM values are
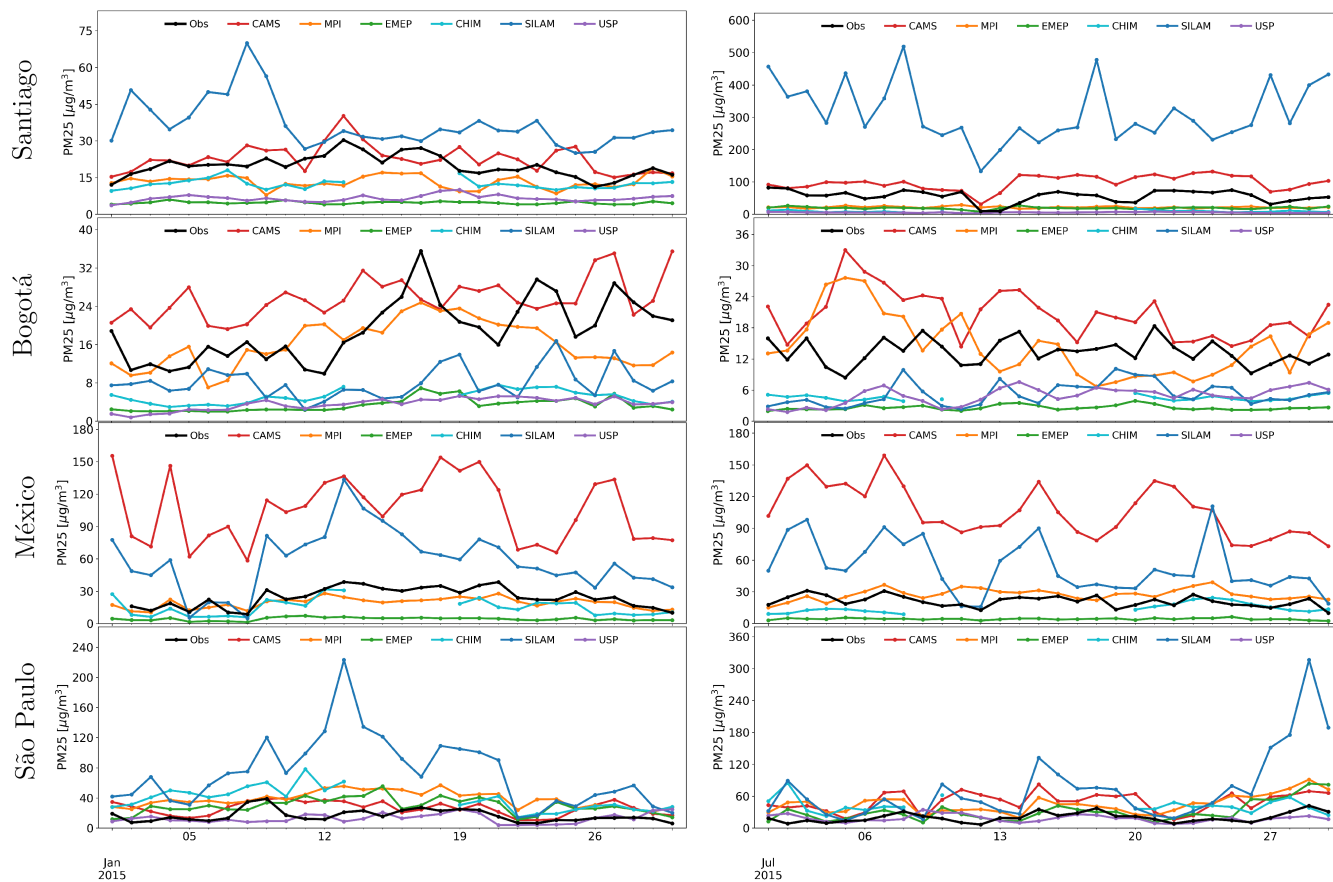
Figure 6. Observed (black) and simulated PM$_{2.5}$ daily mean concentrations in Santiago, (top) Bogotá, México City, São Paulo (bottom) for January (left) and July (right) 2015.

larger (Figure 6). In Bogotá, CAMS overestimates PM$_{2.5}$ (MNBIAS ≈ 37%) whereas SILAM underestimates it (MNBIAS
435   -85%). SILAM correlation coefficient meets the criteria benchmark suggested by (Emery et al., 2017).

Among the regional models, EMEP shows the largest underestimation (MNBIAS < -110%) in all cites, except in São Paulo where the model overestimates PM2.5, but within the criteria benchmark (MNBIAS < ±60%) (Boylan and Russell, 2006) and with a correlation coefficient (R >0.4) that meets the criteria benchmark by (Emery et al., 2017) in July (Table A6). WRF-USP heavily underestimates in Bogotá and Santiago, but performs well in São Paulo with the lowest errors. This difference
440   in behavior might be explained by a good adaptation of the model's inputs to the city. The WRF-MPI model meets goal benchmarks for MNBIAS and FGE in Bogotá and México City.

The largest model variation is observed in México City and Santiago during wintertime with a C.V. greater than 100% (Table A8). Santiago in summer and Bogotá present intermediate values (C.V. 70 to 80%), whereas São Paulo shows the least variability between models (C.V. < 56%).

 Ensemble performance

Considering the large underestimation of most models in Bogotá and Santiago the ensemble displays less bias and errors than some of the individual models (Table A6). In Mexico City, the ensemble outperforms models with a MNBIAS of -5% in January and +30% in July, achieving the goal benchmark suggested by (Boylan and Russell, 2006), as well as the correlation coefficient (R>0.8) in January. For São Paulo, all models tend to overestimate $PM_{2.5}$, so it follows that the ensemble presents the same behavior with MNBIAS > 67%. The correlation coefficient meets the criteria benchmark (R>0.4) in both periods (Emery et al., 2017).

3.2 Spatial seasonal variability of predictions

For all pollutants, models and periods, maps of mean concentrations were constructed to visualize the spatial differences (Appendix D). In order to summarize the results, other spatial plots were also prepared: median ensemble (Figure 7), median absolute deviation (Figure E1), mean standard deviation (Figure E2). In Figure 7, pollution hot spots are clearly visible around major urban areas, in particular, São Paulo in the southeastern coast and México City in the northwestern part of the continent. São Paulo and México City each cover a significant area, of approximately 3600 km^2, spanning at least nine modeling cells (400 km^2 each). This extensive coverage offers some spatial representation of the physical and chemical atmospheric processes. Other regions highlighted on the maps include Lima and Santiago on the Pacific coast, Buenos Aires along the southern shore of the Río de la Plata, and cities in the northern part of South America like Quito, Bogotá, Medellín, and Caracas. However, most of these cities are encompassed by six or fewer modeling cells, limiting the potential for significant spatial variation.

The temporal seasonality can also be observed in Figure 7. The left and right panels show results for January and July, corresponding to the southern hemisphere summer and winter respectively. For SO_2, major hot spots appear in México City, São Paulo and surrounding areas, and the Pacific coast in Chile. The SO_2 concentrations are associated with with volcanic emissions and the use of coal in power generation, cement production and copper smelting that are active in both summer and winter (Huneeus et al., 2006; SEMARNAT and INECC, 2020). Similarly, NO_2 hotspots are common in major urban areas due to transportation emissions.

In January, the median ensemble shows high concentrations of PM_{10} in several areas. In the south of Argentina, the concentrations are primarily due to dust from the Patagonia desertic areas (Gassó and Torres, 2019). In the north of Brazil and the Guianas, increased PM_{10} levels are most likely associated with fires in the Orinoco basin during the dry season (Hernandez et al., 2019). In a similar manner, $PM_{2.5}$ concentrations show an increase in the northern part of Brazil due to biomass burning. Large concentrations of $PM_{2.5}$ in São Paulo in both January and July are probably caused by overestimation of fires, as previously discussed.

During the austral summer, the southeastern part of Brazil (including São Paulo) displays large concentrations of ozone that were simulated mainly by the regional models WRF-Chem, EMEP and the global SILAM (Figure D3). Several studies have shown the influence of urban plumes of NO_2 into the Amazon rainforest, rich in BVOCs, with the consequent generation of ozone (Rafee et al., 2017; Nascimento et al., 2022). In January, simulated O_3 concentrations are also large in Mexico City during winter, a situation that has been observed in other studies (Barrett and Raga, 2016). There is a maximum of CO in the
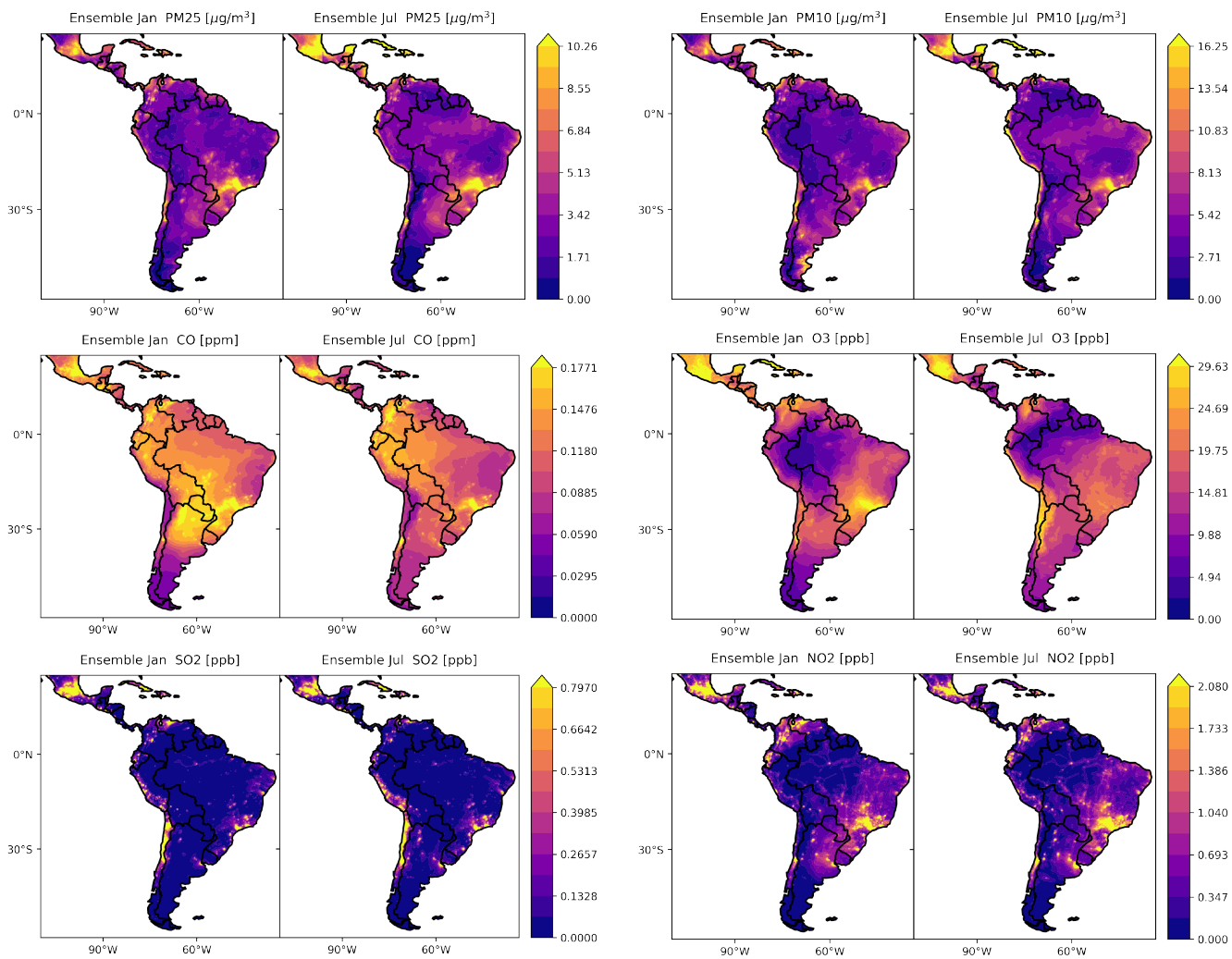
Figure 7. Spatial variability of simulated PM_{10}, $PM_{2.5}$, O_3, CO in LAC for January and July 2015 (based on the median of the models)

area between north of Argentina, south of Bolivia, Paraguay and south of Brazil, probably related to fires and the abundance of BVOCs.

In July, during the austral winter, concentrations of CO, $PM_{2.5}$ and PM_{10} are significant in Santiago due to transportation and residential heating emissions under adverse meteorological conditions. PM_{10} concentrations are large in the Caribbean and central México, primarily due to the transport of Saharan dust into these urban areas (Kramer and Kirtman, 2021; Ramírez-Romero et al., 2021). Similarly, along the Pacific coast between Chile and Peru, increased PM_{10} is probably explained by anthropogenic emissions of copper smelters in connection with strong eastern wind events (Huneeus et al., 2006). Large concentrations of O_3 are visible in México City associated with clear skies under high-pressure atmospheric conditions (Barrett and Raga, 2016). Elevated O_3 values in the Andes mountains between northern Chile and central Peru might be explained by the abundance of VOCs from metropolitan regions and industrial zones (Seguel et al., 2020).

The median absolute deviation maps (Figure E1) and the standard deviation maps (Figure E2), display spatial differences between model simulations. In particular, for particulate matter (PM_{10} and $PM_{2.5}$) notorious dissimilarity is observed in northern Brazil in January, Venezuela in July, and the south of Argentina in both periods. The reason for this disagreement is the simulation of the WRF-MPI model, which contributes with significant PM mass in the mentioned zones, probably due to an overestimation of fires in the northern part of the continent and dust in the southern areas. In July, CO showed large differences in the Colombian and Peruvian Amazon, mostly driven by the EMEP model. This situation might be related to an incorrect estimation of BVOCs emissions as precursors of CO in forested areas. The inadequate simulation of NO_2 by the CAMS model, explained in section 3.1.1, is the cause of the large standard deviation of model results for this pollutant.

3.3 Large versus small urban areas

The coarse resolution used in the modeling systems ($0.2°$x $0.2°$) poses challenges in adequately representing the intricate topography and diverse meteorological conditions of the different cities in LAC. Capturing these physical phenomena can be very difficult and requires a finer scale with much greater computational demand. In the last years, emission inventories for LAC at high spatial and temporal resolution have been constructed (Castesana et al., 2022; Alamos et al., 2022; Puliafito et al., 2015, 2017; Rojas et al., 2023) and it's expected they will complement existing global emission inventories at coarse resolution. We observe that, in large urban areas (> 3500 km^2) the models tend in general to have lower and positive MNBIAS compared to medium size ($600 <$ area < 3600 km^2) or small (area <600 km^2) cities (Figure 8). For example, for México City and São Paulo, the two largest cities in LAC, the mean of the models show the lowest MNBIAS and FGE for CO (-27% to 29%) and NO_2 (-6% to 6%), while in other cities they display larger and negative MNBIAS and FGE (Table A2 and A4). The discrepancies in NO_2 have a corresponding impact in the overestimation of O_3. For particulate matter, a similar pattern is observed, with positive MNBIAS for larger urban areas and negative MNBIAS for medium and small cities. High-resolution simulations are necessary to resolve the spatial variation, but unfortunately global models at high performance are scarce in the Southern Hemisphere (Zhang et al., 2023).

Although the size of cities can influence the performance of the models at coarse resolution, other challenging features for models exist. For instance, Bogotá and Santiago have several challenges in terms of topography and meteorology (Mazzeo
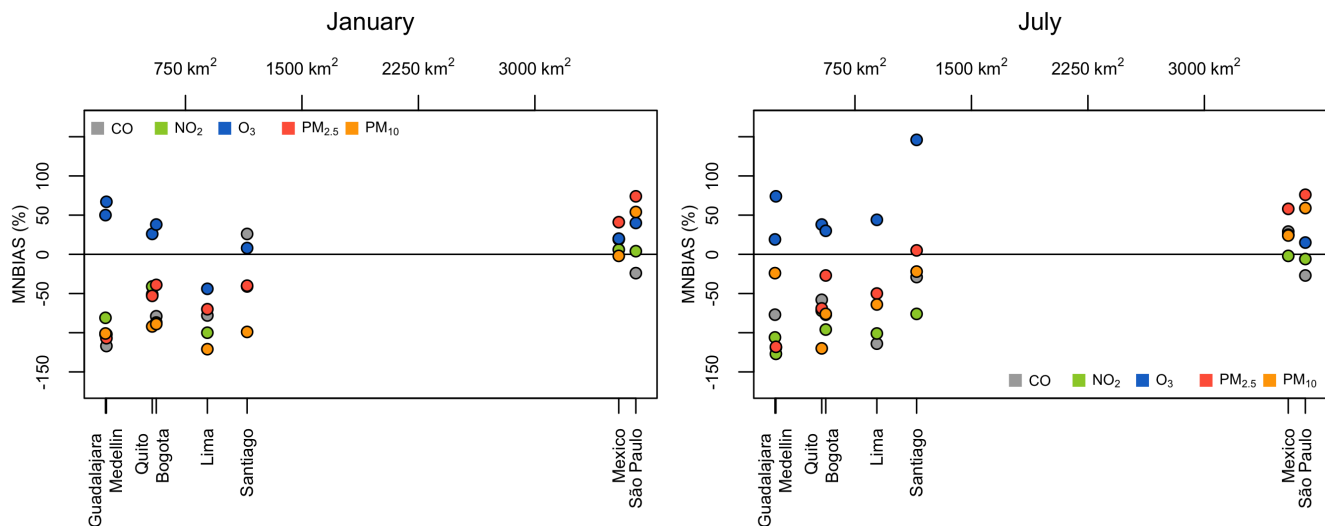
Figure 8. MNBIAS estimated for large and small urban areas.

et al., 2018; Nedbor-Gross et al., 2017; Reboredo et al., 2015) and local emissions not always accounted in global inventories (Castesana et al., 2022; Huneeus et al., 2020; Osses et al., 2022; Rojas et al., 2023). Ideally, we would have access to more

515 cities of various sizes to make this determination with more certainty, unfortunately, local measured data was only available for the cities we considered.

4   Conclusions and future developments

This study performed the first inter-comparison and model evaluation effort in Latin America with the idea to develop an AQF system that can inform the public about air pollution episodes and support policy actions. Despite the limitations of air quality

520 and emissions data, as well as computing resources, the scientific community in Latin America, with international support, has achieved significant progress in air quality modeling and in understanding the fate and transport of pollutants in the region. For instance, the impact of Saharan dust, biomass burning from the Orinoco and the Amazon basis, biogenic VOCs of the Amazon rainforest, are becoming better understood through modeling.

Several challenges still exist. In addition to the intricate topography and diverse meteorological conditions, limitations are

525 found in anthropogenic, volcanic and biogenic emissions, spatial and temporal profiles, land use and vegetation types, as well as other data that are relevant for the calculation of wildfire emissions. This last source is crucial in the region under a climate change scenario, for which adequate parametrization of biomass burning is necessary. The boundary conditions of the models can be improved, which are especially important for long-lived species. The experience of local researchers who have been implementing air quality models for several years can greatly benefit international efforts such as global emissions inventories

530 and the recently-launched WMO GAFIS initiative.

At this first stage of development, interesting and insightful findings were identified for the region. Despite the fact that some of the models were still in an early phase for regional implementation, most models could adequately reproduce air quality observations with the best performance observed for nitrogen dioxide in México City and São Paulo. These enormous urban areas (> 3500 km^2) outperformed Bogotá and Santiago, which are cities between 500 and 1000 km^2. This suggests an accurate portrayal of the temporal and spatial variability in large cities with the current model resolution (0.2°x 0.2°) and the need for a finer model domain in smaller cities that could capture circulation and emission features. At the moment, high-resolution global simulations in the Global South remain rare.

The ensemble median was evaluated on its potential to outperform individual models. In certain periods and cities, the ensemble performed better than any individual models, for example, when the errors of the models compensate for each other, but not when the errors are recurring in all the models. The results varied per city, pollutant and period. Before defining whether the ensemble is the correct approximation for an AQF system, more research is necessary. This work only looked at two months (one in summer and one in winter), a thorough analysis of one entire annual cycle with sufficient spin-up time should be conducted. More observations should also be included for model calibration and evaluation. For 2015, only eight cities in LAC had data that complied with quality and completeness criteria. In recent years, more AQ networks have been implemented and data is more publicly available.

Code and data availability. All model data analyzed in the intercomparison is archived at https://zenodo.org/records/13151018. The tool to create the plots, MOSPAT, can be found in GitHub at https://github.com/NeoMOSPAT/NeoMOSPAT_PAPILA.git.

Author contributions. JE and MO performed the formal analysis of the data; PL, NH, IB, JF, LM, CM, MG, MS, RK, JP, AU, AD, and DS performed the model simulations; JE, MO, PL, NH, and IB prepared the manuscript with contributions from all co-authors; GB and LG provided the financial support for the project leading to this publication; LD, NR, NH, MA coordinated research activities; CL provided technical support; all co-authors reviewed and edited the manuscript.

Competing interests. The authors declare that they have no conflict of interest.

Acknowledgements. The PAPILA (Prediction of Air Pollutants in Latin America) project was funded by the European Commission under the MSCA action for research and innovation staff exchange, Grant agreement ID: 777544. Support of Academy of Finland HEATCOST and ACCC flagship projects (grants Nbr 334798 and 337552), and H2020 project AQ-Watch (grant Nbr 870301) is acknowledged. Support from the German Climate Computer Center (Deutsches Klimarechenzentrum, DKRZ) is acknowledged. Support from the Center for Climate and Resilience Research (FONDAP/ANID 1523A0002) is acknowledged.

References

Alamos, N., Huneeus, N., Opazo, M., Osses, M., Puja, S., Pantoja, N., van der Gon, H. D., Schueftan, A., Reyes, R., and Calvo, R.: High-resolution inventory of atmospheric emissions from transport, industrial, energy, mining and residential activities in Chile, Earth Syst. Sci. Data, 14, 361–379, https://doi.org/10.5194/essd-14-361-2022, 2022.

Albuquerque, T. T., West, J., de F. Andrade, M., Ynoue, R. Y., Andreão, W. L., dos Santos, F. S., Maciel, F. M., Pedruzzi, R., de O. Mateus, V., Martins, J. A., Martins, L. D., Nascimento, E. G. S., and Moreira, D. M.: Analysis of PM2.5 concentrations under pollutant emission control strategies in the metropolitan area of São Paulo, Brazil, Environmental Science and Pollution Research, 26, 33 216–33 227, https://doi.org/10.1007/s11356-019-06447-6, 2019.

Alfaro, S. C. and Gomes, L.: Modeling mineral aerosol production by wind erosion: Emission intensities and aerosol size distributions in source areas, Journal of Geophysical Research: Atmospheres, 106, 18 075–18 084, https://doi.org/https://doi.org/10.1029/2000JD900339, 2001.

Andersson, C., Bergström, R., Bennet, C., Robertson, L., Thomas, M., Korhonen, H., Lehtinen, K. E. J., and Kokkola, H.: MATCH-SALSA – Multi-scale Atmospheric Transport and CHemistry model coupled to the SALSA aerosol microphysics model – Part 1: Model description and evaluation, Geoscientific Model Development, 8, 171–189, https://doi.org/10.5194/gmd-8-171-2015, 2015.

Andersson-Sköld, Y. and Simpson, D.: Comparison of the chemical schemes of the EMEP MSC-W and IVL photochemical trajectory models, Atmospheric Environment, 33, 1111–1129, https://doi.org/https://doi.org/10.1016/S1352-2310(98)00296-9, 1999.

Ballesteros-González, K., Sullivan, A. P., and Morales-Betancourt, R.: Estimating the air quality and health impacts of biomass burning in northern South America using a chemical transport model, Science of The Total Environment, 739, 139 755, https://doi.org/https://doi.org/10.1016/j.scitotenv.2020.139755, 2020.

Ballesteros-González, K., Espitia-Cano, S. O., Rincón-Caro, M. A., Rincón-Riveros, J. M., Perez-Peña, M. P., Sullivan, A., and Betancourt, R. M.: Understanding organic aerosols in Bogotá, Colombia: In-situ observations and regional-scale modeling, Atmospheric Environment, 284, 119 161, https://doi.org/https://doi.org/10.1016/j.atmosenv.2022.119161, 2022.

Barrett, B. S. and Raga, G. B.: Variability of winter and summer surface ozone in Mexico City on the intraseasonal timescale, Atmos. Chem. Phys., 16, 15 359–15 370, https://doi.org/10.5194/acp-16-15359-2016, 2016.

Binkowski, F. S. and Shankar, U.: The Regional Particulate Matter Model: 1. Model description and preliminary results, Journal of Geophysical Research: Atmospheres, 100, 26 191–26 209, https://doi.org/https://doi.org/10.1029/95JD02093, 1995.

Blechschmidt, A.-M., Arteta, J., Coman, A., Curier, L., Eskes, H., Foret, G., Gielen, C., Hendrick, F., Marécal, V., Meleux, F., Parmentier, J., Peters, E., Pinardi, G., Piters, A. J. M., Plu, M., Richter, A., Segers, A., Sofiev, M., Valdebenito, M., Roozendael, M. V., Vira, J., Vlemmix, T., and Burrows, J. P.: Comparison of tropospheric NO2 columns from MAX-DOAS retrievals and regional air quality model simulations, Atmos. Chem. Phys., 20, 2795–2823, https://doi.org/10.5194/acp-20-2795-2020, 2020.

Bouarar, I., Brasseur, G., Petersen, K., Granier, C., Fan, Q., Wang, X., Wang, L., Ji, D., Liu, Z., Xie, Y., Gao, W., and Elguindi, N.: Influence of anthropogenic emission inventories on simulations of air quality in China during winter and summer 2010, Atmospheric Environment, 198, 236–256, https://doi.org/https://doi.org/10.1016/j.atmosenv.2018.10.043, 2019.

Boylan, J. W. and Russell, A. G.: PM and light extinction model performance metrics, goals, and criteria for three-dimensional air quality models, Atmospheric Environment, 40, 4946–4959, https://doi.org/https://doi.org/10.1016/j.atmosenv.2005.09.087, 2006.

Brasseur, G. P., Xie, Y., Petersen, A. K., Bouarar, I., Flemming, J., Gauss, M., Jiang, F., Kouznetsov, R., Kranenburg, R., Mijling, B., Peuch, V.-H., Pommier, M., Segers, A., Sofiev, M., Timmermans, R., van der A, R., Walters, S., Xu, J., and Zhou, G.: Ensemble forecasts

595 of air quality in eastern China – Part 1: Model description and implementation of the MarcoPolo–Panda prediction system, version 1, Geoscientific Model Development, 12, 33–67, https://doi.org/10.5194/gmd-12-33-2019, 2019.

Buchholz, R. R., Emmons, L. K., Tilmes, S., and Team, T. C. D.: CESM2.1/CAM-chem Instantaneous Output for Boundary Conditions, 2019.

Busch, P., Cifuentes, L. A., and Cabrera, C.: Chronic exposure to fine particles (PM2.5) and mortality: Evidence from Chile, Environmen-
600 tal Epidemiology, 7, https://journals.lww.com/environepidem/fulltext/2023/08000/chronic_exposure_to_fine_particles__pm2_5__and.3. aspx, 2023.

Casallas, A., Castillo-Camacho, M. P., Sanchez, E. R., González, Y., Celis, N., Mendez-Espinosa, J. F., Belalcazar, L. C., and Ferro, C.: Surface, satellite ozone variations in Northern South America during low anthropogenic emission conditions: a machine learning approach, Air Quality, Atmosphere Health, 16, 745–764, https://doi.org/10.1007/s11869-023-01303-6, 2023.

605 Casallas, A., Cabrera, A., Guevara-Luna, M.-A., Tompkins, A., González, Y., Aranda, J., Belalcazar, L. C., Mogollon-Sotelo, C., Celis, N., Lopez-Barrera, E., Peña-Rincon, C. A., and Ferro, C.: Air pollution analysis in Northwestern South America: A new Lagrangian framework, Science of The Total Environment, 906, 167 350, https://doi.org/https://doi.org/10.1016/j.scitotenv.2023.167350, 2024.

Castesana, P., Resquin, M. D., Huneeus, N., Puliafito, E., Darras, S., Gómez, D., Granier, C., Alvarado, M. O., Rojas, N., and Dawidowski, L.: PAPILA dataset: a regional emission inventory of reactive gases for South America based on the combination of local and global
610 information, Earth System Science Data, 14, 271–293, https://doi.org/10.5194/essd-14-271-2022, 2022.

Chin, M., Ginoux, P., Kinne, S., Torres, O., Holben, B. N., Duncan, B. N., Martin, R. V., Logan, J. A., Higurashi, A., and Nakajima, T.: Tropo-spheric Aerosol Optical Thickness from the GOCART Model and Comparisons with Satellite and Sun Photometer Measurements, Journal of the Atmospheric Sciences, 59, 461–483, https://doi.org/https://doi.org/10.1175/1520-0469(2002)059<0461:TAOTFT>2.0.CO;2, 2002.

Colette, A., Collin, G., and Barré, J.: Update on European Regional Air Quality Forecast in the Copernicus Atmosphere Monitoring Service
615 (CAMS), in: EGU General Assembly Conference Abstracts, p. 3487, https://doi.org/10.5194/egusphere-egu2020-3487, 2020.

de Ambiente, S. S. D.: Inventario de emisiones de Bogotá, Contaminantes atmosféricos año 2018, 2018.

de Fatima Andrade, M., Kumar, P., de Freitas, E. D., Ynoue, R. Y., Martins, J., Martins, L. D., Nogueira, T., Perez-Martinez, P., de Miranda, R. M., Albuquerque, T., Gonçalves, F. L. T., Oyama, B., and Zhang, Y.: Air quality in the megacity of São Paulo: Evolution over the last 30 years and future perspectives, Atmospheric Environment, 159, 66–82, https://doi.org/https://doi.org/10.1016/j.atmosenv.2017.03.051,
620 2017.

de Foy, B., Krotkov, N. A., Bei, N., Herndon, S. C., Huey, L. G., Martínez, A.-P., Ruiz-Suárez, L. G., Wood, E. C., Zavala, M., and Molina, L. T.: Hit from both sides: tracking industrial and volcanic plumes in Mexico City with surface measurements and OMI SO$_2$ retrievals during the MILAGRO field campaign, Atmos. Chem. Phys., 9, 9599–9617, https://doi.org/10.5194/acp-9-9599-2009, 2009.

de la Barrera, F., Barraza, F., Favier, P., Ruiz, V., and Quense, J.: Megafires in Chile 2017: Monitoring mul-
625 tiscale environmental impacts of burned ecosystems, Science of The Total Environment, 637-638, 1526–1536, https://doi.org/https://doi.org/10.1016/j.scitotenv.2018.05.119, 2018.

Deroubaix, A. M., Hoelzemann, J. J., Ynoue, R., Bouarar, I., de Souza Fernandes Duarte, E., Elbern, H., Lichtig, P., Martins, L. D., Évora do Rosário, N. M., Brasseur, G. P., rafaela Cruz Alves, de Arruda Moreira, G., phiipp franke, de Fatima Andrade, M., Lange, A. C., Andreao, W. L., rizzieri Pedruzzi, de Almeida Albuquerque, T. T., and Lugon, L.: Intercomparison of air qual-
630 ity models in a megacity: Towards an operational ensemble forecasting system for São Paulo, JGR Atmospheres, 129, 1–27, https://doi.org/https://doi.org/10.1029/2022JD038179, 2024.

East, J., Montealegre, J. S., Pachon, J. E., and Garcia-Menendez, F.: Air quality modeling to inform pollution mitigation strategies in a Latin American megacity, Science of The Total Environment, 776, 145 894, https://doi.org/https://doi.org/10.1016/j.scitotenv.2021.145894, 2021.

ECCAD: Global Anthropogenic Emissions (CAMS-GLOB-ANT) for the Copernicus Atmosphere Monitoring Service Simulations of Air Quality Forecasts and Reanalyses, https://doi.org/10.24380/eets-qd81, 2020.

ECCAD: Global Biogenic VOC emissions CAMS-GLOB-BIO v3.0 Snapshot, https://doi.org/10.24380/xs64-gj42, 2021.

Emery, C., Liu, Z., Russell, A. G., Odman, M. T., Yarwood, G., and Kumar, N.: Recommendations on statistics and benchmarks to assess photochemical model performance, Journal of the Air Waste Management Association, 67, 582–598, https://doi.org/10.1080/10962247.2016.1265027, 2017.

Emmons, L. K., Walters, S., Hess, P. G., Lamarque, J.-F., Pfister, G. G., Fillmore, D., Granier, C., Guenther, A., Kinnison, D., Laepple, T., Orlando, J., Tie, X., Tyndall, G., Wiedinmyer, C., Baughcum, S. L., and Kloster, S.: Description and evaluation of the Model for Ozone and Related chemical Tracers, version 4 (MOZART-4), Geoscientific Model Development, 3, 43–67, https://doi.org/10.5194/gmd-3-43-2010, 2010.

Fast, J. D., Jr., W. I. G., Easter, R. C., Zaveri, R. A., Barnard, J. C., Chapman, E. G., Grell, G. A., and Peckham, S. E.: Evolution of ozone, particulates, and aerosol direct radiative forcing in the vicinity of Houston using a fully coupled meteorology-chemistry-aerosol model, Journal of Geophysical Research: Atmospheres, 111, https://doi.org/https://doi.org/10.1029/2005JD006721, 2006.

Flemming, J., Huijnen, V., Arteta, J., Bechtold, P., Beljaars, A., Blechschmidt, A.-M., Diamantakis, M., Engelen, R. J., Gaudel, A., Inness, A., Jones, L., Josse, B., Katragkou, E., Marecal, V., Peuch, V.-H., Richter, A., Schultz, M. G., Stein, O., and Tsikerdekis, A.: Tropospheric chemistry in the Integrated Forecasting System of ECMWF, Geoscientific Model Development, 8, 975–1003, https://doi.org/10.5194/gmd-8-975-2015, 2015.

Flemming, J., Benedetti, A., Inness, A., Engelen, R. J., Jones, L., Huijnen, V., Remy, S., Parrington, M., Suttie, M., Bozzo, A., Peuch, V.-H., Akritidis, D., and Katragkou, E.: The CAMS interim Reanalysis of Carbon Monoxide, Ozone and Aerosol for 2003–2015, Atmospheric Chemistry and Physics, 17, 1945–1983, https://doi.org/10.5194/acp-17-1945-2017, 2017.

Franco, J. F., Gidhagen, L., Morales, R., and Behrentz, E.: Towards a better understanding of urban air quality management capabilities in Latin America, Environmental Science Policy, 102, 43–53, https://doi.org/https://doi.org/10.1016/j.envsci.2019.09.011, 2019.

Freitas, S. R., Longo, K. M., Alonso, M. F., Pirre, M., Marecal, V., Grell, G., Stockler, R., Mello, R. F., and Gácita, M. S.: PREP-CHEM-SRC – 1.0: a preprocessor of trace gas and aerosol emission fields for regional and global atmospheric chemistry models, Geosci. Model Dev., 4, 419–433, https://doi.org/10.5194/gmd-4-419-2011, 2011.

Gallardo, L., Olivares, G., Langner, J., and Aarhus, B.: Coastal lows and sulfur air pollution in Central Chile, Atmospheric Environment, 36, 3829–3841, https://doi.org/https://doi.org/10.1016/S1352-2310(02)00285-6, 2002.

Gallardo, L., Escribano, J., Dawidowski, L., Rojas, N., de Fátima Andrade, M., and Osses, M.: Evaluation of vehicle emission inventories for carbon monoxide and nitrogen oxides for Bogotá, Buenos Aires, Santiago, and São Paulo, Atmospheric Environment, 47, 12–19, https://doi.org/https://doi.org/10.1016/j.atmosenv.2011.11.051, 2012.

Gassó, S. and Torres, O.: Temporal Characterization of Dust Activity in the Central Patagonia Desert (Years 1964–2017), Journal of Geophysical Research: Atmospheres, 124, 3417–3434, https://doi.org/https://doi.org/10.1029/2018JD030209, 2019.

Gavidia-Calderón, M., Schuch, D., Vara-Vela, A., Inoue, R., Freitas, E. D., de A Albuquerque, T. T., Zhang, Y., de Fatima Andrade, M., and Bell, M. L.: Air quality modeling in the metropolitan area of São Paulo, Brazil: A review, Atmospheric Environment, 319, 120 301, https://doi.org/https://doi.org/10.1016/j.atmosenv.2023.120301, 2024.

670 Gery, M. W., Whitten, G. Z., Killus, J. P., and Dodge, M. C.: A photochemical kinetics mechanism for urban and regional scale computer modeling, Journal of Geophysical Research: Atmospheres, 94, 12 925–12 956, https://doi.org/https://doi.org/10.1029/JD094iD10p12925, 1989.

Ginoux, P., Chin, M., Tegen, I., Prospero, J. M., Holben, B., Dubovik, O., and Lin, S.-J.: Sources and distributions of dust aerosols simulated with the GOCART model, Journal of Geophysical Research: Atmospheres, 106, 20 255–20 273,

675 https://doi.org/https://doi.org/10.1029/2000JD000053, 2001.

González, C. M., Ynoue, R. Y., Vara-Vela, A., Rojas, N. Y., and Aristizábal, B. H.: High-resolution air quality modeling in a medium-sized city in the tropical Andes: Assessment of local and global emissions in understanding ozone and PM10 dynamics, Atmospheric Pollution Research, 9, 934–948, https://doi.org/10.1016/j.apr.2018.03.003, 2018.

Gouveia, N., Junger, W. L., Romieu, I., Cifuentes, L. A., de Leon, A. P., Vera, J., Strappa, V., Hurtado-Díaz, M., Miranda-Soberanis, V.,

680 Rojas-Bracho, L., Carbajal-Arroyo, L., and Tzintzun-Cervantes, G.: Effects of air pollution on infant and children respiratory mortality in four large Latin-American cities, Environmental Pollution, 232, 385–391, https://doi.org/https://doi.org/10.1016/j.envpol.2017.08.125, 2018.

Granier, C., Bessagnet, B., Bond, T., D'Angiola, A., van der Gon, H. D., Frost, G. J., Heil, A., Kaiser, J. W., Kinne, S., Klimont, Z., Kloster, S., Lamarque, J.-F., Liousse, C., Masui, T., Meleux, F., Mieville, A., Ohara, T., Raut, J.-C., Riahi, K., Schultz, M. G., Smith, S. J.,

685 Thompson, A., van Aardenne, J., van der Werf, G. R., and van Vuuren, D. P.: Evolution of anthropogenic and biomass burning emissions of air pollutants at global and regional scales during the 1980–2010 period, Climatic Change, 109, 163, https://doi.org/10.1007/s10584-011-0154-1, 2011.

Grell, G. A., Peckham, S. E., Schmitz, R., McKeen, S. A., Frost, G., Skamarock, W. C., and Eder, B.: Fully coupled "online" chemistry within the WRF model, Atmospheric Environment, 39, 6957–6975, https://doi.org/https://doi.org/10.1016/j.atmosenv.2005.04.027, 2005.

690 Grewe, V.: Technical Note: A diagnostic for ozone contributions of various NO_x emissions in multi-decadal chemistry-climate model simulations, Atmos. Chem. Phys., 4, 729–736, https://doi.org/10.5194/acp-4-729-2004, 2004.

Guenther, A., Karl, T., Harley, P., Wiedinmyer, C., Palmer, P. I., and Geron, C.: Estimates of global terrestrial isoprene emissions using MEGAN (Model of Emissions of Gases and Aerosols from Nature), Atmospheric Chemistry and Physics, 6, 3181–3210, https://doi.org/10.5194/acp-6-3181-2006, 2006.

695 Hernandez, A. J., Morales-Rincon, L. A., Wu, D., Mallia, D., Lin, J. C., and Jimenez, R.: Transboundary transport of biomass burning aerosols and photochemical pollution in the Orinoco River Basin, Atmospheric Environment, 205, 1–8, https://doi.org/https://doi.org/10.1016/j.atmosenv.2019.01.051, 2019.

Huneeus, N., Gallardo, L., and Rutllant, J. A.: Offshore transport episodes of anthropogenic sulfur in northern Chile: Potential impact on the stratocumulus cloud deck, Geophysical Research Letters, 33, https://doi.org/https://doi.org/10.1029/2006GL026921, 2006.

700 Huneeus, N., van der Gon, H. D., Castesana, P., Menares, C., Granier, C., Granier, L., Alonso, M., de Fatima Andrade, M., Dawidowski, L., Gallardo, L., Gomez, D., Klimont, Z., Janssens-Maenhout, G., Osses, M., Puliafito, E., Rojas, N., Sánchez-Ccoyllo, O., Tolvett, S., and Ynoue, R. Y.: Evaluation of anthropogenic air pollutant emission inventories for South America at national and city scale, Atmospheric Environment, p. 117606, https://doi.org/https://doi.org/10.1016/j.atmosenv.2020.117606, 2020.

IDEAM: Primer inventario indicativo Nacional de emisiones de contaminantes criterio y carbono negro 2010-2014, https://documentacion.

705 ideam.gov.co/openbiblio/bvirtual/023893/1InventarioBLACK.pdf, 2020.

Inness, A., Ades, M., Agustí-Panareda, A., Barré, J., Benedictow, A., Blechschmidt, A.-M., Dominguez, J. J., Engelen, R., Eskes, H., Flemming, J., Huijnen, V., Jones, L., Kipling, Z., Massart, S., Parrington, M., Peuch, V.-H., Razinger, M., Remy, S., Schulz, M., and Suttie,

M.: The CAMS reanalysis of atmospheric composition, Atmos. Chem. Phys., 19, 3515–3556, https://doi.org/10.5194/acp-19-3515-2019, 2019.

710 Kaiser, J. W., Heil, A., Andreae, M. O., Benedetti, A., Chubarova, N., Jones, L., Morcrette, J.-J., Razinger, M., Schultz, M. G., Suttie, M., and van der Werf, G. R.: Biomass burning emissions estimated with a global fire assimilation system based on observed fire radiative power, Biogeosciences, 9, 527–554, https://doi.org/10.5194/bg-9-527-2012, 2012.

Kouznetsov, R. and Sofiev, M.: A methodology for evaluation of vertical dispersion and dry deposition of atmospheric aerosols, Journal of Geophysical Research: Atmospheres, 117, https://doi.org/https://doi.org/10.1029/2011JD016366, 2012.

715 Kramer, S. J. and Kirtman, B. P.: Saharan Dust Transport Predictability Utilizing a Subseasonal Experiment (SubX) Model, Journal of Geophysical Research: Atmospheres, 126, e2020JD033 802, https://doi.org/https://doi.org/10.1029/2020JD033802, 2021.

Kukkonen, J., Olsson, T., Schultz, D. M., Baklanov, A., Klein, T., Miranda, A. I., Monteiro, A., Hirtl, M., Tarvainen, V., Boy, M., Peuch, V.-H., Poupkou, A., Kioutsioukis, I., Finardi, S., Sofiev, M., Sokhi, R., Lehtinen, K. E. J., Karatzas, K., José, R. S., Astitha, M., Kallos, G., Schaap, M., Reimer, E., Jakobs, H., and Eben, K.: A review of operational, regional-scale, chemical weather forecasting models in
720 Europe, Atmos. Chem. Phys., 12, 1–87, https://doi.org/10.5194/acp-12-1-2012, 2012.

Lapere, R.: Modeling the Impacts of Future Emission Scenarios on Air Pollution in Santiago, Chile, pp. 1–44, 2018.

Lapere, R., Menut, L., Mailler, S., and Huneeus, N.: Seasonal variation in atmospheric pollutants transport in central Chile: dynamics and consequences, Atmos. Chem. Phys., 21, 6431–6454, https://doi.org/10.5194/acp-21-6431-2021, 2021.

Longo, K. M., Freitas, S. R., Pirre, M., Marécal, V., Rodrigues, L. F., Panetta, J., Alonso, M. F., Rosário, N. E., Moreira, D. S., Gácita, M. S.,
725 Arteta, J., Fonseca, R., Stockler, R., Katsurayama, D. M., Fazenda, A., and Bela, M.: The Chemistry CATT-BRAMS model (CCATT-BRAMS 4.5): a regional atmospheric model system for integrated air quality and weather forecasting and research, Geosci. Model Dev., 6, 1389–1405, https://doi.org/10.5194/gmd-6-1389-2013, 2013.

Mailler, S., Menut, L., Khvorostyanov, D., Valari, M., Couvidat, F., Siour, G., Turquety, S., Briant, R., Tuccella, P., Bessagnet, B., Colette, A., Létinois, L., Markakis, K., and Meleux, F.: CHIMERE-2017: from urban to hemispheric chemistry-transport modeling, Geosci. Model
730 Dev., 10, 2397–2423, https://doi.org/10.5194/gmd-10-2397-2017, 2017.

Marlier, M. E., Bonilla, E. X., and Mickley, L. J.: How Do Brazilian Fires Affect Air Pollution and Public Health?, GeoHealth, 4, e2020GH000 331, https://doi.org/https://doi.org/10.1029/2020GH000331, 2020.

Martins, L. D., de Castro Vasconcellos, P., de Carvalho, L. R. F., and de Fátima Andrade, M.: Estimated impact of biogenic hydrocarbon emissions on photochemical oxidant formation en São Paulo during two periods of the winters of 1999-2000, Revista Brasileira de
735 Meteorologia, 21, 190–200, 2006.

Marécal, V., Peuch, V.-H., Andersson, C., Andersson, S., Arteta, J., Beekmann, M., Benedictow, A., Bergström, R., Bessagnet, B., Cansado, A., Chéroux, F., Colette, A., Coman, A., Curier, R. L., van der Gon, H. A. C. D., Drouin, A., Elbern, H., Emili, E., Engelen, R. J., Eskes, H. J., Foret, G., Friese, E., Gauss, M., Giannaros, C., Guth, J., Joly, M., Jaumouillé, E., Josse, B., Kadygrov, N., Kaiser, J. W., Krajsek, K., Kuenen, J., Kumar, U., Liora, N., Lopez, E., Malherbe, L., Martinez, I., Melas, D., Meleux, F., Menut, L., Moinat, P., Morales, T., Par-
740 mentier, J., Piacentini, A., Plu, M., Poupkou, A., Queguiner, S., Robertson, L., Rouïl, L., Schaap, M., Segers, A., Sofiev, M., Tarasson, L., Thomas, M., Timmermans, R., Valdebenito, , van Velthoven, P., van Versendaal, R., Vira, J., and Ung, A.: A regional air quality forecasting system over Europe: the MACC-II daily ensemble production, Geosci. Model Dev., 8, 2777–2813, https://doi.org/10.5194/gmd-8-2777-2015, 2015.

Mazzeo, A., Huneeus, N., Ordoñez, C., Orfanoz-Cheuquelaf, A., Menut, L., Mailler, S., Valari, M., van der Gon, H. D., Gallardo, L., Muñoz, R., Donoso, R., Galleguillos, M., Osses, M., and Tolvett, S.: Impact of residential combustion and transport emissions on air pollution in Santiago during winter, Atmospheric Environment, 190, 195–208, https://doi.org/https://doi.org/10.1016/j.atmosenv.2018.06.043, 2018.

Mendez-Espinosa, J. F., Belalcazar, L. C., and Betancourt, R. M.: Regional air quality impact of northern South America biomass burning emissions, Atmospheric Environment, 203, 131–140, https://doi.org/https://doi.org/10.1016/j.atmosenv.2019.01.042, 2019.

Mendez-Espinosa, J. F., Rojas, N. Y., Vargas, J., Pachón, J. E., Belalcazar, L. C., and Ramírez, O.: Air quality variations in Northern South America during the COVID-19 lockdown, Science of The Total Environment, p. 141621, https://doi.org/https://doi.org/10.1016/j.scitotenv.2020.141621, 2020.

Menut, L., Bessagnet, B., Khvorostyanov, D., Beekmann, M., Blond, N., Colette, A., Coll, I., Curci, G., Foret, G., Hodzic, A., Mailler, S., Meleux, F., Monge, J.-L., Pison, I., Siour, G., Turquety, S., Valari, M., Vautard, R., and Vivanco, M. G.: CHIMERE 2013: a model for regional atmospheric composition modelling, Geosci. Model Dev., 6, 981–1028, https://doi.org/10.5194/gmd-6-981-2013, 2013.

Menut, L., Bessagnet, B., Mailler, S., Pennel, R., and Siour, G.: Impact of Lightning NOx Emissions on Atmospheric Composition and Meteorology in Africa and Europe, Atmosphere, 11, https://doi.org/10.3390/atmos11101128, 2020.

Menut, L., Bessagnet, B., Briant, R., Cholakian, A., Couvidat, F., Mailler, S., Pennel, R., Siour, G., Tuccella, P., Turquety, S., and Valari, M.: The CHIMERE v2020r1 online chemistry-transport model, Geoscientific Model Development, 14, 6781–6811, https://doi.org/10.5194/gmd-14-6781-2021, 2021.

METEO-FRANCE: CAMS Regional air quality production systems, https://atmosphere.copernicus.eu/sites/default/files/2020-09/CAMS50_2018SC2_D2.0.2-U2_Models_documentation_202003_v2.pdf, 2020.

Molina, L. T., Gallardo, L., Andrade, M., Baumgardner, D., Borbor-Córdova, M., Bórquez, R., Casassa, G., Cereceda-Balic, F., Dawidowski, L., Garreaud, R., Huneeus, N., Lambert, F., McCarty, J. L., Phee, J. M., Mena-Carrasco, M., Raga, G. B., Schmitt, C., and Schwarz, J. P.: Pollution and its Impacts on the South American Cryosphere, Earth's Future, 3, 345–369, https://doi.org/https://doi.org/10.1002/2015EF000311, 2015.

Monahan, E. C.: The Ocean as a Source for Atmospheric Particles, pp. 129–163, Springer Netherlands, https://doi.org/10.1007/978-94-009-4738-2_6, 1986.

Morcrette, J.-J., Boucher, O., Jones, L., Salmond, D., Bechtold, P., Beljaars, A., Benedetti, A., Bonet, A., Kaiser, J. W., Razinger, M., Schulz, M., Serrar, S., Simmons, A. J., Sofiev, M., Suttie, M., Tompkins, A. M., and Untch, A.: Aerosol analysis and forecast in the European Centre for Medium-Range Weather Forecasts Integrated Forecast System: Forward modeling, Journal of Geophysical Research: Atmospheres, 114, https://doi.org/https://doi.org/10.1029/2008JD011235, 2009.

Nascimento, J. P., Barbosa, H. M. J., Banducci, A. L., Rizzo, L. V., Vara-Vela, A. L., Meller, B. B., Gomes, H., Cezar, A., Franco, M. A., Ponczek, M., Wolff, S., Bela, M. M., and Artaxo, P.: Major Regional-Scale Production of O3 and Secondary Organic Aerosol in Remote Amazon Regions from the Dynamics and Photochemistry of Urban and Forest Emissions, Environmental Science Technology, 56, 9924–9935, https://doi.org/10.1021/acs.est.2c01358, 2022.

Nations, U.: The World's Cities in 2018—Data Booklet, 2018.

Nedbor-Gross, R., Henderson, B. H., Davis, J. R., Pachón, J. E., Rincón, A., Guerrero, O. J., and Grajales, F.: Comparing Standard to Feature-Based Meteorological Model Evaluation Techniques in Bogotá, Colombia, Journal of Applied Meteorology and Climatology, https://doi.org/10.1175/jamc-d-16-0058.1, 2017.

780   Nedbor-Gross, R., Henderson, B., Perez-Peña, M., and Pachon, J. E.: Air quality modeling in Bogotá, Colombia using local emissions and natural mitigation factor adjustment for re-suspended particulate matter, Atmospheric Pollution Research, 9, 95–104, https://doi.org/http://dx.doi.org/10.1016/j.apr.2017.07.004, 2018.

Osses, M., Rojas, N., Ibarra, C., Valdebenito, V., Laengle, I., Pantoja, N., Osses, D., Basoa, K., Tolvett, S., Huneeus, N., Gallardo, L., and Gómez, B.: High-resolution spatial-distribution maps of road transport exhaust emissions in Chile, 1990–2020, Earth System Science

785   Data, 14, 1359–1376, https://doi.org/10.5194/essd-14-1359-2022, 2022.

Pachón, J., Galvis, B., Lombana, O., Carmona, L., Fajardo, S., Rincón, A., Meneses, S., Chaparro, R., Nedbor-Gross, R., and Henderson, B.: Development and evaluation of a comprehensive atmospheric emission inventory for air quality modeling in the megacity of Bogotá, Atmosphere, 9, https://doi.org/10.3390/atmos9020049, 2018.

Pereira, G., Shimabukuro, Y. E., Moraes, E. C., Freitas, S. R., Cardozo, F. S., and Longo, K. M.: Monitoring the transport of biomass burning

790   emission in South America, Atmospheric Pollution Research, 2, 247–254, https://doi.org/https://doi.org/10.5094/APR.2011.031, 2011.

Petersen, A. K., Brasseur, G. P., Bouarar, I., Flemming, J., Gauss, M., Jiang, F., Kouznetsov, R., Kranenburg, R., Mijling, B., Peuch, V.-H., Pommier, M., Segers, A., Sofiev, M., Timmermans, R., van der A, R., Walters, S., Xie, Y., Xu, J., and Zhou, G.: Ensemble forecasts of air quality in eastern China – Part 2: Evaluation of the MarcoPolo–Panda prediction system, version 1, Geoscientific Model Development, 12, 1241–1266, https://doi.org/10.5194/gmd-12-1241-2019, 2019.

795   Puliafito, S. E., Allende, D., Pinto, S., and Castesana, P.: High resolution inventory of GHG emissions of the road transport sector in Argentina, Atmospheric Environment, 101, 303–311, https://doi.org/https://doi.org/10.1016/j.atmosenv.2014.11.040, 2015.

Puliafito, S. E., Allende, D. G., Castesana, P. S., and Ruggeri, M. F.: High-resolution atmospheric emission inventory of the argentine energy sector. Comparison with edgar global emission database, Heliyon, 3, e00 489, https://doi.org/https://doi.org/10.1016/j.heliyon.2017.e00489, 2017.

800   Pérez-Peña, M., Henderson, B., Nedbor-Gross, R., and Pachón, J.: Natural mitigation factor adjustment for re-suspended particulate matter emissions inventory for Bogotá, Colombia, Atmospheric Pollution Research, 8, https://doi.org/10.1016/j.apr.2016.07.006, 2017.

Rafee, S. A. A., Martins, L. D., Kawashima, A. B., Almeida, D. S., Morais, M. V. B., Souza, R. V. A., Oliveira, M. B. L., Souza, R. A. F., Medeiros, A. S. S., Urbina, V., Freitas, E. D., Martin, S. T., and Martins, J. A.: Contributions of mobile, stationary and biogenic sources to air pollution in the Amazon rainforest: a numerical study with the WRF-Chem model, Atmos. Chem. Phys., 17, 7977–7995,

805   https://doi.org/10.5194/acp-17-7977-2017, 2017.

Ramírez, O., de la Campa, A. M. S., Amato, F., Catacolí, R. A., Rojas, N. Y., and de la Rosa, J.: Chemical composition and source apportionment of PM10 at an urban background site in a high–altitude Latin American megacity (Bogota, Colombia), Environmental Pollution, 233, 142–155, https://doi.org/https://doi.org/10.1016/j.envpol.2017.10.045, 2018.

Ramírez-Romero, C., Jaramillo, A., Córdoba, M. F., Raga, G. B., Miranda, J., Alvarez-Ospina, H., Rosas, D., Amador, T., Kim, J. S., Yakobi-

810   Hancock, J., Baumgardner, D., and Ladino, L. A.: African dust particles over the western Caribbean – Part I: Impact on air quality over the Yucatán Peninsula, Atmos. Chem. Phys., 21, 239–253, https://doi.org/10.5194/acp-21-239-2021, 2021.

Reboredo, B., Arasa, R., and Codina, B.: Evaluating Sensitivity to Different Options and Parameterizations of a Coupled Air Quality Modelling System over Bogotá, Colombia. Part I: WRF Model Configuration, Open Journal of Air Pollution, 4, 47–64, https://doi.org/10.4236/ojap.2015.42006., 2015.

815   Resquin, M. D., Santágata, D., Gallardo, L., Gómez, D., Rössler, C., and Dawidowski, L.: Local and remote black carbon sources in the Metropolitan Area of Buenos Aires, Atmospheric Environment, 182, 105–114, https://doi.org/https://doi.org/10.1016/j.atmosenv.2018.03.018, 2018.

Rodríguez-Villamizar, A. L., Rojas-Roa, Y. N., Blanco-Becerra, C. L., Herrera-Galindo, M. V., and Fernández-Niño, A. J.: Short-Term Effects of Air Pollution on Respiratory and Circulatory Morbidity in Colombia 2011–2014: A Multi-City, Time-Series Analysis, https://doi.org/10.3390/ijerph15081610, 2018.

820

Rojas, N. Y., Mangones, S. C., Osses, M., Granier, C., Laengle, I., A., J. V. A., and Mendez, J. A.: Road transport exhaust emissions in Colombia. 1990–2020 trends and spatial disaggregation, Transportation Research Part D: Transport and Environment, 121, 103 780, https://doi.org/https://doi.org/10.1016/j.trd.2023.103780, 2023.

Romieu, I., Gouveia, N., Cifuentes, L. A., de Leon, A. P., Junger, W., Vera, J., Strappa, V., Hurtado-Díaz, M., Miranda-Soberanis, V., Rojas-

825 Bracho, L., Carbajal-Arroyo, L., Tzintzun-Cervantes, G., and Committee, H. H. R.: Multicity study of air pollution and mortality in Latin America (the ESCALA study)[Abstract], Research report (Health Effects Institute), 2012.

Saide, P. E., Mena-Carrasco, M., Tolvett, S., Hernandez, P., and Carmichael, G. R.: Air quality forecasting for winter-time PM2.5 episodes occurring in multiple cities in central and southern Chile, Journal of Geophysical Research: Atmospheres, 121, 558–575, https://doi.org/https://doi.org/10.1002/2015JD023949, 2016.

830 Sarricolea, P., Serrano-Notivoli, R., Fuentealba, M., Hernández-Mora, M., de la Barrera, F., Smith, P., and Óliver Meseguer-Ruiz: Recent wildfires in Central Chile: Detecting links between burned areas and population exposure in the wildland urban interface, Science of The Total Environment, 706, 135 894, https://doi.org/https://doi.org/10.1016/j.scitotenv.2019.135894, 2020.

Seguel, R. J., Gallardo, L., Fleming, Z. L., and Landeros, S.: Two decades of ozone standard exceedances in Santiago de Chile, Air Quality, Atmosphere Health, 13, 593–605, https://doi.org/10.1007/s11869-020-00822-w, 2020.

835 Seguel, R. J., Castillo, L., Opazo, C., Rojas, N. Y., Nogueira, T., Cazorla, M., Gavidia-Calderón, M., Gallardo, L., Garreaud, R., Carrasco-Escaff, T., and Elshorbany, Y.: Changes in South American surface ozone trends: exploring the influences of precursors and extreme events, Atmos. Chem. Phys., 24, 8225–8242, https://doi.org/10.5194/acp-24-8225-2024, 2024.

SEMARNAT and INECC: Calidad del Aire en la Cuenca Atmosférica de Tula, https://www.gob.mx/cms/uploads/attachment/file/571616/Calidad_del_Aire_Cuenca_Atm_de_Tula-FINAL.pdf, 2020.

840 Silva-Quiroz, R., Rivera, A. L., Ordoñez, P., Gay-Garcia, C., and Frank, A.: Atmospheric blockages as trigger of environmental contingencies in Mexico City, Heliyon, 5, e02 099, https://doi.org/https://doi.org/10.1016/j.heliyon.2019.e02099, 2019.

Simpson, D., Benedictow, A., Berge, H., Bergström, R., Emberson, L. D., Fagerli, H., Flechard, C. R., Hayman, G. D., Gauss, M., Jonson, J. E., Jenkin, M. E., Ny{ı}ri, A., Richter, C., Semeena, V. S., Tsyro, S., Tuovinen, J.-P., Valdebenito, , and Wind, P.: The EMEP MSC-W chemical transport model ndash; technical description, Atmospheric Chemistry and Physics, 12, 7825–7865, https://doi.org/10.5194/acp-

845 12-7825-2012, 2012.

Soares, J. and Sofiev, M.: A Global Wildfire Emission and Atmospheric Composition: Refinement of the Integrated System for Wild-Land Fires IS4FIRES, in: Air Pollution Modeling and its Application XXIII, edited by Steyn, D. and Mathur, R., pp. 253–258, Springer International Publishing, 2014.

Sofiev, M.: Extended resistance analogy for construction of the vertical diffusion scheme for dispersion models, Journal of Geophysical

850 Research: Atmospheres, 107, ACH 10–1–ACH 10–8, https://doi.org/https://doi.org/10.1029/2001JD001233, 2002.

Sofiev, M., Siljamo, P., Valkama, I., Ilvonen, M., and Kukkonen, J.: A dispersion modelling system SILAM and its evaluation against ETEX data, Atmospheric Environment, 40, 674–685, https://doi.org/https://doi.org/10.1016/j.atmosenv.2005.09.069, 2006.

Sofiev, M., Vankevich, R., Lotjonen, M., Prank, M., Petukhov, V., Ermakova, T., Koskinen, J., and Kukkonen, J.: An operational system for the assimilation of the satellite information on wild-land fires for the needs of air quality modelling and forecasting, Atmos. Chem. Phys.,

855 9, 6833–6847, https://doi.org/10.5194/acp-9-6833-2009, 2009.

Sofiev, M., Genikhovich, E., Keronen, P., and Vesala, T.: Diagnosing the Surface Layer Parameters for Dispersion Models within the Meteorological-to-Dispersion Modeling Interface, Journal of Applied Meteorology and Climatology, 49, 221–233, https://doi.org/https://doi.org/10.1175/2009JAMC2210.1, 2010.

Sofiev, M., Vira, J., Kouznetsov, R., Prank, M., Soares, J., and Genikhovich, E.: Construction of the SILAM Eulerian atmospheric dispersion model based on the advection algorithm of Michael Galperin, Geoscientific Model Development, 8, 3497–3522, https://doi.org/10.5194/gmd-8-3497-2015, 2015.

Wiedinmyer, C., Akagi, S. K., Yokelson, R. J., Emmons, L. K., Al-Saadi, J. A., Orlando, J. J., and Soja, A. J.: The Fire INventory from NCAR (FINN): a high resolution global model to estimate the emissions from open burning, Geosci. Model Dev., 4, 625–641, https://doi.org/10.5194/gmd-4-625-2011, 2011.

WMO: Global Air Quality Forecasting and Information System (GAFIS), https://community.wmo.int/en/activity-areas/gaw/science-for-services/gafis, 2022.

Worden, H. M., Bloom, A. A., Worden, J. R., Jiang, Z., Marais, E. A., Stavrakou, T., Gaubert, B., and Lacey, F.: New constraints on biogenic emissions using satellite-based estimates of carbon monoxide fluxes, Atmospheric Chemistry and Physics, 19, 13 569–13 579, 2019.

Zaveri, R. A. and Peters, L. K.: A new lumped structure photochemical mechanism for large-scale applications, Journal of Geophysical Research: Atmospheres, 104, 30 387–30 415, https://doi.org/https://doi.org/10.1029/1999JD900876, 1999.

Zeng, G., Williams, J. E., Fisher, J. A., Emmons, L., Jones, N. B., Morgenstern, O., Robinson, J., Smale, D., Paton-Walsh, C., and Griffith, D. W.: Multi-model simulation of CO and HCHO in the Southern Hemisphere: comparison with observations and impact of biogenic emissions, Atmospheric Chemistry and Physics, 15, 7217–7245, 2015.

Zhai, H., Huang, L., Emery, C., Zhang, X., Wang, Y., Yarwood, G., Fu, J. S., and Li, L.: Recommendations on benchmarks for photochemical air quality model applications in China — NO2, SO2, CO and PM10, Atmospheric Environment, 319, 120 290, https://doi.org/https://doi.org/10.1016/j.atmosenv.2023.120290, 2024.

Zhang, D., Martin, R. V., Bindle, L., Li, C., Eastham, S. D., van Donkelaar, A., and Gallardo, L.: Advances in Simulating the Global Spatial Heterogeneity of Air Quality and Source Sector Contributions: Insights into the Global South, Environmental Science Technology, 57, 6955–6964, https://doi.org/10.1021/acs.est.2c07253, 2023.

Zhang, Y., Bocquet, M., Mallet, V., Seigneur, C., and Baklanov, A.: Real-time air quality forecasting, part I: History, techniques, and current status, Atmospheric Environment, 60, 632–655, https://doi.org/https://doi.org/10.1016/j.atmosenv.2012.06.031, 2012.

Zimmerman, P. R., Greenberg, J. P., and Westberg, C. E.: Measurements of atmospheric hydrocarbons and biogenic emission fluxes in the Amazon Boundary layer, Journal of Geophysical Research: Atmospheres, 93, 1407–1416, https://doi.org/https://doi.org/10.1029/JD093iD02p01407, 1988.

 Appendix A: Evaluation scores

Table A1. Metrics used for model evaluation.

Metric	Formula for each city, model and month
Model/Observation Ratio	$ratio = \frac{\overline{m}}{\overline{O}} = \frac{\sum_d m_d}{\sum_d O_d}$
Mean Bias	$BIAS = \frac{1}{N}\sum_d (m_d - O_d)$
Modified Normalized Bias	$MNBIAS = \frac{2}{N}\sum_d \frac{m_d - O_d}{m_d + O_d}$
Fractional Gross Error	$FGE = \frac{2}{N}\sum_d |\frac{m_d - O_d}{m_d + O_d}|$
Root Mean Square Error	$RMSE = \sqrt{\frac{1}{N}\sum_d (m_d - O_d)^2}$
Correlation Coefficient	$R = \frac{1}{N}\frac{\sum_d (m_d - \overline{m})(O_d - \overline{O})}{\sigma_m \sigma_O}$
Coefficient of Variation	$CV = \frac{\sigma_m}{\overline{m}}$ or $CV = \frac{\sigma_O}{\overline{O}}$

Metric	Formula for each pixel and hour
Median of Models (Ensemble)	$MED = Median(\{m_i\})$ with $i \in N, 1 \geq i \geq 6$

Metric	Formula for each pixel
Median Absolute Deviation	$MAD = Median(\{|m_{i,d} - MED_d|\})$ $i \in N, 1 \leq i \leq 6$ and $d \in N, 1 \leq d \leq 31$

Metric	Formula for each city, day and model
Observation	$O_d = \sum_{j,k} g_{A_{j,k}} M_{j,k}$ with $\sum_{j,k} g_{A_{j,k}} = 1$ $j,k \in N$ representing a specific pixel $g_{A_{j,k}}$ proportion of area of the pixel with the area of the polygon of the city

with O_d and m_d being the observation and modeled value for each day. $\overline{m}$ the mean of the models for each month and $\overline{O}$ the mean of the observations for each city. σ_m the standard deviation for each model. N is the number of model-observation pairs available for each month.

Table A2. NO$_2$ model evaluation scores (January / July)

		ENSEMBLE		Mean		CAMS		MPI		EMEP		CHIM		SILAM		USP	
NO$_2$	City	Jan	Jul	Jan	Jul	Jan	Jul	Jan	Jul	Jan	Jul	Jan	Jul	Jan	Jul	Jan	Jul
Model/Observations	Santiago	0.81	0.44	0.89	0.58	0.31	0.63	0.78	0.39	1.06	0.75	0.94	0.27	1.60	1.26	0.63	0.10
	Bogotá	0.40	0.34	0.42	0.38	0.24	0.13	0.48	0.49	0.68	0.60	0.26	0.18	0.37	0.22	0.42	0.59
	México	1.04	0.97	1.15	1.18	0.78	0.44	1.11	1.06	1.46	2.21	1.57	1.44	0.87	0.85		
	São Paulo	1.18	1.06	1.24	1.11	0.14	0.37	1.69	1.72	2.04	1.61	1.72	1.28	1.20	0.92	0.71	0.83
MNBIAS [%]	Santiago	−18.8	−73.5	−9.7	−47.9	−106	−46.7	−22.6	−83.3	7.2	−24.5	−2.2	−118	47.0	24.6	−44.6	−160
	Bogotá	−85.8	−97.8	−81.6	−88.7	−121	−156	−68.7	−67.0	−39.2	−49.6	−111	−138	−92.1	−128	−84.5	−52.2
	México	1.7	−2.9	12.0	17.0	−35.0	−83.7	10.4	7.3	35.5	74.0	44.0	30.8	−18.2	−20.3		
	São Paulo	17.7	6.8	22.8	10.8	−157	−107	51.2	51.1	69.1	44.3	54.0	28.3	14.1	−14.7	−40.6	−24.2
RMSE [ppb]	Santiago	3.11	23.64	2.45	18.36	8.23	17.17	3.58	25.67	3.07	14.65	2.27	32.10	7.53	15.15	4.88	35.30
	Bogotá	11.22	10.16	10.89	9.55	14.41	13.22	9.73	7.98	6.60	6.63	12.85	12.44	11.83	11.92	10.81	6.92
	México	5.06	3.97	7.13	5.81	10.26	14.93	5.22	5.23	15.87	31.52	21.45	12.25	6.48	6.01		
	São Paulo	5.90	7.03	6.59	6.94	15.92	16.31	13.74	19.38	19.57	18.07	15.56	12.38	7.70	8.82	8.70	10.81
FGE	Santiago	0.24	0.74	0.18	0.48	1.06	0.48	0.27	0.84	0.21	0.36	0.16	1.19	0.47	0.30	0.46	1.60
	Bogotá	0.86	0.98	0.82	0.89	1.22	1.56	0.69	0.67	0.39	0.50	1.12	1.39	0.92	1.28	0.84	0.52
	México	0.14	0.13	0.18	0.19	0.43	0.84	0.14	0.17	0.36	0.74	0.45	0.36	0.24	0.26		
	São Paulo	0.24	0.23	0.26	0.24	1.58	1.09	0.51	0.52	0.69	0.47	0.56	0.41	0.29	0.34	0.56	0.45
R	Santiago	0.57	0.26	0.64	0.53	0.65	0.44	0.32	0.02	0.08	0.11	0.55	0.24	0.51	0.52	0.44	0.57
	Bogotá	0.74	0.25	0.76	0.31	−0.12	0.44	0.74	0.34	0.66	0.15	0.14	0.15	0.56	0.43	0.65	0.17
	México	0.80	0.73	0.78	0.73	0.58	0.40	0.80	0.48	0.69	0.52	0.68	−0.21	0.81	0.80		
	São Paulo	0.63	0.49	0.62	0.60	0.36	0.47	0.54	0.62	0.48	0.52	0.49	−0.20	0.67	0.64	0.29	0.18

*ENSEMBLE: based on the median value of the models; MEAN: arithmetic mean of the models; CAMS: Copernicus Atmosphere Monitoring Service's (CAMS); MPI: WRF-Chem executed by MPIM; EMEP: European Monitoring and Evaluation Programme; CHIM: CHIMERE transport model; SILAM: System for Integrated modeling of Atmospheric composition; USP: WRF-Chem executed by University of São Paulo.

Table A3. O$_3$ model evaluation scores (January / July)

		ENSEMBLE		Mean		CAMS		MPI		EMEP		CHIM		SILAM		USP	
O$_3$	City	Jan	Jul	Jan	Jul	Jan	Jul	Jan	Jul	Jan	Jul	Jan	Jul	Jan	Jul	Jan	Jul
Model/Observations	Santiago	1.21	4.51	1.19	4.95	0.32	5.01	1.67	6.78	1.75	6.12	1.06	5.72	1.60	5.76	0.69	0.74
	Bogotá	1.24	1.20	1.35	1.22	0.34	0.35	2.36	1.57	2.27	2.30	1.54	1.38	0.82	0.45	0.78	1.29
	México	1.12	1.05	1.19	1.23	0.54	0.31	1.58	1.70	1.76	2.33	1.12	0.68	0.87	0.93		
	São Paulo	1.39	0.97	1.44	1.11	0.29	0.72	2.65	1.71	1.84	1.67	1.30	0.58	1.34	0.90	1.13	0.89
MNBIAS [%]	Santiago	18.8	127	16.8	133	−104	133	47.7	149	54.2	142	6.1	147	44.0	118	−38.0	−20.8
	Bogotá	23.5	19.9	31.4	21.3	−95.2	−94.0	79.7	43.8	77.7	78.0	43.6	32.3	−18.7	−73.9	−25.9	24.8
	México	12.6	4.1	17.5	20.0	−56.1	−102	45.3	50.2	49.3	77.0	9.1	−42.1	−12.4	−10.3		
	São Paulo	30.0	−3.4	35.1	11.0	−104	−29.6	86.4	46.8	56.8	45.6	32.3	−50.8	19.6	−30.3	4.5	−13.0
RMSE [ppb]	Santiago	5.62	13.44	4.84	14.88	15.29	15.17	16.39	21.13	17.01	19.66	3.23	17.76	14.85	20.92	8.52	2.55
	Bogotá	4.08	4.05	5.63	4.08	8.84	7.70	18.57	8.12	16.87	15.43	7.53	5.63	3.16	6.77	6.28	5.69
	México	9.62	9.38	10.78	11.45	12.62	21.93	16.81	24.96	24.98	44.77	11.24	14.21	10.60	10.19		
	São Paulo	13.90	7.06	14.58	7.45	19.00	7.30	43.50	14.24	24.62	16.06	16.30	9.90	14.31	10.84	12.89	6.24
FGE	Santiago	0.19	1.30	0.17	1.34	1.04	1.34	0.48	1.49	0.54	1.42	0.11	1.48	0.44	1.32	0.40	0.51
	Bogotá	0.25	0.27	0.33	0.28	0.95	0.94	0.80	0.45	0.78	0.78	0.44	0.40	0.22	0.74	0.46	0.34
	México	0.31	0.23	0.34	0.27	0.57	1.02	0.45	0.53	0.56	0.77	0.31	0.50	0.39	0.29		
	São Paulo	0.43	0.41	0.43	0.39	1.06	0.50	0.88	0.58	0.57	0.52	0.49	0.71	0.47	0.65	0.52	0.43
R	Santiago	0.68	−0.22	0.76	−0.06	0.42	−0.40	0.76	−0.20	0.59	−0.19	0.74	0.33	0.64	0.17	−0.20	−0.06
	Bogotá	0.42	−0.19	0.05	−0.36	0.15	−0.12	0.02	−0.29	−0.16	−0.12	0.56	−0.13	0.69	−0.09	−0.53	−0.23
	México	0.07	0.02	0.09	0.09	0.26	−0.00	0.32	0.14	0.08	0.13	0.04	−0.19	−0.26	0.11		
	São Paulo	0.52	0.16	0.48	0.18	0.16	−0.01	0.40	0.29	0.39	0.13	0.08	−0.33	0.61	0.16	0.26	0.28

*ENSEMBLE: based on the median value of the models; MEAN: arithmetic mean of the models; CAMS: Copernicus Atmosphere Monitoring Service's (CAMS); MPI: WRF-Chem executed by MPIM; EMEP: European Monitoring and Evaluation Programme; CHIM: CHIMERE transport model; SILAM: System for Integrated modeling of Atmospheric composition; USP: WRF-Chem executed by University of São Paulo.

Table A4. CO model evaluation scores (January / July)

CO	City	ENSEMBLE		Mean		CAMS		MPI		EMEP		CHIM		SILAM		USP	
		Jan	Jul	Jan	Jul	Jan	Jul	Jan	Jul	Jan	Jul	Jan	Jul	Jan	Jul	Jan	Jul
Model/Observations	Santiago	1.31	0.55	1.62	0.98	1.05	0.97	1.14	0.38	1.86	0.89	1.70	0.32	3.47	2.94	0.54	0.12
	Bogotá	0.36	0.41	0.40	0.45	0.38	0.33	0.42	0.52	0.52	0.60	0.31	0.25	0.51	0.50	0.21	0.40
	México	1.14	1.18	1.45	1.61	0.60	0.48	0.94	1.01	2.28	3.48	2.40	1.99	1.16	1.28		
	São Paulo	0.87	0.80	0.89	0.85	0.42	0.48	1.11	1.08	1.23	1.08	0.94	0.81	1.26	1.19	0.36	0.44
MNBIAS [%]	Santiago	26.5	−51.4	47.6	3.4	2.2	−0.8	12.6	−81.4	59.4	−6.1	52.4	−108	109	98.5	−60.3	−151
	Bogotá	−90.0	−83.3	−83.1	−76.1	−84.8	−99.9	−78.0	−62.8	−60.2	−49.6	−99.7	−118	−63.0	−68.3	−130	−87.3
	México	10.4	17.8	32.6	48.2	−49.8	−69.0	−5.8	3.9	73.9	108	72.3	59.0	9.8	21.6		
	São Paulo	−15.0	−22.8	−12.7	−17.2	−84.7	−73.3	10.4	6.1	18.9	1.8	−8.1	−15.3	17.2	8.9	−94.2	−76.2
RMSE [ppm]	Santiago	0.08	0.64	0.15	0.38	0.06	0.40	0.05	0.80	0.22	0.40	0.18	0.96	0.61	2.38	0.11	1.08
	Bogotá	0.47	0.38	0.45	0.36	0.47	0.43	0.43	0.31	0.37	0.27	0.49	0.48	0.39	0.33	0.58	0.39
	México	0.18	0.15	0.45	0.43	0.34	0.38	0.14	0.16	1.20	1.77	1.40	0.67	0.23	0.26		
	São Paulo	0.17	0.27	0.17	0.26	0.39	0.44	0.18	0.28	0.27	0.38	0.25	0.29	0.31	0.43	0.43	0.50
FGE	Santiago	0.26	0.59	0.48	0.30	0.18	0.27	0.15	0.85	0.59	0.32	0.52	1.08	1.09	0.98	0.60	1.52
	Bogotá	0.90	0.83	0.83	0.76	0.85	1.00	0.78	0.63	0.60	0.50	1.00	1.19	0.63	0.69	1.31	0.87
	México	0.16	0.19	0.34	0.48	0.50	0.69	0.16	0.19	0.74	1.09	0.72	0.59	0.21	0.24		
	São Paulo	0.26	0.32	0.24	0.31	0.85	0.74	0.23	0.30	0.28	0.36	0.27	0.30	0.30	0.41	0.94	0.76
R	Santiago	0.36	0.20	0.22	0.28	0.54	0.38	0.17	0.32	−0.04	0.21	0.30	−0.00	−0.16	0.24	0.50	0.02
	Bogotá	0.72	0.27	0.71	0.28	0.07	0.18	0.77	0.36	0.60	0.32	0.42	0.22	0.29	0.19	0.67	0.11
	México	0.85	0.87	0.73	0.85	0.78	0.68	0.75	0.49	0.59	0.65	0.74	−0.04	0.85	0.82		
	São Paulo	0.50	0.48	0.49	0.48	0.57	0.62	0.46	0.44	0.31	0.37	0.36	0.07	0.54	0.45	0.09	0.15

*ENSEMBLE: based on the median value of the models; MEAN: arithmetic mean of the models; CAMS: Copernicus Atmosphere Monitoring Service's (CAMS); MPI: WRF-Chem executed by MPIM; EMEP: European Monitoring and Evaluation Programme; CHIM: CHIMERE transport model; SILAM: System for Integrated modeling of Atmospheric composition; USP: WRF-Chem executed by University of São Paulo.

Table A5. SO$_2$ model evaluation scores (January / July)

SO$_2$	City	ENSEMBLE		Mean		CAMS		MPI		EMEP		CHIM		SILAM		USP	
		Jan	Jul	Jan	Jul	Jan	Jul	Jan	Jul	Jan	Jul	Jan	Jul	Jan	Jul	Jan	Jul
Model/Observations	Santiago	3.38	4.82	4.69	5.82	11.64	8.99	6.87	8.52	1.59	2.09	1.93	3.65	5.55	10.93	0.01	0.01
	Bogotá	0.58	0.50	0.64	0.56	0.52	0.40	1.17	1.10	1.13	0.98	0.36	0.20	0.56	0.50	0.00	0.00
	México	3.53	4.85	12.43	12.46	46.93	42.11	5.83	6.92	2.12	3.02	1.65	1.98	3.12	4.44		
	São Paulo	6.27	5.69	8.13	8.01	3.08	5.73	21.01	22.41	7.46	5.68	4.70	4.64	11.57	8.43	0.01	0.01
MNBIAS [%]	Santiago	107	130	129	140	168	159	147	157	45.4	69.3	61.2	109	138	162	−196	−197
	Bogotá	−50.2	−63.5	−42.4	−53.3	−58.8	−79.9	16.0	12.9	7.2	0.4	−89.2	−127	−55.8	−62.0	−199	−199
	México	111	131	169	170	191	190	141	149	76.2	101	57.0	69.8	102	124		
	São Paulo	144	139	156	153	101	136	181	181	151	134	129	128	167	154	−196	−193
RMSE [ppb]	Santiago	3.58	7.05	5.46	8.76	15.67	14.51	8.79	13.64	0.94	2.11	1.53	4.85	6.79	19.21	1.46	1.82
	Bogotá	0.87	0.93	0.83	0.84	0.96	1.09	0.75	0.49	0.97	0.48	1.15	1.15	0.93	0.95	1.79	1.70
	México	12.44	12.10	52.40	35.18	207.29	125.97	22.42	18.35	6.08	6.33	4.62	3.39	10.63	11.19		
	São Paulo	5.26	6.17	7.04	9.28	2.11	6.34	19.66	28.76	6.49	6.66	3.71	5.16	10.68	10.32	1.01	1.33
FGE	Santiago	1.08	1.30	1.29	1.41	1.68	1.60	1.48	1.58	0.45	0.69	0.61	1.09	1.38	1.62	1.96	1.97
	Bogotá	0.52	0.64	0.49	0.53	0.59	0.80	0.31	0.24	0.38	0.21	0.89	1.28	0.60	0.62	1.99	1.99
	México	1.14	1.31	1.69	1.70	1.91	1.91	1.42	1.49	0.82	1.01	0.73	0.70	1.06	1.24		
	São Paulo	1.44	1.39	1.56	1.54	1.01	1.37	1.82	1.81	1.52	1.34	1.30	1.29	1.67	1.54	1.97	1.94
R	Santiago	−0.09	−0.17	−0.13	0.02	0.00	0.54	−0.23	0.16	−0.26	0.00	−0.43	0.25	−0.06	−0.20	0.29	0.37
	Bogotá	0.24	0.70	0.07	0.68	0.03	0.42	−0.01	0.55	−0.01	0.52	0.37	0.37	0.17	0.44	0.10	0.48
	México	0.24	0.18	0.17	0.16	0.10	−0.03	0.20	−0.04	0.19	0.21	0.14	0.04	0.11	0.04		
	São Paulo	0.36	0.50	0.55	0.54	0.39	0.54	0.61	0.47	0.30	0.36	0.57	−0.06	0.56	0.46	0.11	0.05

*ENSEMBLE: based on the median value of the models; MEAN: arithmetic mean of the models; CAMS: Copernicus Atmosphere Monitoring Service's (CAMS); MPI: WRF-Chem executed by MPIM; EMEP: European Monitoring and Evaluation Programme; CHIM: CHIMERE transport model; SILAM: System for Integrated modeling of Atmospheric composition; USP: WRF-Chem executed by University of São Paulo.

Table A6. PM$_{2.5}$ model evaluation scores (January / July)

		ENSEMBLE		Mean		CAMS		MPI		EMEP		CHIM		SILAM		USP	
PM$_{2.5}$	City	Jan	Jul	Jan	Jul	Jan	Jul	Jan	Jul	Jan	Jul	Jan	Jul	Jan	Jul	Jan	Jul
Model/Observations	Santiago	0.61	0.40	0.78	1.45	1.15	1.74	0.66	0.39	0.20	0.34	0.62	0.17	1.66	5.55	0.34	0.10
	Bogotá	0.34	0.42	0.55	0.67	1.34	1.54	0.85	1.09	0.18	0.20	0.26	0.34	0.42	0.39	0.19	0.37
	México	1.02	1.38	1.72	2.06	4.35	5.06	0.79	1.30	0.18	0.20	0.62	0.70	2.38	2.56		
	São Paulo	1.90	1.88	2.23	2.14	1.60	2.46	2.33	2.23	1.79	1.54	2.33	2.11	4.44	3.63	0.79	0.90
MNBIAS [%]	Santiago	−46.9	−75.3	−23.1	41.4	14.0	57.5	−40.3	−78.9	−129	−89.5	−40.0	−144	48.0	138	−97.9	−156
	Bogotá	−95.8	−81.4	−53.2	−38.3	32.9	41.0	−15.0	1.8	−139	−133	−109	−95.8	−79.9	−90.8	−135	−93.6
	México	−5.0	29.8	53.4	69.5	125	133	−18.0	26.9	−138	−130	−46.6	−34.8	69.6	79.1		
	São Paulo	66.0	61.5	77.7	71.2	48.5	82.6	83.5	75.3	58.2	35.0	85.7	76.2	117	92.4	−23.4	−7.4
RMSE [$\mu g/m^2$]	Santiago	8.61	38.52	5.92	31.44	5.47	46.62	8.22	39.07	16.27	41.00	7.48	53.00	16.82	269.80	13.80	53.60
	Bogotá	13.64	8.02	9.98	5.17	9.25	8.64	6.84	7.28	16.60	10.97	13.77	8.83	12.42	8.50	16.47	8.87
	México	7.72	12.00	18.45	23.41	83.04	87.94	7.63	9.43	21.60	17.48	9.59	9.89	39.20	39.23		
	São Paulo	16.90	20.90	23.07	27.26	12.99	32.92	23.86	28.83	16.68	19.52	26.71	28.98	69.79	78.88	10.30	10.15
FGE	Santiago	0.47	0.87	0.25	0.42	0.20	0.57	0.41	0.90	1.30	0.94	0.40	1.44	0.48	1.38	0.98	1.57
	Bogotá	0.96	0.81	0.53	0.41	0.38	0.41	0.32	0.42	1.40	1.34	1.09	0.96	0.80	0.91	1.35	0.94
	México	0.23	0.36	0.53	0.70	1.25	1.34	0.28	0.34	1.39	1.31	0.47	0.43	0.79	0.80		
	São Paulo	0.66	0.63	0.78	0.72	0.50	0.84	0.84	0.76	0.65	0.55	0.86	0.80	1.17	0.94	0.51	0.40
R	Santiago	0.50	−0.15	0.43	0.42	0.60	0.51	0.20	0.05	0.13	0.25	0.26	0.00	0.02	0.37	0.21	0.33
	Bogotá	0.67	0.47	0.69	0.05	0.30	0.17	0.41	−0.42	0.77	0.38	0.44	0.37	0.43	0.43	0.61	0.16
	México	0.83	0.35	0.89	0.66	0.69	0.62	0.84	0.11	0.74	0.32	0.75	−0.19	0.83	0.63		
	São Paulo	0.53	0.59	0.54	0.63	0.51	0.56	0.45	0.49	0.37	0.50	0.45	−0.11	0.53	0.63	0.08	0.22

*ENSEMBLE: based on the median value of the models; MEAN: arithmetic mean of the models; CAMS: Copernicus Atmosphere Monitoring Service's (CAMS); MPI: WRF-Chem executed by MPIM; EMEP: European Monitoring and Evaluation Programme; CHIM: CHIMERE transport model; SILAM: System for Integrated modeling of Atmospheric composition; USP: WRF-Chem executed by University of São Paulo.

Table A7. PM$_{10}$ model evaluation scores (January / July)

PM$_{10}$	City	ENSEMBLE Jan	ENSEMBLE Jul	Mean Jan	Mean Jul	CAMS Jan	CAMS Jul	MPI Jan	MPI Jul	EMEP Jan	EMEP Jul	CHIM Jan	CHIM Jul	SILAM Jan	SILAM Jul	USP Jan	USP Jul
Model/Observations	Santiago	0.31	0.35	0.41	1.08	0.57	1.43	0.31	0.24	0.29	0.39	0.27	0.13	0.88	3.89	0.12	0.06
	Bogotá	0.21	0.22	0.33	0.40	0.75	0.83	0.59	0.84	0.19	0.18	0.12	0.16	0.21	0.19	0.08	0.15
	México	0.57	0.87	1.10	1.31	2.96	3.30	0.42	0.91	0.41	0.51	0.28	0.35	1.21	1.16		
	São Paulo	1.46	1.53	1.76	1.80	1.28	2.02	1.52	1.54	2.04	1.93	1.54	1.66	3.61	3.08	0.45	0.54
MNBIAS [%]	Santiago	−102	−85.2	−81.6	13.9	−53.8	39.9	−103	−110	−108	−79.5	−111	−155	−13.1	118	−156	−173
	Bogotá	−130	−127	−98.4	−82.9	−25.6	−18.4	−52.3	−26.6	−136	−136	−153	−141	−130	−137	−170	−147
	México	−62.9	−15.4	6.2	27.0	96.5	105	−79.5	−11.0	−89.3	−65.6	−115	−92.6	4.2	7.2		
	São Paulo	39.4	42.1	54.9	53.8	24.2	64.1	42.6	40.4	64.8	45.6	46.4	53.8	104	84.1	−75.1	−57.0
RMSE [$\mu g/m^2$]	Santiago	39.65	72.46	34.40	32.08	25.86	53.34	39.82	81.63	41.21	67.84	40.52	99.01	16.89	295.63	50.28	97.44
	Bogotá	39.06	27.77	33.59	21.92	16.96	10.48	23.52	18.66	39.84	29.01	40.77	29.11	39.54	28.84	45.34	30.23
	México	25.44	12.05	12.80	18.74	105.46	110.21	32.93	13.46	32.46	25.05	36.82	29.92	24.00	22.35		
	São Paulo	17.51	24.28	26.48	35.41	15.11	40.68	21.35	28.36	36.89	55.94	23.75	33.12	91.62	102.20	20.03	20.42
FGE	Santiago	1.03	0.93	0.82	0.30	0.54	0.43	1.04	1.17	1.08	0.83	1.12	1.55	0.27	1.19	1.56	1.73
	Bogotá	1.31	1.27	0.98	0.83	0.31	0.27	0.56	0.53	1.37	1.36	1.54	1.42	1.31	1.38	1.71	1.48
	México	0.64	0.25	0.20	0.31	0.96	1.05	0.80	0.27	0.90	0.66	1.16	0.93	0.38	0.34		
	São Paulo	0.41	0.47	0.55	0.57	0.34	0.67	0.48	0.51	0.66	0.62	0.48	0.58	1.04	0.87	0.78	0.65
R	Santiago	0.30	−0.17	0.35	0.44	0.44	0.48	0.20	−0.33	−0.03	0.26	0.07	0.03	0.03	0.45	0.07	0.37
	Bogotá	0.72	0.37	0.65	−0.00	0.33	0.20	0.33	−0.17	0.74	0.05	0.45	0.42	0.32	0.24	0.65	−0.02
	México	0.69	0.46	0.77	0.37	0.58	0.14	0.36	0.20	0.64	0.08	0.66	−0.24	0.76	0.37		
	São Paulo	0.51	0.45	0.56	0.50	0.43	0.51	0.12	0.13	0.41	0.37	0.45	−0.01	0.58	0.52	0.11	0.19

*ENSEMBLE: based on the median value of the models; MEAN: arithmetic mean of the models; CAMS: Copernicus Atmosphere Monitoring Service's (CAMS); MPI: WRF-Chem executed by MPIM; EMEP: European Monitoring and Evaluation Programme; CHIM: CHIMERE transport model; SILAM: System for Integrated modeling of Atmospheric composition; USP: WRF-Chem executed by University of São Paulo.

Table A8. Coefficient of Variation (CV) per city during January and July

City	NO$_2$	O$_3$	CO	SO$_2$	PM$_{2.5}$
Santiago	22% 29%	13% 58%	10% 33%	15% 20%	22% 32%
Bogota	22% 18%	23% 23%	29% 17%	28% 34%	33% 18%
São Paulo	35% 31%	37% 38%	26% 31%	37% 41%	49% 45%
Mexico	24% 23%	31% 20%	24% 26%	60% 30%	37% 24%

Appendix B: Air quality observations

Table B1. Stations availability and location for México City.

		Obs		ENSEMBLE		CAMS		MPI		EMEP		CHIM		SILAM		USP	
		Jan	Jul	Jan	Jul	Jan	Jul	Jan	Jul	Jan	Jul	Jan	Jul	Jan	Jul	Jan	Jul
CO																	
México	Number Stations	21	24	21	24	21	24	21	24	21	24	21	24	21	24		
	Availability [%]	96.67	100	100	100	100	100	100	100	100	100	83.33	66.67	100	100		
	CV	0.24	0.26	0.29	0.22	0.26	0.20	0.24	0.15	0.36	0.29	0.50	0.16	0.35	0.35		
NO$_2$																	
México	Number Stations	24	24	24	24	24	24	24	24	24	24	24	24	24	24		
	Availability [%]	100	100	100	100	100	100	100	100	100	100	83.33	66.67	100	100		
	CV	0.24	0.23	0.29	0.21	0.46	0.52	0.22	0.15	0.30	0.24	0.38	0.14	0.38	0.38		
O$_3$																	
México	Number Stations	21	29	28	29	28	29	28	29	28	29	28	29	28	29		
	Availability [%]	96.67	100	100	100	100	100	100	100	100	100	83.33	66.67	100	100		
	CV	0.31	0.20	0.25	0.22	0.17	0.14	0.27	0.23	0.41	0.26	0.32	0.33	0.28	0.30		
PM$_{10}$																	
México	Number Stations	17	24	17	24	17	24	17	24	17	24	17	24	17	24		
	Availability [%]	96.67	100	100	100	100	100	100	100	100	100	83.33	66.67	100	100		
	CV	0.27	0.20	0.55	0.27	0.28	0.23	0.24	0.26	0.48	0.31	0.52	0.25	0.48	0.43		
PM$_{2.5}$																	
México	Number Stations	14	16	14	16	14	16	14	16	14	16	14	16	14	16		
	Availability [%]	96.67	100	100	100	100	100	100	100	100	100	83.33	66.67	100	100		
	CV	0.37	0.24	0.52	0.32	0.28	0.22	0.25	0.19	0.34	0.19	0.52	0.30	0.48	0.46		
SO$_2$																	
México	Number Stations	23	26	23	26	23	26	23	26	23	26	23	26	23	26		
	Availability [%]	96.67	100	100	100	100	100	100	100	100	100	83.33	66.67	100	100		
	CV	0.60	0.30	0.35	0.20	0.25	0.09	0.26	0.15	0.30	0.14	0.38	0.18	0.35	0.28		

The observations availability refers to the percentage of days in each period when at least one station records enough data to construct their daily average (minimum of 18 hours). Additionally, only stations that maintain at least 75% of daily availability throughout the entire period are considered (at least 23 days with 18 hours minimum). The model availability refers to the percentage of days for which we have modeled data, being CHIMERE the only one with missing days, and USP missing information for México given their simulation domain did not include it.

Table B2. Stations availability and location for Bogotá

		Obs		ENSEMBLE		CAMS		MPI		EMEP		CHIM		SILAM		USP	
		Jan	Jul	Jan	Jul	Jan	Jul	Jan	Jul	Jan	Jul	Jan	Jul	Jan	Jul	Jan	Jul
CO																	
Bogotá	Number Stations	7	8	7	8	7	8	7	8	7	8	7	8	7	8	7	8
	Availability [%]	100	100	100	100	100	100	100	100	100	100	83.33	66.67	100	100	100	100
	CV	0.29	0.17	0.16	0.17	0.10	0.13	0.18	0.14	0.26	0.17	0.18	0.14	0.25	0.31	0.33	0.30
NO_2																	
Bogotá	Number Stations	8	7	8	7	8	7	8	7	8	7	8	7	8	7	8	7
	Availability [%]	100	100	100	100	100	100	100	100	100	100	83.33	66.67	100	100	100	100
	CV	0.22	0.18	0.24	0.26	0.42	0.57	0.21	0.14	0.30	0.15	0.28	0.39	0.28	0.24	0.37	0.29
O_3																	
Bogotá	Number Stations	10	11	10	11	10	11	10	11	10	11	10	11	10	11	10	11
	Availability [%]	100	100	100	100	100	100	100	100	100	100	83.33	66.67	100	100	100	100
	CV	0.23	0.23	0.11	0.13	0.08	0.11	0.22	0.21	0.14	0.19	0.18	0.15	0.18	0.27	0.35	0.24
PM_{10}																	
Bogotá	Number Stations	10	10	10	10	10	10	10	10	10	10	10	10	10	10	10	10
	Availability [%]	100	100	100	100	100	100	100	100	100	100	83.33	66.67	100	100	100	100
	CV	0.27	0.22	0.31	0.19	0.16	0.21	0.33	0.52	0.37	0.17	0.26	0.14	0.37	0.40	0.33	0.34
$PM_{2.5}$																	
Bogotá	Number Stations	9	10	9	10	9	10	9	10	9	10	9	10	9	10	9	10
	Availability [%]	100	100	100	100	100	100	100	100	100	100	83.33	66.67	100	100	100	100
	CV	0.33	0.18	0.29	0.22	0.16	0.22	0.29	0.40	0.40	0.18	0.28	0.11	0.40	0.42	0.34	0.33
SO_2																	
Bogotá	Number Stations	7	6	7	6	7	6	7	6	7	6	7	6	7	6	7	6
	Availability [%]	100	100	100	100	100	100	100	100	100	100	83.33	66.67	100	100	100	100
	CV	0.28	0.34	0.22	0.20	0.12	0.15	0.24	0.20	0.41	0.24	0.24	0.45	0.32	0.18	0.30	0.37

The observations availability refers to the percentage of days in each period when at least one station records enough data to construct their daily average (minimum of 18 hours). Additionally, only stations that maintain at least 75% of daily availability throughout the entire period are considered (at least 23 days with 18 hours minimum). The model availability refers to the percentage of days for which we have modeled data, being CHIMERE the only one with missing days, and USP missing information for México given their simulation domain did not include it.

Table B3. Stations availability and location for Santiago

		Obs		ENSEMBLE		CAMS		MPI		EMEP		CHIM		SILAM		USP	
		Jan	Jul	Jan	Jul	Jan	Jul	Jan	Jul	Jan	Jul	Jan	Jul	Jan	Jul	Jan	Jul
CO																	
Santiago	Number Stations	8	9	8	9	8	9	8	9	8	9	8	9	8	9	8	9
	Availability [%]	100	100	100	100	100	100	100	100	100	100	83.33	66.67	100	100	100	100
	CV	0.10	0.33	0.10	0.19	0.27	0.29	0.13	0.10	0.13	0.16	0.12	0.29	0.17	0.25	0.13	0.20
NO_2																	
Santiago	Number Stations	9	9	10	10	10	10	10	10	10	10	10	10	10	10	10	10
	Availability [%]	100	100	100	100	100	100	100	100	100	100	83.33	66.67	100	100	100	100
	CV	0.22	0.29	0.11	0.16	0.36	0.32	0.17	0.14	0.14	0.13	0.11	0.28	0.17	0.26	0.21	0.27
O_3																	
Santiago	Number Stations	9	9	9	9	9	9	9	9	9	9	9	9	9	9	9	9
	Availability [%]	100	100	100	100	100	100	100	100	100	100	83.33	66.67	100	100	100	100
	CV	0.13	0.58	0.16	0.24	0.16	0.20	0.24	0.14	0.13	0.29	0.17	0.22	0.24	0.60	0.25	0.40
PM_{10}																	
Santiago	Number Stations	10	10	10	10	10	10	10	10	10	10	10	10	10	10	10	10
	Availability [%]	100	100	100	100	100	100	100	100	100	100	83.33	66.67	100	100	100	100
	CV	0.20	0.36	0.15	0.20	0.24	0.23	0.24	0.17	0.14	0.22	0.16	0.31	0.23	0.27	0.20	0.22
$PM_{2.5}$																	
Santiago	Number Stations	10	10	10	10	10	10	10	10	10	10	10	10	10	10	10	10
	Availability [%]	100	100	100	100	100	100	100	100	100	100	83.33	66.67	100	100	100	100
	CV	0.22	0.32	0.15	0.13	0.24	0.23	0.20	0.13	0.12	0.19	0.16	0.32	0.29	0.29	0.20	0.22
SO_2																	
Santiago	Number Stations	4	4	4	4	4	4	4	4	4	4	4	4	4	4	4	4
	Availability [%]	100	100	100	100	100	100	100	100	100	100	83.33	66.67	100	100	100	100
	CV	0.15	0.20	0.16	0.18	0.11	0.16	0.18	0.14	0.12	0.19	0.21	0.22	0.17	0.36	0.12	0.17

The observations availability refers to the percentage of days in each period when at least one station records enough data to construct their daily average (minimum of 18 hours). Additionally, only stations that maintain at least 75% of daily availability throughout the entire period are considered (at least 23 days with 18 hours minimum). The model availability refers to the percentage of days for which we have modeled data, being CHIMERE the only one with missing days, and USP missing information for México given their simulation domain did not include it.

Table B4. Stations availability and location for São Paulo

		Obs		ENSEMBLE		CAMS		MPI		EMEP		CHIM		SILAM		USP	
		Jan	Jul	Jan	Jul	Jan	Jul	Jan	Jul	Jan	Jul	Jan	Jul	Jan	Jul	Jan	Jul
CO																	
São Paulo	Number Stations	17	17	17	17	17	17	17	17	17	17	17	17	17	17	17	17
	Availability [%]	100	100	100	100	100	100	100	100	100	100	83.33	66.67	100	100	100	100
	CV	0.26	0.31	0.26	0.31	0.37	0.42	0.22	0.34	0.29	0.48	0.42	0.26	0.40	0.50	0.41	0.34
NO$_2$																	
São Paulo	Number Stations	18	18	18	18	18	18	18	18	18	18	18	18	18	18	18	18
	Availability [%]	100	100	100	100	100	100	100	100	100	100	83.33	66.67	100	100	100	100
	CV	0.35	0.31	0.28	0.27	1.13	0.87	0.27	0.33	0.26	0.36	0.34	0.20	0.45	0.53	0.49	0.45
O$_3$																	
São Paulo	Number Stations	20	20	20	20	20	20	20	20	20	20	20	20	20	20	20	20
	Availability [%]	100	100	100	100	100	100	100	100	100	100	83.33	66.67	100	100	100	100
	CV	0.37	0.38	0.35	0.44	0.32	0.36	0.33	0.48	0.35	0.57	0.38	0.43	0.47	0.85	0.43	0.41
PM$_{10}$																	
São Paulo	Number Stations	23	22	23	22	23	22	23	22	23	22	23	22	23	22	23	22
	Availability [%]	100	100	100	100	100	100	100	100	100	100	83.33	66.67	100	100	100	100
	CV	0.39	0.37	0.27	0.33	0.34	0.36	0.27	0.36	0.40	0.75	0.39	0.33	0.56	0.76	0.47	0.38
PM$_{2.5}$																	
São Paulo	Number Stations	9	9	9	9	9	9	9	9	9	9	9	9	9	9	9	9
	Availability [%]	100	100	100	100	100	100	100	100	100	100	83.33	66.67	100	100	100	100
	CV	0.49	0.45	0.29	0.37	0.34	0.36	0.26	0.38	0.35	0.60	0.40	0.32	0.61	0.88	0.47	0.37
SO$_2$																	
São Paulo	Number Stations	8	8	8	8	8	8	8	8	8	8	8	8	8	8	8	8
	Availability [%]	100	100	100	100	100	100	100	100	100	100	83.33	66.67	100	100	100	100
	CV	0.37	0.41	0.28	0.31	0.28	0.36	0.26	0.40	0.31	0.48	0.30	0.39	0.35	0.46	0.34	0.34

The observations availability refers to the percentage of days in each period when at least one station records enough data to construct their daily average (minimum of 18 hours). Additionally, only stations that maintain at least 75% of daily availability throughout the entire period are considered (at least 23 days with 18 hours minimum). The model availability refers to the percentage of days for which we have modeled data, being CHIMERE the only one with missing days, and USP missing information for México given their simulation domain did not include it.

Table B5. Stations availability and location for Quito

		Obs		ENSEMBLE		CAMS		MPI		EMEP		CHIM		SILAM		USP	
		Jan	Jul	Jan	Jul	Jan	Jul	Jan	Jul	Jan	Jul	Jan	Jul	Jan	Jul	Jan	Jul
CO																	
Quito	Number Stations	6	6	6	6	6	6	6	6	6	6	6	6	6	6	6	6
	Availability [%]	100	100	100	100	100	100	100	100	100	100	83.33	66.67	100	100	100	100
	CV	0.17	0.16	0.15	0.15	0.07	0.06	0.14	0.12	0.31	0.32	0.18	0.12	0.15	0.16	0.34	0.26
NO$_2$																	
Quito	Number Stations	5	5	5	5	5	5	5	5	5	5	5	5	5	5	5	5
	Availability [%]	100	100	100	100	100	100	100	100	100	100	83.33	66.67	100	100	100	100
	CV	0.24	0.18	0.16	0.28	0.49	0.46	0.20	0.16	0.26	0.31	0.22	0.27	0.18	0.18	0.37	0.32
O$_3$																	
Quito	Number Stations	7	7	7	7	7	7	7	7	7	7	7	7	7	7	7	7
	Availability [%]	100	100	100	100	100	100	100	100	100	100	83.33	66.67	100	100	100	100
	CV	0.17	0.20	0.13	0.13	0.08	0.07	0.21	0.21	0.26	0.20	0.20	0.12	0.24	0.27	0.33	0.18
PM$_{10}$																	
Quito	Number Stations	3	3	3	3	3	3	3	3	3	3	3	3	3	3	3	3
	Availability [%]	96.67	100	100	100	100	100	100	100	100	100	83.33	66.67	100	100	100	100
	CV	0.34	0.24	0.22	0.23	0.14	0.12	0.25	0.33	0.26	0.41	0.19	0.16	0.22	0.38	0.40	0.26
PM$_{2.5}$																	
Quito	Number Stations	5	5	5	5	5	5	5	5	5	5	5	5	5	5	5	5
	Availability [%]	96.67	100	100	100	100	100	100	100	100	100	83.33	66.67	100	100	100	100
	CV	0.19	0.24	0.20	0.19	0.14	0.12	0.21	0.24	0.23	0.32	0.19	0.13	0.23	0.33	0.40	0.26
SO$_2$																	
Quito	Number Stations	7	7	7	7	7	7	7	7	7	7	7	7	7	7	7	7
	Availability [%]	100	100	100	100	100	100	100	100	100	100	83.33	66.67	100	100	100	100
	CV	0.33	0.35	0.21	0.33	0.09	0.08	0.19	0.17	0.19	0.27	0.19	0.25	0.12	0.19	0.34	0.34

The observations availability refers to the percentage of days in each period when at least one station records enough data to construct their daily average (minimum of 18 hours). Additionally, only stations that maintain at least 75% of daily availability throughout the entire period are considered (at least 23 days with 18 hours minimum). The model availability refers to the percentage of days for which we have modeled data, being CHIMERE the only one with missing days, and USP missing information for México given their simulation domain did not include it.

Table B6. Stations availability and location for Medellín

		Obs		ENSEMBLE		CAMS		MPI		EMEP		CHIM		SILAM		USP	
		Jan	Jul	Jan	Jul	Jan	Jul	Jan	Jul	Jan	Jul	Jan	Jul	Jan	Jul	Jan	Jul
CO																	
Medellin	Number Stations	2	2	2	2	2	2	2	2	2	2	2	2	2	2	2	2
	Availability [%]	76.67	100	100	100	100	100	100	100	100	100	83.33	66.67	100	100	100	100
	CV	0.14	0.11	0.10	0.09	0.08	0.13	0.13	0.13	0.34	0.30	0.19	0.09	0.14	0.12	0.18	0.14
NO$_2$																	
Medellin	Number Stations	4	4	4	4	4	4	4	4	4	4	4	4	4	4	4	4
	Availability [%]	100	100	100	100	100	100	100	100	100	100	83.33	66.67	100	100	100	100
	CV	0.19	0.16	0.13	0.17	0.68	0.70	0.16	0.15	0.37	0.25	0.25	0.18	0.24	0.16	0.20	0.20
O$_3$																	
Medellin	Number Stations	4	3	4	3	4	3	4	3	4	3	4	3	4	3	4	3
	Availability [%]	100	100	100	100	100	100	100	100	100	100	83.33	66.67	100	100	100	100
	CV	0.21	0.17	0.13	0.10	0.12	0.14	0.13	0.18	0.17	0.21	0.11	0.11	0.18	0.26	0.30	0.17
PM$_{10}$																	
Medellin	Number Stations	1	1	1	1	1	1	1	1	1	1	1	1	1	1	1	1
	Availability [%]	100	100	100	100	100	100	100	100	100	100	83.33	66.67	100	100	100	100
	CV	0.16	0.20	0.14	0.15	0.17	0.29	0.32	0.39	0.22	0.33	0.13	0.16	0.22	0.18	0.31	0.37
PM$_{2.5}$																	
Medellin	Number Stations	5	5	5	5	5	5	5	5	5	5	5	5	5	5	5	5
	Availability [%]	100	100	100	100	100	100	100	100	100	100	83.33	66.67	100	100	100	100
	CV	0.15	0.14	0.14	0.15	0.18	0.30	0.27	0.30	0.18	0.25	0.14	0.13	0.22	0.20	0.27	0.35
SO$_2$																	
Medellin	Number Stations	1	1	1	1	1	1	1	1	1	1	1	1	1	1	1	1
	Availability [%]	10	100	100	100	100	100	100	100	100	100	83.33	66.67	100	100	100	100
	CV	0.20	0.19	0.26	0.20	0.20	0.23	0.28	0.22	0.74	0.52	0.17	0.15	0.27	0.31	0.22	0.25

The observations availability refers to the percentage of days in each period when at least one station records enough data to construct their daily average (minimum of 18 hours). Additionally, only stations that maintain at least 75% of daily availability throughout the entire period are considered (at least 23 days with 18 hours minimum). The model availability refers to the percentage of days for which we have modeled data, being CHIMERE the only one with missing days, and USP missing information for México given their simulation domain did not include it.

Table B7. Stations availability and location for Lima

		Obs		ENSEMBLE		CAMS		MPI		EMEP		CHIM		SILAM		USP	
		Jan	Jul	Jan	Jul	Jan	Jul	Jan	Jul	Jan	Jul	Jan	Jul	Jan	Jul	Jan	Jul
CO																	
Lima	Number Stations	8	7	8	7	8	7	8	7	8	7	8	7	8	7	8	7
	Availability [%]	100	100	100	100	100	100	100	100	100	100	83.33	66.67	100	100	100	100
	CV	0.21	0.17	0.08	0.09	0.08	0.10	0.11	0.09	0.10	0.08	0.36	0.13	0.33	0.19	0.20	0.14
NO_2																	
Lima	Number Stations	2	6	2	6	2	6	2	6	2	6	2	6	2	6	2	6
	Availability [%]	93.33	96.67	100	100	100	100	100	100	100	100	83.33	66.67	100	100	100	100
	CV	0.23	0.16	0.10	0.13	0.38	0.70	0.08	0.11	0.14	0.10	0.25	0.12	0.20	0.19	0.20	0.19
O_3																	
Lima	Number Stations	3	6	3	6	3	6	3	6	3	6	3	6	3	6	3	6
	Availability [%]	100	100	100	100	100	100	100	100	100	100	83.33	66.67	100	100	100	100
	CV	0.47	0.29	0.14	0.13	0.18	0.15	0.17	0.08	0.12	0.10	0.12	0.12	0.19	0.18	0.31	0.25
PM_{10}																	
Lima	Number Stations	8	8	8	8	8	8	8	8	8	8	8	8	8	8	8	8
	Availability [%]	100	100	100	100	100	100	100	100	100	100	83.33	66.67	100	100	100	100
	CV	0.13	0.27	0.09	0.12	0.13	0.18	0.16	0.19	0.24	0.23	0.11	0.11	0.20	0.18	0.16	0.23
$PM_{2.5}$																	
Lima	Number Stations	9	8	9	8	9	8	9	8	9	8	9	8	9	8	9	8
	Availability [%]	96.67	100	100	100	100	100	100	100	100	100	83.33	66.67	100	100	100	100
	CV	0.16	0.22	0.12	0.13	0.13	0.18	0.18	0.14	0.20	0.11	0.18	0.13	0.28	0.23	0.16	0.23
SO_2																	
Lima	Number Stations	4	2	4	2	4	2	4	2	4	2	4	2	4	2	4	2
	Availability [%]	100	100	100	100	100	100	100	100	100	100	83.33	66.67	100	100	100	100
	CV	0.19	0.37	0.15	0.11	0.12	0.05	0.10	0.12	0.19	0.10	0.22	0.21	0.24	0.16	0.19	0.15

The observations availability refers to the percentage of days in each period when at least one station records enough data to construct their daily average (minimum of 18 hours). Additionally, only stations that maintain at least 75% of daily availability throughout the entire period are considered (at least 23 days with 18 hours minimum). The model availability refers to the percentage of days for which we have modeled data, being CHIMERE the only one with missing days, and USP missing information for México given their simulation domain did not include it.

Table B8. Stations availability and location for Guadalajara

		Obs		ENSEMBLE		CAMS		MPI		EMEP		CHIM		SILAM		USP
		Jan	Jul	Jan	Jul	Jan	Jul	Jan	Jul	Jan	Jul	Jan	Jul	Jan	Jul	Jan Jul
CO																
Guadalajara	Number Stations	7	7	7	7	7	7	7	7	7	7	7	7	7	7	
	Availability [%]	96.67	100	100	100	100	100	100	100	100	100	83.33	66.67	100	100	
	CV	0.20	0.12	0.22	0.14	0.20	0.13	0.14	0.18	0.28	0.20	0.32	0.16	0.30	0.27	
NO$_2$																
Guadalajara	Number Stations	8	8	8	8	8	8	8	8	8	8	8	8	8	8	
	Availability [%]	100	100	100	100	100	100	100	100	100	100	83.33	66.67	100	100	
	CV	0.25	0.17	0.30	0.17	0.64	0.88	0.16	0.18	0.34	0.24	0.39	0.28	0.32	0.33	
O$_3$																
Guadalajara	Number Stations	8	8	8	8	8	8	8	8	8	8	8	8	8	8	
	Availability [%]	96.67	100	100	100	100	100	100	100	100	100	83.33	66.67	100	100	
	CV	0.16	0.31	0.16	0.16	0.28	0.24	0.22	0.27	0.22	0.16	0.18	0.12	0.26	0.27	
PM$_{10}$																
Guadalajara	Number Stations	8	8	8	8	8	8	8	8	8	8	8	8	8	8	
	Availability [%]	96.67	100	100	100	100	100	100	100	100	100	83.33	66.67	100	100	
	CV	0.22	0.20	0.32	0.20	0.28	0.29	0.34	0.47	0.34	0.25	0.31	0.19	0.36	0.37	
SO$_2$																
Guadalajara	Number Stations	8	8	8	8	8	8	8	8	8	8	8	8	8	8	
	Availability [%]	96.67	100	100	100	100	100	100	100	100	100	83.33	66.67	100	100	
	CV	0.52	0.41	0.33	0.12	0.26	0.17	0.20	0.21	0.26	0.16	0.28	0.23	0.30	0.28	

The observations availability refers to the percentage of days in each period when at least one station records enough data to construct their daily average (minimum of 18 hours). Additionally, only stations that maintain at least 75% of daily availability throughout the entire period are considered (at least 23 days with 18 hours minimum). The model availability refers to the percentage of days for which we have modeled data, being CHIMERE the only one with missing days, and USP missing information for México given their simulation domain did not include it.

Appendix C: Particular hourly simulations
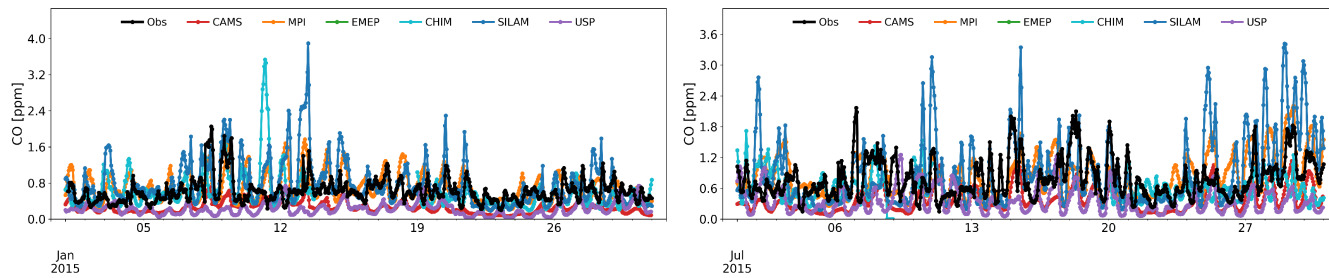
Figure C1. Hourly CO simulations in São Paulo for January and July of 2015
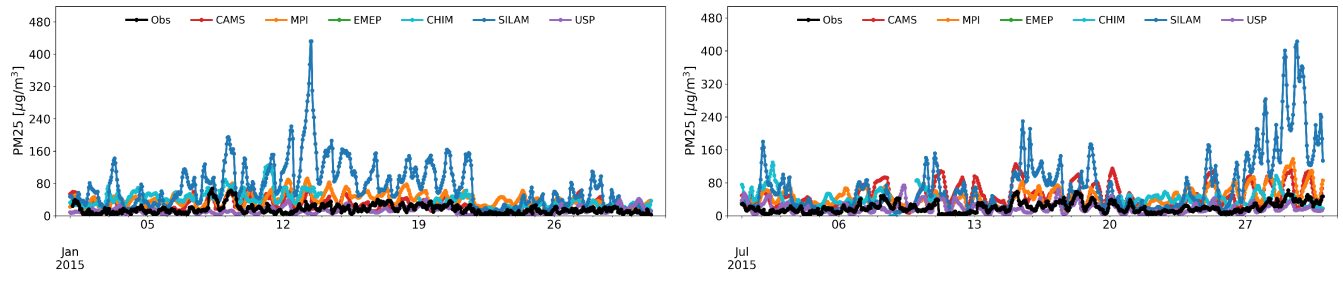
Figure C2. Hourly PM$_{2.5}$ simulations in São Paulo for January and July of 2015
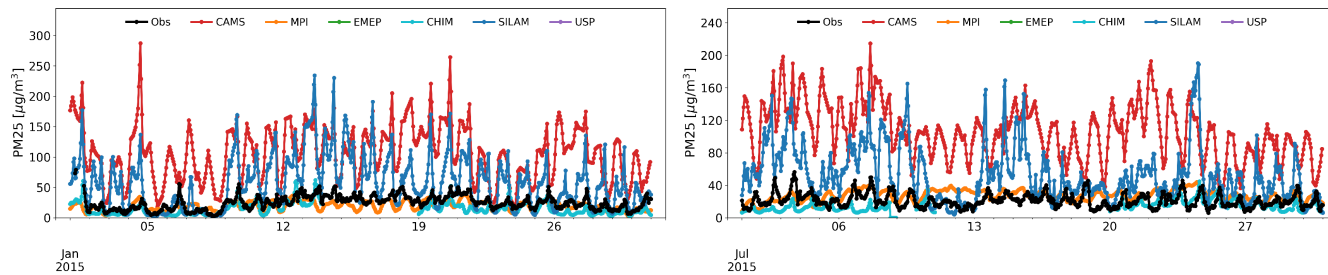
Figure C3. Hourly PM$_{2.5}$ simulations in México City for January and July of 2015

Appendix D: Simulation of all models
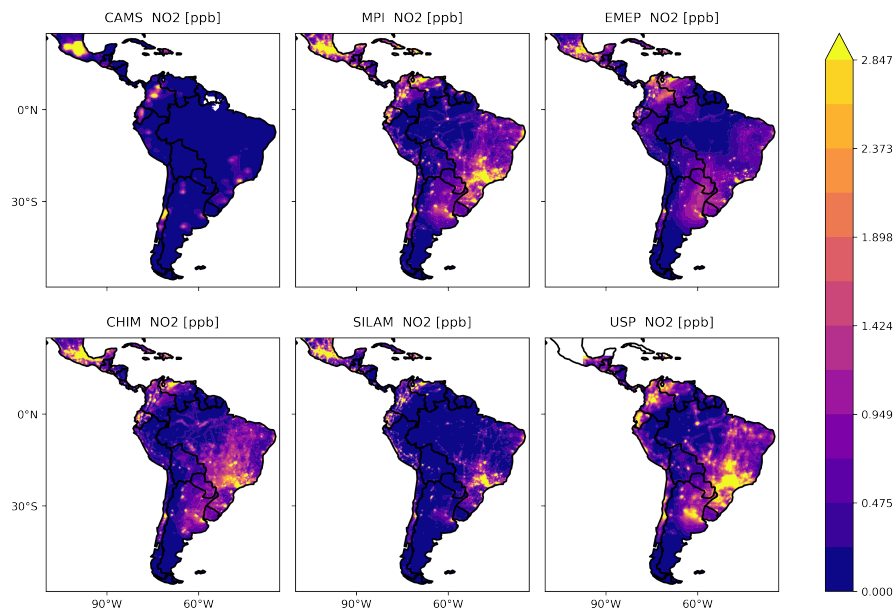
Figure D1. NO$_2$ simulations of January 2015 for all models
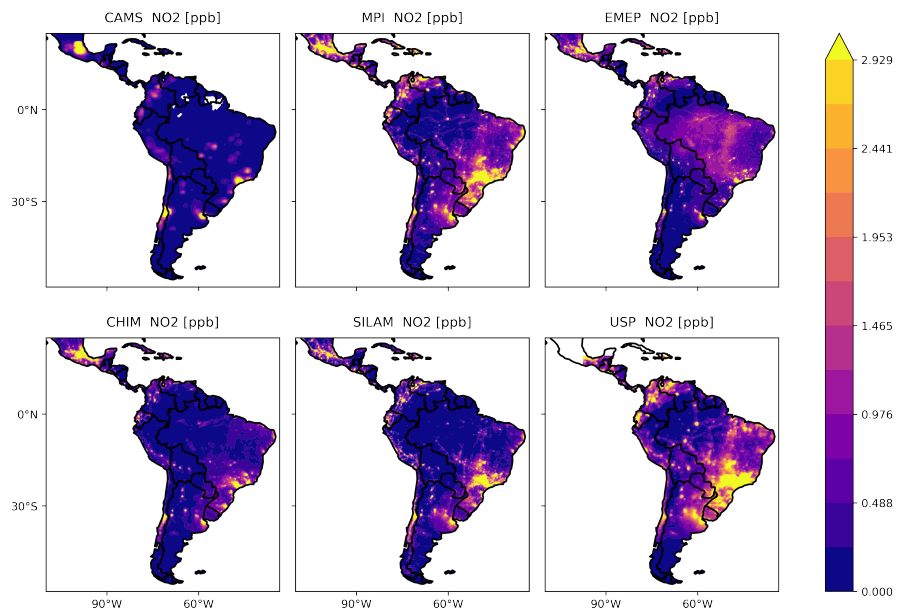
Figure D2. NO$_2$ simulations of July 2015 for all models
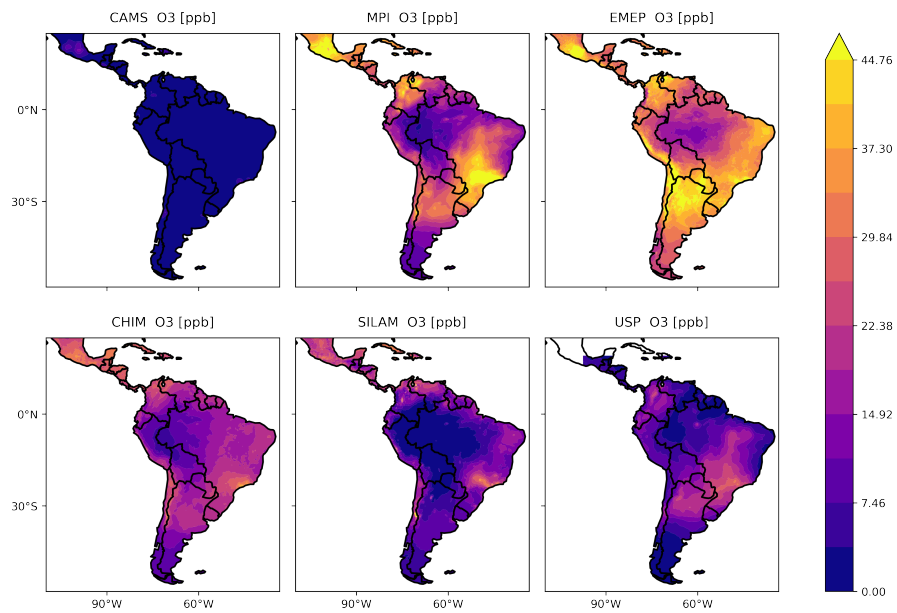
Figure D3. O$_3$ simulations of January 2015 for all models
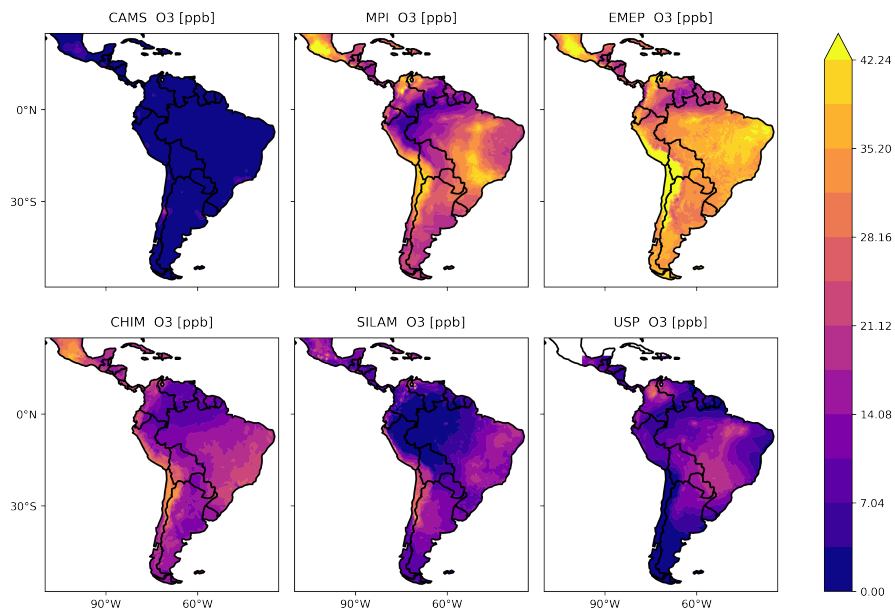
Figure D4. O$_3$ simulations of July 2015 for all models
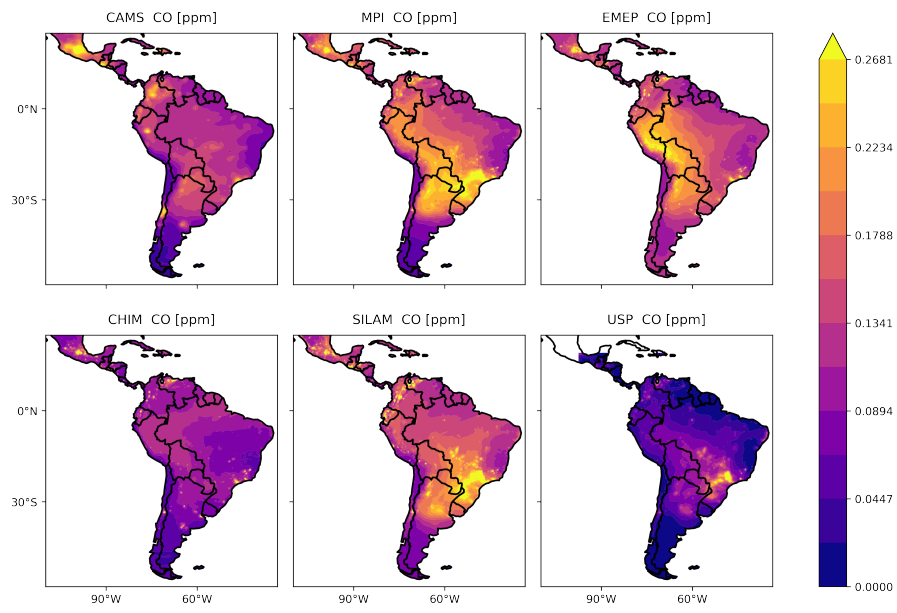
Figure D5. CO simulations of January 2015 for all models
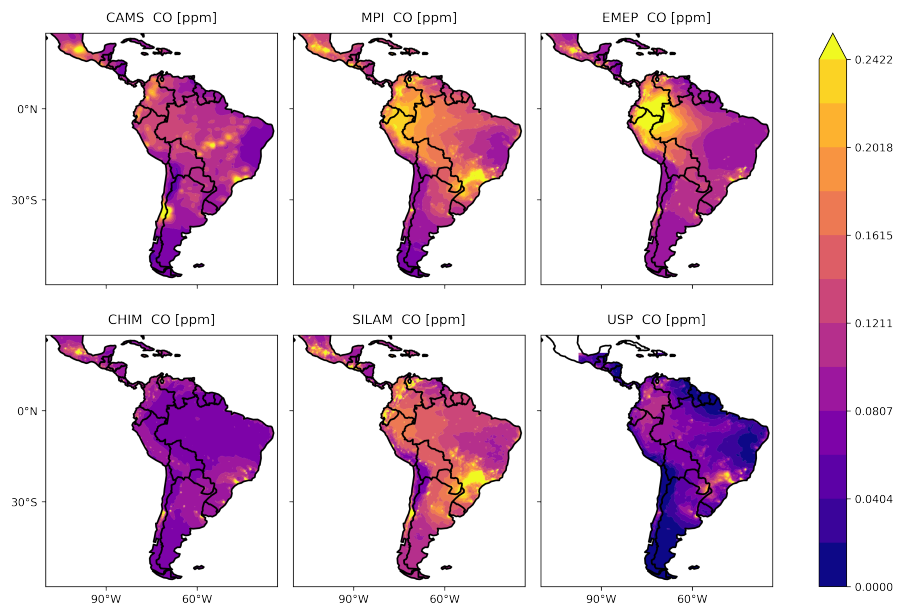
Figure D6. CO simulations of July 2015 for all models
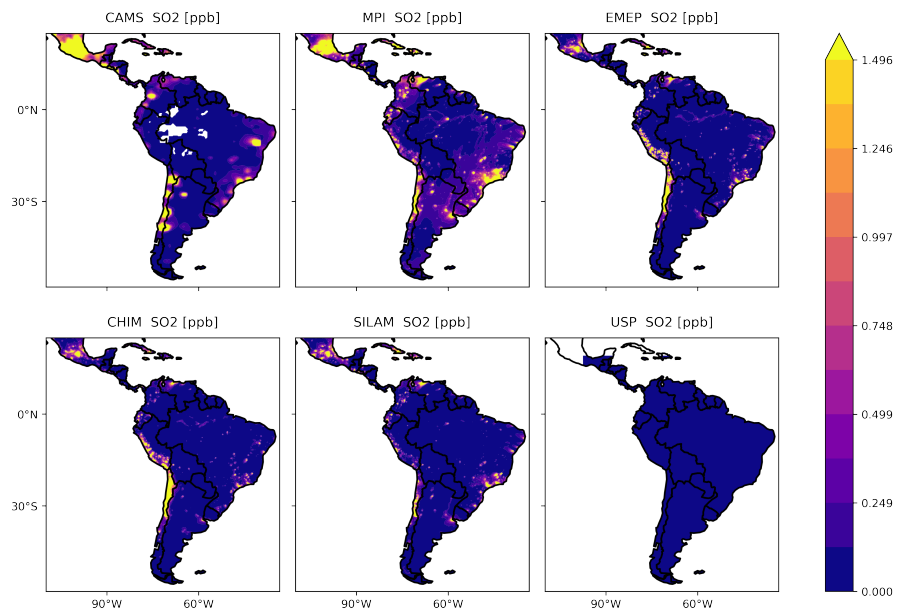
Figure D7. SO$_2$ simulations of January 2015 for all models
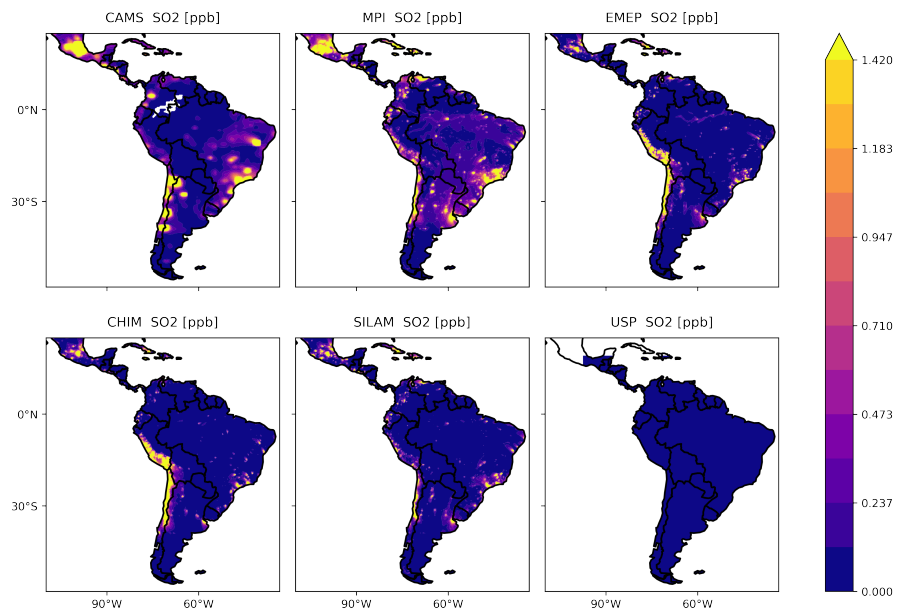
Figure D8. SO$_2$ simulations of July 2015 for all models
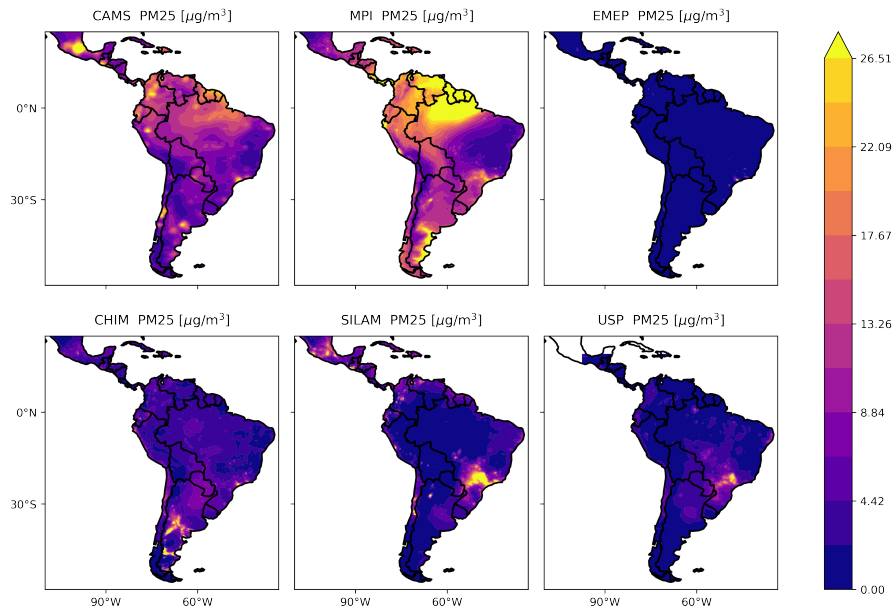
Figure D9. PM$_{2.5}$ simulations of January 2015 for all models
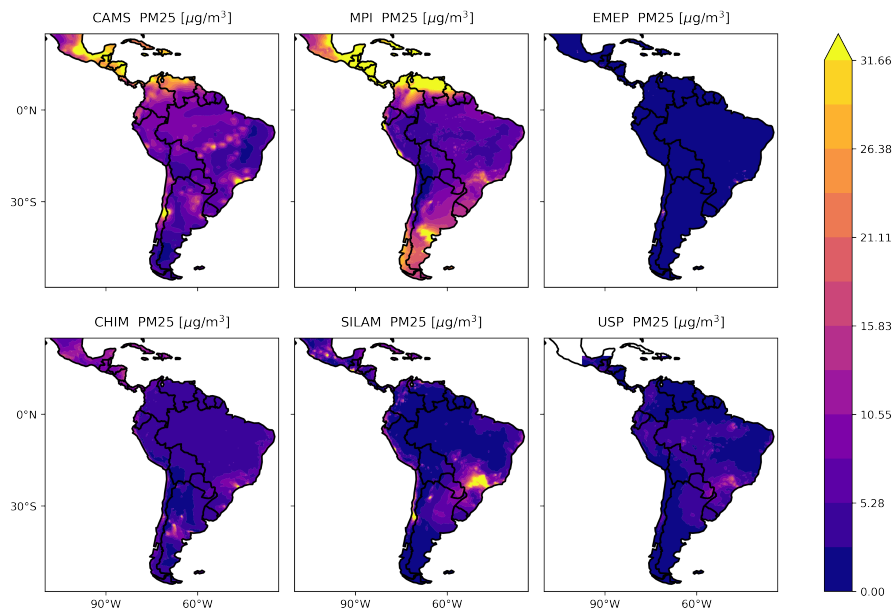
Figure D10. PM$_{2.5}$ simulations of July 2015 for all models

Appendix E: Model deviations
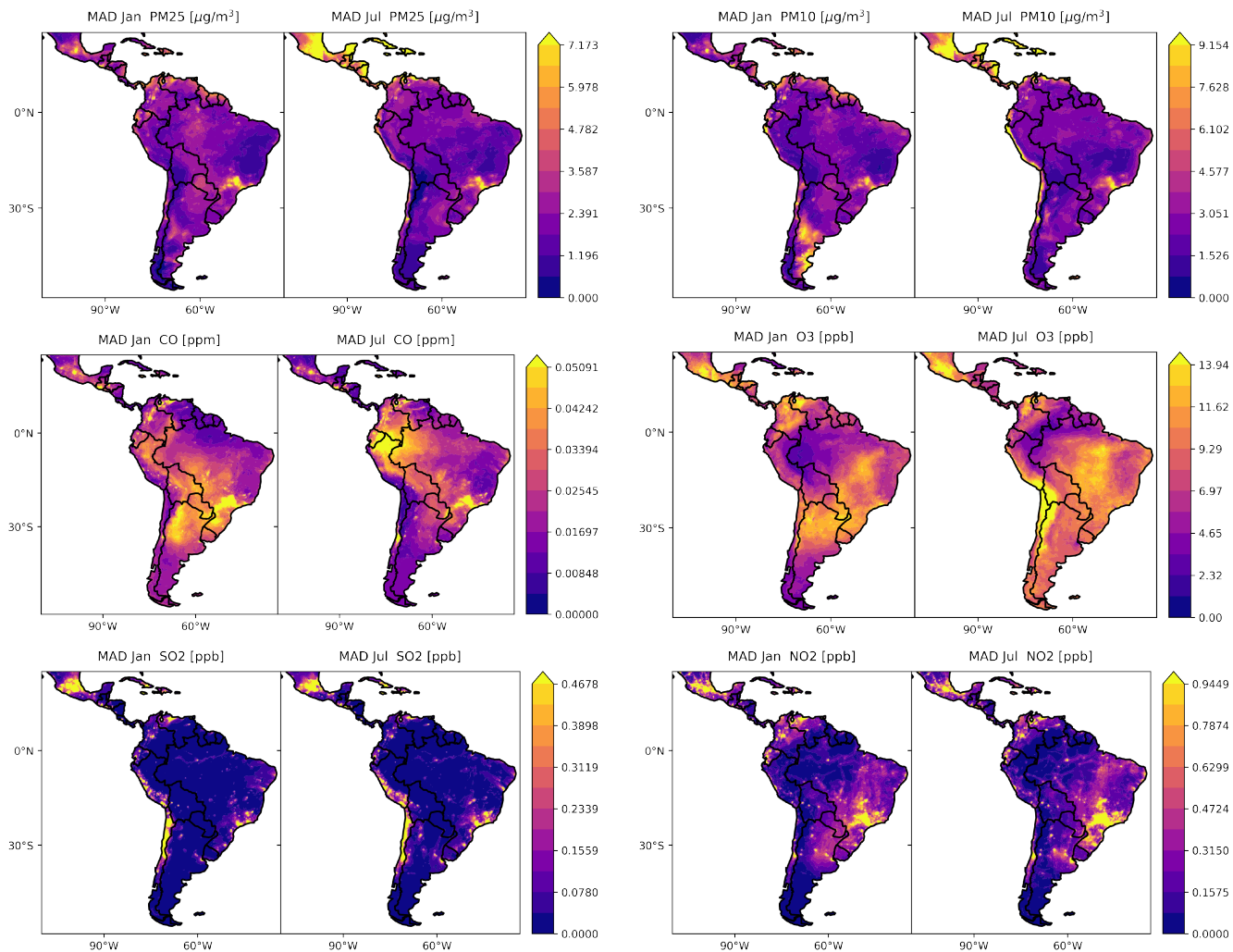
Figure E1. Median absolute deviation of the models with respect to the ensemble for PM_{10}, $PM_{2.5}$, O_3, CO, SO_2 and NO_2 in LAC for January and July 2015
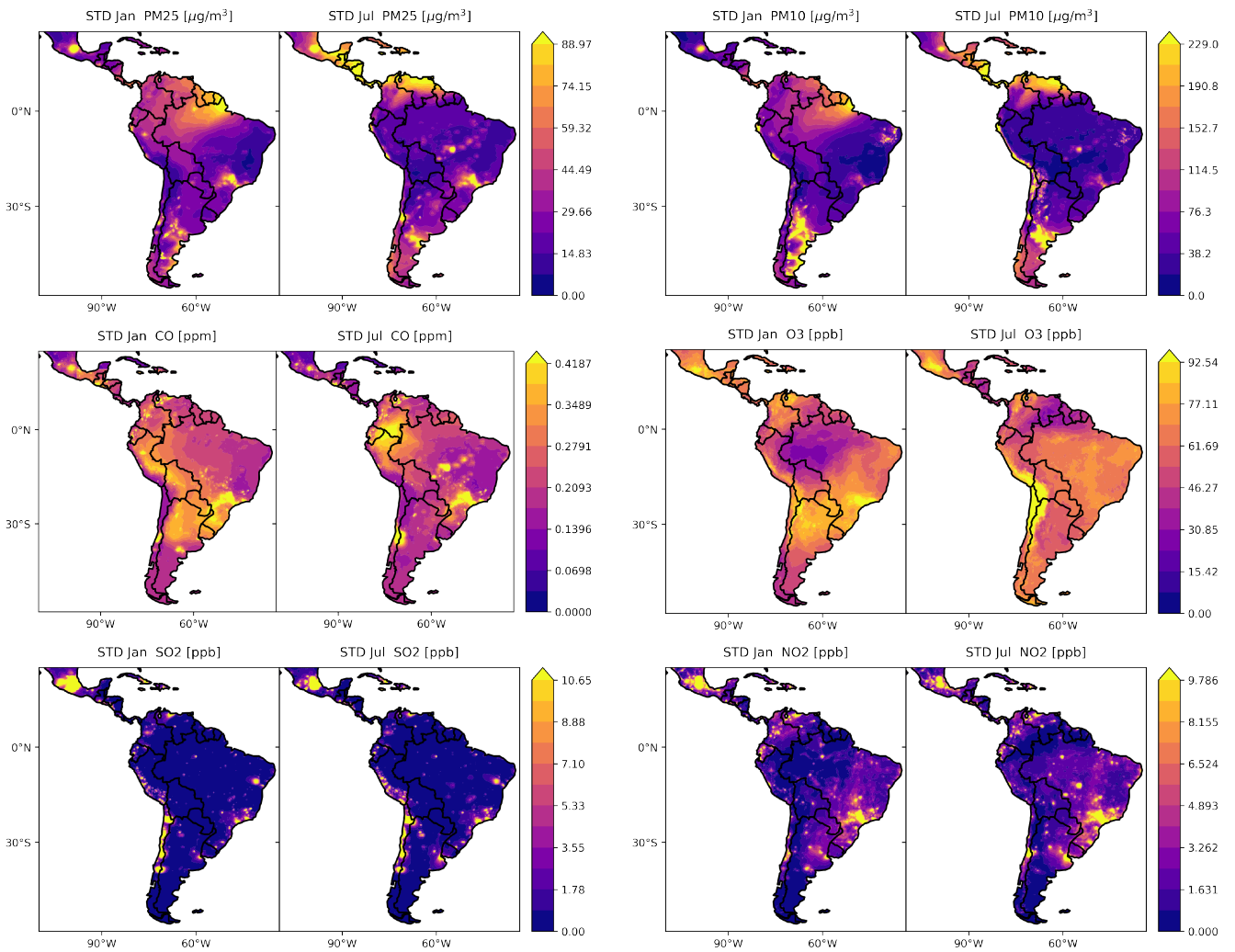
Figure E2. Standard deviation of the models with respect to their mean for PM_{10}, $PM_{2.5}$, O_3, CO, SO_2 and NO_2 in LAC for January and July 2015